creative commons
COMMONS DEED

저작자표시-비영리-동일조건변경허락 2.0 대한민국

이용자는 아래의 조건을 따르는 경우에 한하여 자유롭게

- 이 저작물을 복제, 배포, 전송, 전시, 공연 및 방송할 수 있습니다.
- 이차적 저작물을 작성할 수 있습니다.

다음과 같은 조건을 따라야 합니다:

저작자표시. 귀하는 원저작자를 표시하여야 합니다.

비영리. 귀하는 이 저작물을 영리 목적으로 이용할 수 없습니다.

동일조건변경허락. 귀하가 이 저작물을 개작, 변형 또는 가공했을 경우에는, 이 저작물과 동일한 이용허락조건하에서만 배포할 수 있습니다.

- 귀하는, 이 저작물의 재이용이나 배포의 경우, 이 저작물에 적용된 이용허락조건을 명확하게 나타내어야 합니다.
- 저작권자로부터 별도의 허가를 받으면 이러한 조건들은 적용되지 않습니다.

저작권법에 따른 이용자의 권리는 위의 내용에 의하여 영향을 받지 않습니다.

이것은 이용허락규약(Legal Code)을 이해하기 쉽게 요약한 것입니다.

Disclaimer

dCollection

Ph.D DISSERTATION

A STUDY ON SERIES SLOT ARRAY ANTENNA DESIGN METHODOLOGY AND ITS APPLICATION TO DUAL LINEAR POLARIZATION

직렬 슬롯 배열안테나 설계 기법과 이중 선형편파로의 응용에 관한 연구

BY
DONGYEON KIM

FEBRUARY 2014

SCHOOL OF ELECTRICAL ENGINEERING AND
COMPUTER SCIENCE COLLEGE OF ENEGINEEING
SEOUL NATIONAL UNIVERSITY

공학박사 학위논문

A STUDY ON SERIES SLOT ARRAY ANTENNA DESIGN METHODOLOGY AND ITS APPLICATION TO DUAL LINEAR POLARIZATION

직렬 슬롯 배열안테나 설계 기법과 이중 선형편파로의 응용에 관한 연구

2014년 2월

서울대학교 대학원

전기·컴퓨터 공학부

김 동 연

Abstract

This thesis presents series slot array antenna design methodology for arbitrary inclined linear polarization. In order to realize 45°-inclined linear polarization, impedance matching, and grating lobe suppression, new concept of an 'alternating reactance slot pair' is proposed. The slot spacings are set for a half guided-wavelength of radiating waveguides and then avoid grating lobes in longitudinal directions. The proposed antenna is realized by a substrate integrated waveguide (SIW) technology and verified by full-wave EM simulations and measurements.

First, a linear and a 16 × 8 planar slot array antennas for Ka-band are proposed using a SIW technology on a multi-layered structure for 45°-inclined linear polarization. Uniform field distributions are verified in terms of amplitude and phase from an equivalent circuit analysis and compared with full-wave simulations.

Secondly, the excitation control method is proposed for low sidelobe levels. The mode currents flowing each radiating slots can be controlled by axial displacements along the center line of a radiating waveguide. In order to confirm the tapered excitation control method, –20 and –26 dB Dolph-Chebyshev polynomials are applied for linear slot array antennas.

Finally, a ±45° dual linear polarization is applied for a monopulse tracking radar to enhance channel capacity and clear the target images. The crossed ±45°

radiating slots are arranged on a common radiating aperture under orthogonal condition for minimal mutual coupling. The monopulse operation in Ka-band is realized by the proposed dual linear polarized 8 × 8 SIW monopulse antenna with outstanding isolations. The electrical performances such as S-parameters, sum and difference radiation patterns, and gains are verified by full-wave simulation and experimental results.

Keywords: 45 degree linear polarization, alternating reactance slot pair, dual linear polarization, isolation, millimeter wave antenna, monopulse antenna, mutual coupling, resonant slot arrays, series slot arrays, sidelobe suppression, substrate integrated waveguide (SIW), waveguide comparator.

Student number: 2010-30211

Contents

Abstract ..... **i**

Contents ..... **iii**

List of Figures ..... **vi**

List of Tables ..... **xii**

1. Introduction **1**

1.1 Conventional Slot Array Antennas for Linear Polarization 3

1.2 Substrated Integrated Waveguide (SIW) Technology 5

2. Linear Slot Array Antenna for 45°-Inclined Linear Polarization **9**

2.1 Introduction 9

2.2 Proposed Antenna Configuration 10

2.2.1 Single Slot Module and Impedance Extraction 11

2.2.2 Alternating Reactance Slot Pair 14

2.2.3 Equivalent Circuit Analysis using Recursive Formulas 17

2.2.4 Centered-Inclined Series-to-Series Coupling Slot 20

2.3 Simulation and Measurement 22

2.4 Summary 25

3. Planar Slot Array Antenna for 45º-Inclined Linear Polarization 30

3.1 Introduction 30

3.2 Proposed Antenna Configuration 33

3.3 Feeding Network Design and Analysis 35

3.4 Coupling and Radiating Slot Arrangement for In-Phase Excitation 41

3.5 Wideband Coax-to-SIW Transition Design and Analysis 42

3.6 Simulation and Measurement 48

3.6.1 Uniform Electric Field Distribution 48

3.6.2 Back-to-Back Coax-to-SIW Transition 52

3.6.3 Reflection Coefficient, Gain, and Radiation Patterns 54

3.7 Summary 57

4. Excitation Control Method for Low Sidelobe Level 63

4.1 Introduction 63

4.2 Axial Displacements for Excitation Control 66

4.3 Design Procedure for Excitation Control 73

4.4 Simulation and Measurement 77

4.5 Summary 82

5. Dual Linear Polarized SIW Monopulse Antenna for Tracking Radar..... 85

5.1 Introduction..... 85

5.2 Design Considerations for Dual LP Radiating SIWs..... 88

5.3 The Proposed Dual LP 8 × 8 SIW Monopulse Protptype Antenna 92

5.3.1 Folded Short-Circuited Stubs..... 95

5.3.2 Shunt-to-Series Coupling Slots..... 96

5.3.3 Series-to-Series Coupling Slots 97

5.4 RWG Comparator for Monopulse Operation..... 98

5.5 Experimental Results 103

5.5.1 Dual LP SIW Sub-Array Antenna..... 103

5.5.2 Dual LP SIW Monopulse Antenna..... 107

5.6 Summary..... 109

6. Conclusion 116

List of Figures

Fig. 1.1 Conventional slot array antennas using (a) shunt and (b) series radiating slots. (c) Standing-wave (or resonant) and (d) traveling-wave slot array antennas for arbitrary linear polarization 4

Fig. 1.2 SIW and its metallic rectangular waveguide equivalent model. 6

Fig. 2.1 Geometry of the proposed SIW series slot array antenna. (a) Front view of the multi-layered total antenna structure. (b) Front view of the feeding SIW including the series-to-series coupling slot. (c) Lateral view. 12

Fig. 2.2 A SIW single module of the series slot tilted at an angle of 45°. (a) The structure with the dimensions given in TABLE I and its equivalent circuit, where Z_0 is the wave impedance of the SIW and β_{10} is the propagation constant of the TE_{10}-mode. (b) The normalized resistance and reactance characteristics, as well as the phase with respect to the normalized half-length of the slot. 13

Fig. 2.3 The proposed alternating reactance slot pair etched on the broad wall of a radiating SIW. (a) The structure and its equivalent circuit, where Z_0^{rad} is the wave impedance and β_{10}^{rad} is the propagation constant of the TE_{10} mode. (b)

The phase difference (θ_d) between the normalized self-impedances (z_c and z_i) of an alternating reactance slot pair. 15

Fig. 2.4 The left section of a linear slot array antenna (Fig. 2.1(a)) with the surface current density patterns and 45º-inclined electric fields on radiating slots. 18

Fig. 2.5 The equivalent circuit of a linear slot array antenna referenced to a coupling slot location. 18

Fig. 2.6 Simulated and calculated results of magnitude and phase of uniformly excited electric field generated by 16 series radiating slots. 24

Fig. 2.7 Reflection coefficients and realized gain results. Inset shows a photograph of a fabricated antenna; Antenna size is 60.6 (L) × 17 (W) mm. 24

Fig. 2.8 Simulated and measured radiation patterns. (a) zx-plane and (b) yz-plane. . 26

Fig. 3.1 The proposed planar antenna geometry. (a) Top view. (b) The feeding structure that has series-to-series coupling slot arrays. (c) Lateral view. 34

Fig. 3.2 The equivalent circuit of a feeding SIW. 36

Fig. 3.3 The four-port series-to-series coupling slot junction and an equivalent circuit, where β_{10}^{rad} is the propagation constant of the TE_{10} mode. 36

Fig. 3.4 The input impedance characteristics of a linear slot array as a function of the coupling slot length (l_i) and the tilt angle (p) when the width (w_c) of the coupling slot is 0.5 mm. (a) Input resistance and (b) Input susceptance. 38

Fig. 3.5 The resonant condition for the series-to-series coupling slot which is

terminated with a linear slot array at port 3 and 4. 39

Fig. 3.6 The arrangement of the coupling and radiating slots for in-phase distribution with surface current density patterns. 41

Fig. 3.7 The wideband stepped coax-to-SIW transition structure. 43

Fig. 3.8 The equivalent circuit model of the proposed wideband stepped coax-to-SIW transition. 44

Fig. 3.9 S-parameter results of circuit and full-wave simulations for a single-ended stepped coax-to-SIW transition 46

Fig. 3.10 The return loss variation according to (a) the width of a feeding SIW (w_f), (b) the length of an open-circuited SIW stub (l_1), and (c) the radius of the coaxial aperture radius (r_2). 47

Fig. 3.11 The near aperture field distribution with respect to the phase and amplitude (a) for the radiating SIW #1 and (b) for 9th radiating elements (slot #9) of every radiating SIW. 50

Fig. 3.12 The simulated aperture distribution with respect to the electric field amplitude. 51

Fig. 3.13 The fabricated back-to-back stepped coax-to-SIW transition. 53

Fig. 3.14 The simulated and measured s-parameter results of the proposed coax-to-SIW transition. 53

Fig. 3.15 The fabricated slot array antenna for 45º-inclined LP. 55

Fig. 3.16 The simulated and measured reflection coefficients and realized gain..... 55

Fig. 3.17 Radiation patterns for (a) *zx* plane and (b) *yz* plane, respectively..... 56

Fig. 4.1 SIW linear slot array antenna structure (a) for arbitrary excitation coefficients using axial displacements (from x_1 to x_8). In this case, the axial displacements are employed just for inductive radiating slots (x_2, x_4, x_6, and x_8) not capacitive radiating slots (x_1, x_3, x_5, and x_7). (b) Lateral view..... 65

Fig. 4.2 Equivalent rectangular waveguide slot array model with axial displacements on each radiating slots and its transmission line circuit model. . 68

Fig. 4.3 The magnitude and phase variation of radiating electric fields with respect to the direction of axial displacements for (a) inductive (slots #8 and #9) and (b) capacitive (slots #7 and #10) radiating slots, respectively. For the verification, the calculated results from recursive formulas are depicted..... 72

Fig. 4.4 The slot voltage characteristics according to the progressive axial displacement variations. The calculated results from the equivalent circuit are shown with EM results. 74

Fig. 4.5 Excitation coefficient design results for (a) –20 dB and (b) –26 dB, respectively, with electric field distribution (E_z) inside a radiating SIW. 75

Fig. 4.6 The reflection coefficients and realized gain results with fabricated antenna pictures of (a) –20 dB SLL and (b) –26 dB SLL slot array antennas, respectively.. 78

Fig. 4.7 The measured radiation patterns (*zx*-plane) with calculated array factor and full-wave simulation results for 45°-inclined LP of two types of linear array antennas. (a) –20 dB SLL, (b) –26 dB SLL. 80

Fig. 5.1 The arrangement of ±45º dual linear polarized radiating slots on radiating SIWs. The SIW transmission lines consist of via arrays with a diameter (*d*) and spacing (*s*) of 0.4 mm and 0.75 mm. The length of the alternating reactance slot pair are set to 2.9 mm (l_i) and 3.6 mm (l_c) as inductive and capacitive loads. The width of all radiating slots is 0.4 mm (*sw*)..... 89

Fig. 5.2 The orthogonal conditions for a dual linear polarized slot array antenna with respect to the width variation of a radiating SIW for given PCBs..... 91

Fig. 5.3 The proposed dual LP monopulse antenna structure with top and side views. (SIW transmission lines that are consisted with metallic via arrays are replaced with equivalent conventional RWGs.) 93

Fig. 5.4 The proposed folded short-circuited stubs. (a) Wide *x*-directed slot spacing between two sub-arrays. (b) Reduced slot spacing as $0.8 \cdot \lambda_0$ without any slot free regions. (c) The arrangements of shunt-to-series coupling slots and radiating slots of two adjacent sub-arrays. (d) The arrangement of a series-to-series coupling slot with adjacent two shunt-to-series coupling slots for in-phase excitation. 94

Fig. 5.5 The feeding network for 2-D monopulse operation. (a) A block diagram.

(b) The picture of fabricated RWG comparator. 99

Fig. 5.6 measured return losses for each input ports of a RWG comparator. 100

Fig. 5.7 The measured amplitude results of four output ports for (a) sum (Σ), two difference input ports (b) Δ_{AZ} and (c) Δ_{EL}. 101

Fig. 5.8 The measured phase imbalance results for (a) sum (Σ), two difference input ports (b) Δ_{AZ} and (c) Δ_{EL}. 102

Fig. 5.9 The picture of fabricated dual LP sub-array antenna. 104

Fig. 5.10 The simulated and measured results of reflection coefficients, isolations, and realized gains for fabricated dual LP SIW sub-array antenna. 104

Fig. 5.11 The simulated and measured radiation patterns for –45º LP (port #1). (a) *yz*-plane. (b) *zx*-plane. 105

Fig. 5.12 The simulated and measured radiation patterns for +45º LP (port #2). (a) *yz*-plane. (b) *zx*-plane. 106

Fig. 5.13 The fabricated monopulse antenna. (a) SIW main radiator, (b) back view for –45° LP operation, (c) back view for +45° LP operation. 108

Fig. 5.14 The +45° LP sum radiation patterns at 34.7 GHz. (a) In azimuth angle (*zx*-plane), (b) In elevation angle (*yz*-plane). 110

Fig. 5.15 The +45° LP difference radiation patterns at 34.7 GHz. (a) In azimuth angle (*zx*-plane), (b) In elevation angle (*yz*-plane). 111

List of Tables

TABLE 2.1 Optimized values for the design parameters of the proposed antenna .. 22

TABLE 2.2 Simulated and calculated results for the normalized electric field of the radiating slots 23

TABLE 2.3 Measured elecrical performance of the proposed antenna 27

TABLE 3.1 Design parameters and optimized values 49

TABLE 3.2 Measured elecrical performances 57

TABLE 4.1 The design parameters and optimized values 76

TABLE 4.2 Radiation characteristics for two types of antennas 81

TABLE 5.1 The design parameters and optimized values 97

Chapter 1

Introduction

Modern radars are widely applied to portable systems, short range millimeter-wave sensors, and military defense. Their commercial demands are also rapidly increasing and the operating frequency bands are changed from L, S, and X-bands to Ku, Ka, and W-bands.

The polarization diversity is suggested to several communication and radar systems in order to enhance the channel capacity and clear the target image from the glint angle noise **[1-3]**. A two-beam slotted leaky waveguide array antenna had been proposed for dual-polarization direct broadcast satellite (DBS) using cross slot arrays **[1]**. The coupling between two left- and right-handed circular polarizations is relatively high, and there is increased cross polarization level about –10 dB in each dual circular polarized radiation patterns. The air-filled waveguide slot array antenna

is suggested for X-band synthesis aperture radar (SAR) application to achieve clear target images **[2]**. A dual linear polarization (LP) was achieved by shunt slot arrays of ridged waveguides and series slot arrays etched on the narrow wall of adjacent waveguides, respectively, for horizontal and vertical LPs. There are extremely pure polarization properties between each radiator due to their orthogonal arrangement. In **[3]**, the Ka-band monopulse antenna was invented for a missile seeker using ±45º-inclined radiating slots that are excited by ridged waveguides with open-ended cavities. As a result, sufficiently low cross polarization level (less than –25 dB) can be achieved from isolated dual LP radiating slots. As mentioned above reference papers, the most important design issue is the suppression of the mutual coupling between dual polarizations sharing a common radiating aperture for the same operating frequency bands. At the same time, simple radiating and feeding structures are preferable.

In this dissertation, a series slot array antenna design methodology is presented for arbitrary inclined LP. All radiating slots are etched on a center line of the broad wall of radiating waveguides with an identical tilt angle. Finally, the proposed design methodology is applied for a ±45º dual LP monopulse antenna that has a common radiating aperture. Every radiating and feeding transmission line is realized in printed circuit boards (PCBs) to avoid grating lobes and total structures are designed by substrate integrated waveguide (SIW) technology.

1.1 Conventional Slot Array Antennas for Linear Polarization

The conventional slot array antennas employ shunt or series radiating slots as shown in Fig. 1.1(a), (b). All shunt and series radiating slots are located on a broad wall of a radiating waveguide along the center line with offsets (for a shunt array) or alternating tilt angles (for a series array). Also, these radiating slots are separated by a half guided-wavelength for standing-wave (i.e. resonant) excitation. Furthermore, the rigorous design methods for shunt and series slot array antennas are presented in previous works that are considering and compensating external mutual coupling between adjacent radiating slots **[4, 5]**.

These typical slot array antennas are realized on air-filled waveguide transmission lines for radiating and feeding lines and thus have low loss and high radiation efficiency. However, their vertical or horizontal LPs are inappropriate for some radar applications such as the collision avoidance system requiring a 45º-inclined LP. Accordingly, some applied slot array antennas were proposed for an arbitrary LP as shown in Fig. 1.1(c) and (d). Based on a conventional series slot array antenna of Fig. 1.1(b), the resonant series radiating slots with a fixed tilt angle should be arranged with a guided-wavelength due to in-phase excitation and inclined LP generation as shown in Fig. 1.1(c). But, there are some disadvantages such as large sidelobe levels (i.e. grating lobes), tilt angle limitation, and an impedance matching problem. In addition, a traveling-wave type slot array antenna can be used

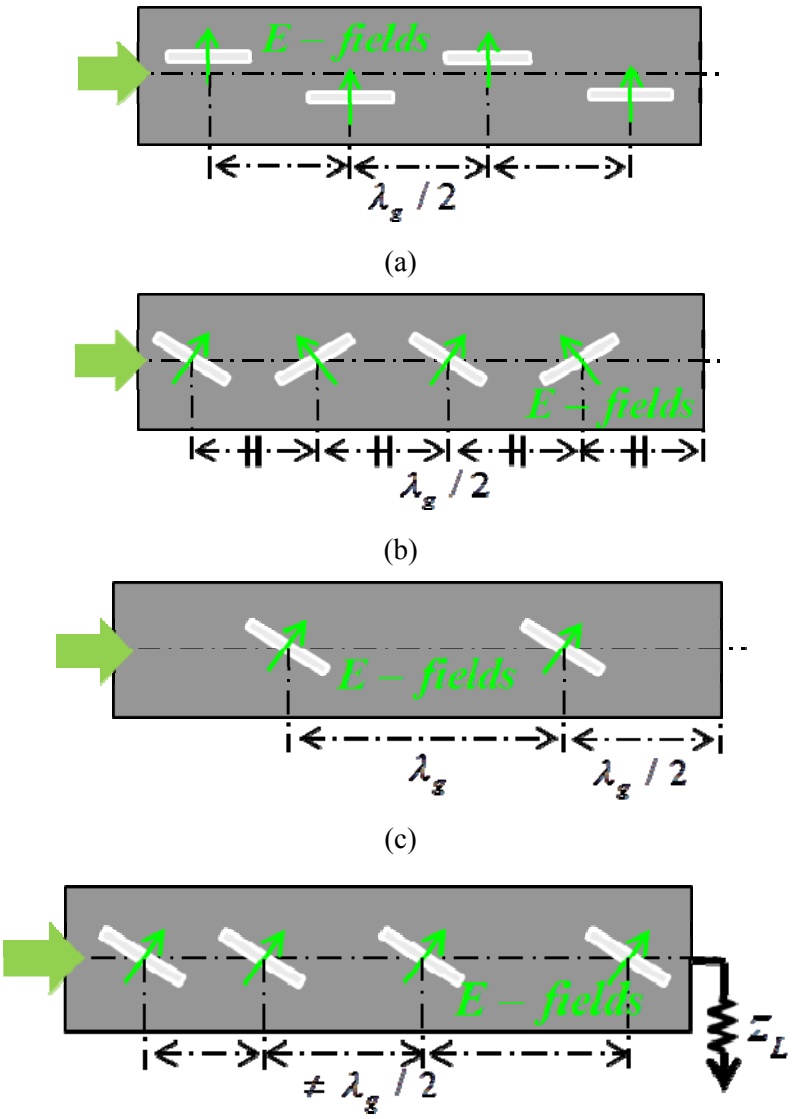

Fig. 1.1 Conventional slot array antennas using (a) shunt and (b) series radiating slots **[4, 5]**. (c) Standing-wave (or resonant) and (d) traveling-wave slot array antennas for arbitrary linear polarization **[6]**.

for arbitrary inclined LP as depicted in Fig. 1.1(d). The slot spacing is not a half guided-wavelength for a travelling-wave type antenna, and the radiating waveguide is terminated with its characteristic impedance **[6]**. Even though this traveling-wave has wide impedance bandwidth, the main beam is tilted from boresight direction.

1.2 Substrate Integrated Waveguide (SIW) Technology

As shown in Fig. 1.2, a SIW transmission line can be embedded in a general PCB connecting the top and bottom metal plates with metalized via arrays acting as a perfect electric wall (PEW) like a rectangular waveguide (RWG). The width (w) of a radiating SIW, the diameter (d), and the spacing (s) of vias are the critical design parameters for the transmission characteristics of a SIW such as the cut-off frequency and attenuations for a fundamental TE_{10} mode. In order to determine the above design parameters for the operating frequency bands, it is desirable to set the center frequency between the cut-off frequencies of the TE_{10} and TE_{20} modes. When the SIW transmission line is identified with the equivalent RWG, the cut-off frequency of the TE_{10} mode is defined by

$$f_{c,TE10} = \frac{c}{2\pi\sqrt{\varepsilon_r}} \cdot \frac{\pi}{w_{eff}} \tag{1.1}$$

and the effective width of the SIW transmission line can be obtained by

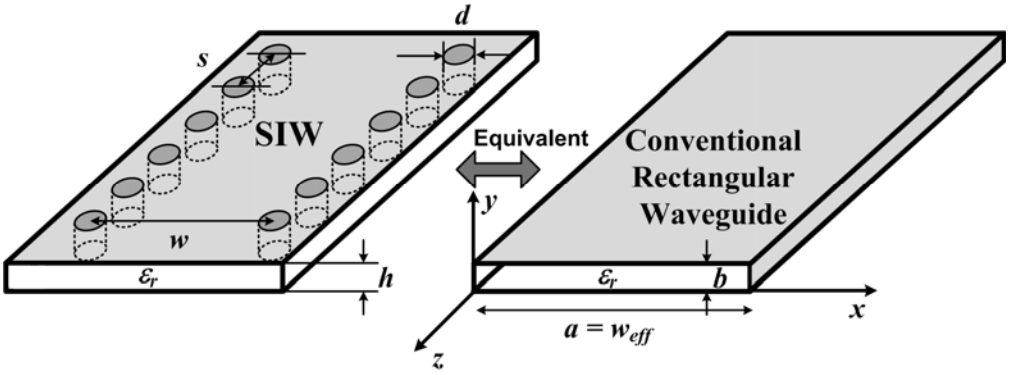

Fig. 1.2 SIW and its metallic rectangular waveguide equivalent model.

$$w_{eff} = w - 1.08 \cdot \frac{d^2}{s} + 0.1 \cdot \frac{d^2}{w} \tag{1.2}$$

where c and ε_r are the light velocity and the dielectric constant of a PCB, respectively **[7]**. Furthermore, radiation, conduction, and dielectric losses should be reduced according to the design principle for the operating frequency. To minimize these losses, the diameter of via was chosen with the following design role **[7]**:

$$s / 2.5 < d < w / 8 \tag{1.3}$$

Reference

[1] K. Sakakibara, Y. Kimura, J. Hirokawa, M. Ando, and N. Goto, "A two-beam slotted leaky waveguide array for mobile reception of dual-polarization DBS," *IEEE Trans. Veh. Technol.*, vol. 48, no. 1, pp. 1–7, Jan. 1999.

[2] W. Wang, J. Jin, J.-G. Lu, and S.-S. Zhong, "Waveguide slotted antenna array with broadband, dual-polarization and low cross-polarization for X-band SAR applications," in *Proc. IEEE Int. Radar Conf.*, Arlington, VA. May 2005, pp. 653–656.

[3] M. Guler and S. Kim, "Dual-polarized, millimeter wave slot array," *in Proc. Aerospace Conference 2003*, vol. 2, pp. 1077–1083, 2003.

[4] R. S. Elliott, "An improved design procedure for small arrays of shunt slots," *IEEE Trans. Antennas Propag.*, vol. AP-31, pp. 48–53, Jan. 1983.

[5] M. Orefice and R. S. Elliott, "Design of waveguide-fed series slot arrays," *IEE Proc.*, vol. 129, pp. 165–169, Aug. 1982, Dt. H.

[6] A. Mizutani, K. Sakakibara, N. Kikuma, and H. Hirayama, "Grating lobe suppression of narrow-wall slotted hollow waveguide millimeter-wave planar antenna for arbitrarily linear polarization," *IEEE Trans. Antennas*

Propag., vol. 55, no. 2, pp. 313–320, Feb. 2007.

[7] F. Xu and K. Wu, "Guided-wave and leakage characteristics of substrate integrated waveguide," *IEEE Microw. Theory Tech.*, vol. 53, no. 1, pp. 66–73, Jan. 2005.

Chapter 2

Linear Slot Array Antenna for 45°-Inclined Linear Polarizations

2.1 Introduction

Over recent decades, design techniques for waveguide (WG) shunt slot array antennas have been thoroughly established **[1]**. In addition, series slot array antennas have also been investigated and analyzed, in a similar way to the shunt slot array design procedure, by Orefice and Elliott **[2]**. Most of the previous research has been based on designing WG slot array antennas for vertical or horizontal polarizations. On the other hand, the 45°-inclined LP slot array antennas are required for many radar systems such as collision avoidance automotive radar, monopulse tracking radar, and synthesis aperture radar (SAR). Even though there have been several

papers describing the aspects of a 45°-inclined LP **[3-6]**, most of the research has been on the traveling-wave type **[3-5]**. In one study, a single main radiating slot and a pair of reflection cancelling slots were adopted as the radiating unit used to generate the 45°-inclined LP and, simultaneously, to satisfy input matching **[3]**. For the same reasons, a reflection cancelling inductive post combined with a radiating slot has been used **[4]**. Moreover, a narrow-wall slotted hollow WG planar antenna with rectangular posts, which controls the amount of coupling to produce arbitrary levels of inclined LP has been described **[5]**. A resonant type slot array antenna was introduced in **[6]**. The 45°-inclined LP can be generated by the longitudinal and transverse offsets of the radiating slot that cuts the surface current of the broad wall of the radiating WG. It is possible that this antenna suffers from strong mutual coupling due to the narrow slot spacing.

In this dissertation, a new type of resonant series slot array antenna is described. The proposed antenna is able to generate a 45°-inclined LP by using alternating reactance slot pairs. Furthermore, through the use of the radiating units, impedance matching, uniform excitation, and grating lobe suppression can be easily and simultaneously achieved. The proposed antenna for Ka band was fabricated using a multi-layered SIW structure and was tested to confirm its design validity.

2.2 Proposed Antenna Configuration

The proposed antenna consists of a radiating SIW (upper printed circuit board (PCB)) and a feeding SIW (lower PCB) as depicted in Fig. 2.1. The radiating series slots are arrayed on the broad wall of a radiating SIW and fed by the series-to-series coupling slot of a feeding SIW. The centered and 45°-inclined radiating slots are aligned in the longitudinal direction (*x*-axis) with spacing of one-half guided wavelength. Notice that all sixteen radiating slot arrays (eight alternating reactance slot pairs) are placed in an alternating arrangement of shorter and longer slots (compared to the resonant slot length), which correspond to the inductive and capacitive series impedances, respectively.

2.2.1 Single Slot Module and Impedance Extraction

The centered and inclined radiating series slot can be modeled and characterized by an equivalent series loaded transmission line as shown in Fig. 2.2(a). As an initial design consideration, it is essential for the impedance of a single SIW series slot module to satisfy the impedance matching requirement and to synthesize the proposed linear array antenna. As illustrated in Fig. 2.2(a), a single SIW series slot module is placed on RO3035^{TM} (Rogers) substrate, with a relative permittivity of 3.5, a loss tangent of 0.0018 at 10 GHz, and a thickness of 1.52 mm,

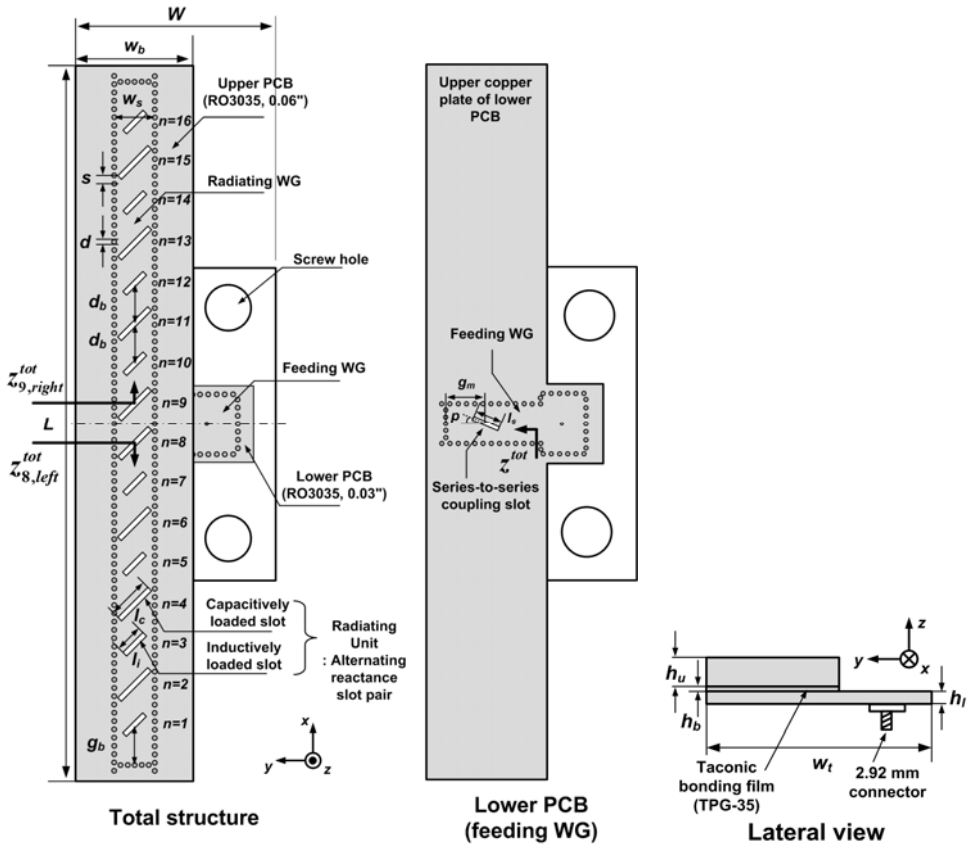

Fig. 2.1 Geometry of the proposed SIW series slot array antenna. (a) Front view of the multi-layered total antenna structure. (b) Front view of the feeding SIW including the series-to-series coupling slot. (c) Lateral view.

as a radiating SIW. In the design of the SIW transmission line, the metalized via arrays are located with appropriate values of via diameter (d), via spacing (s), and the width of the radiating WG (w_s) for minimum radiation, conduction, and

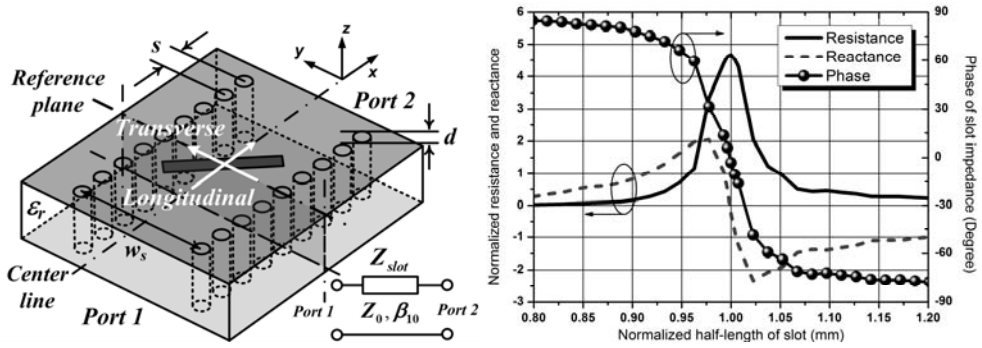

(a) (b)

Fig. 2.2 A SIW single module of the series slot tilted at an angle of 45°. (a) The structure with the dimensions given in TABLE 2.1 and its equivalent circuit, where Z_0 is the wave impedance of the SIW and β_{10} is the propagation constant of the TE_{10}-mode. (b) The normalized resistance and reactance characteristics, as well as the phase with respect to the normalized half-length of the slot.

dielectric losses **[7]**. These design parameters are also applied to the feeding SIW. The width of a radiating SIW was determined to be 3.44 mm for the propagation of the fundamental TE_{10}-mode without any higher order modes and the suppression of the grating lobes, simultaneously.

The slot impedance extraction was conducted by fixing the reference planes of two waveguide ports to the center of a 45°-inclined radiating series slot using the finite-difference time-domain (FDTD) full-wave simulator, CST-Microwave studio **[8]**. As a result, the normalized resistance and reactance of the radiating series slot is obtained from

$$\frac{Z_{\text{slot}}}{Z_0^{rad}} = \frac{1 + S_{11} - S_{21}}{1 - S_{11}} \tag{2.1}$$

where Z_o^{rad} is wave impedance of a given SIW transmission line and the *S*-parameters come from a two-port single slot module **[9]**. Consequently, the normalized impedance is plotted with respect to the variation of the normalized half-length of slot as shown in Fig. 2.2(b). The resonant half-length and the corresponding resistance of the series slot at the design frequency of 35 GHz are 1.34 mm and 4.67· Z_o^{rad}, respectively.

2.2.2 Alternating Reactance Slot Pair

It was found that, the interpolated self-impedance of the resonant slot with a slot width of 0.4 mm has a real high resistance of 4.67·Z_0^{rad}. As a result, it is hard to match the input impedance of a 45°-inclined series slot array antenna to the wave impedance of a given radiating SIW (Z_0^{rad}) without any matching circuits. Therefore, the conventional WG-fed series slot array antenna presented in **[2]** with its impedance matching and bore sight main beam are infeasible with only 45°-inclined resonant radiating slots due to their high input impedances and out-of-phase slot

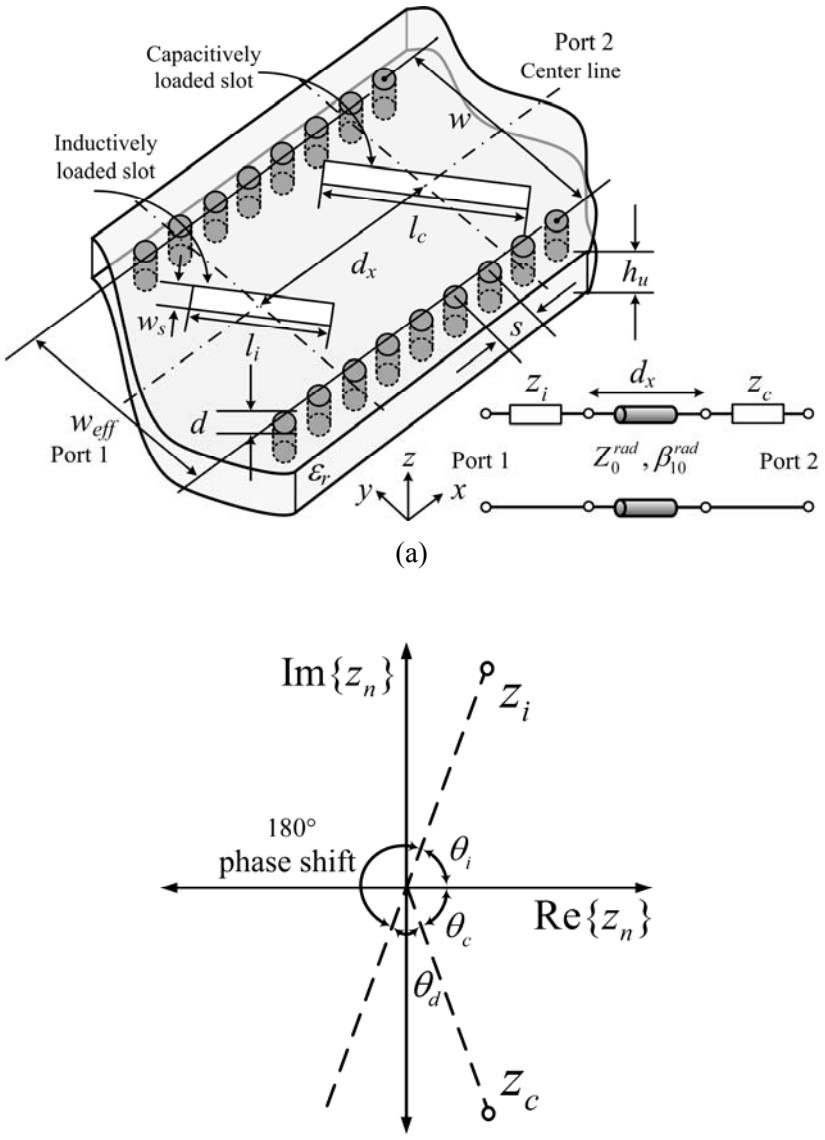

Fig. 2.3 The proposed alternating reactance slot pair etched on the broad wall of a radiating SIW. (a) The structure and its equivalent circuit, where Z_0^{rad} is the wave impedance and β_{10}^{rad} is the propagation constant of the TE_{10} mode. (b) The phase difference (θ_d) between the normalized self-impedances (z_c and z_i) of an alternating reactance slot pair.

mode voltages, respectively.

For that reason, the alternating reactance slot pairs were proposed as depicted in Fig. 2.3(a) comprised of shorter and longer slot lengths rather than resonant one representing inductive and capacitive load impedance, respectively. The currents flowing into these series connected slots have equal amplitude and out-of-phase due to the spacing of the one-half guided wavelength transmission line at the operating frequency as shown in Fig. 2.3(a). Therefore, the mode voltages can be calculated with just the self-impedances of an alternating reactance slot pair as shown in Fig. 2.3(b). The inductive and capacitive self-impedances denoted by z_i and z_c that are normalized to the wave impedance of a given radiating SIW can be plotted in the complex plane with respect to the amplitude and phase. The phase of these inductive and capacitive self-impedances are then given by

$$\theta_n = \tan^{-1}\frac{\mathrm{Im}\{z_n\}}{\mathrm{Re}\{z_n\}}, n = i \; and \; c \tag{2.2}$$

Besides, the phase difference of the alternating reactance slot pair separated by a half guided wavelength can also be obtained by

$$\theta_d = 180° - \theta_i - \left|\theta_c\right| \tag{2.3}$$

The normalized self-impedances of an alternating reactance slot pair were chosen as 0.123+j0.7269 and 0.1253−j0.7523, respectively, based on the linearly interpolated slot impedance data. The phase difference of the mode voltages between these slots can be calculated using (2.2) and (2.3) with 19.07°. As a result, almost in-phase electric fields can be induced in the narrow width of each radiating slot. Moreover, the amplitudes of mode voltages are also nearly the same because of the symmetric impedance property of a single series slot module. In this calculation, the mutual coupling effects were not considered.

2.2.3 Equivalent Circuit Analysis using Recursive Formulas

As shown in Fig. 2.4, the proposed linear slot array antenna has a periodic arrangement of alternating reactance slot pairs and it is fed by a series-to-series coupling slot at the center of a radiating SIW. Furthermore, the series connected radiating slots are terminated by short-circuited SIW stubs with a half guided wavelength from the last radiating slot #1 and #16, and represent the standing-wave (or resonant) excitation due to the equal radiating slot spacing (d_x). The surface current density patterns on the top metal plate of the radiating SIW containing the 45°-inclined series slots are depicted in Fig. 2.4. Although the 45°-inclined series slots generally cut the surface currents, the directions of the currents for the

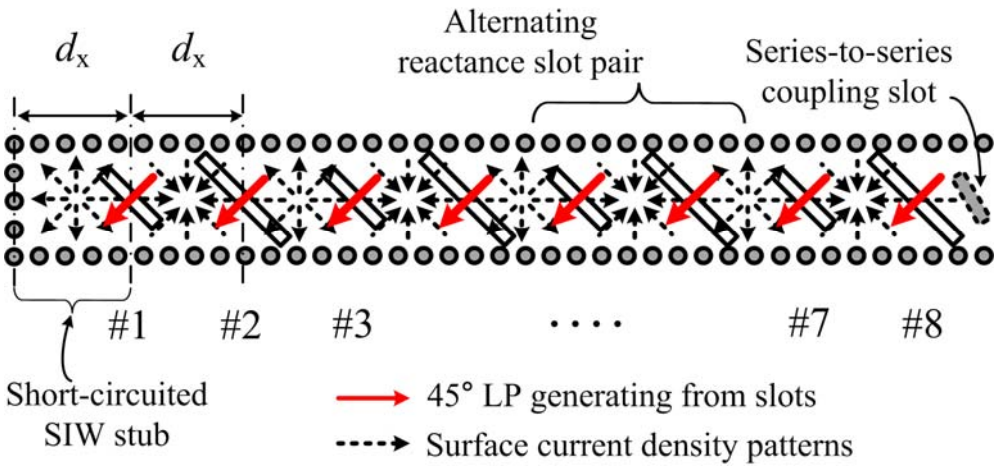

Fig. 2.4 The left section of a linear slot array antenna (Fig. 2.1(a)) with the surface current density patterns and 45º-inclined electric fields on radiating slots.

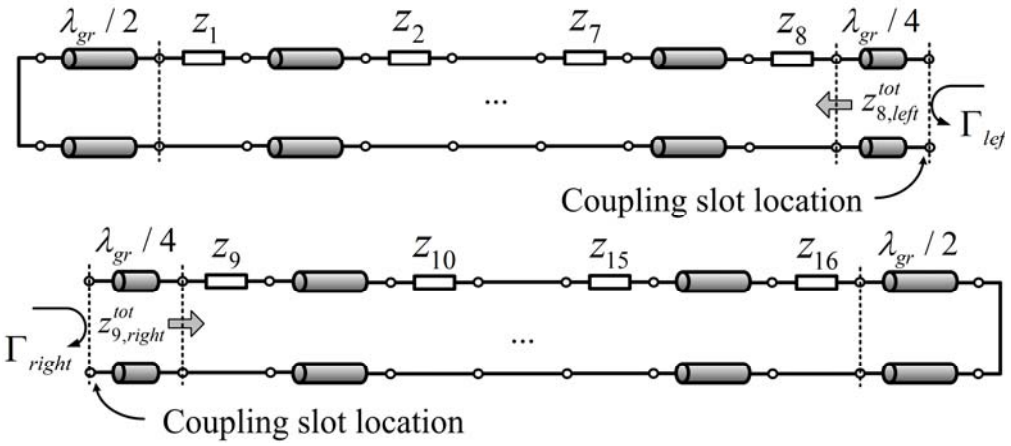

Fig. 2.5 The equivalent circuit of a linear slot array antenna referenced to a coupling slot location.

inductively and capacitively loaded slots are opposite to each other. Therefore, the alternating reactance slot pair has an out-of-phase current distribution. Nevertheless, the in-phase 45°-inclined electric fields can be induced due to the alternating reactance components. It was observed that the alternating reactance slot pairs act as slot offsets and alternating tilt angles of shunt and series slot array antennas, respectively, for in-phase electric field radiation **[1], [2]**.

The proposed linear slot array antenna can be presented by the equivalent circuit with a transmission line network referenced to the coupling slot location as shown in Fig. 2.5. The series connected impedances (z_n) stand for the self-impedances of the 45°-inclined series slot modules, which are normalized to the wave impedance of the radiating SIW. The normalized input impedance as seen from slot #8 and #9 toward the left and right sides of a radiating SIW are obtained from the following recursive impedance formulas, respectively **[11]**.

$$\begin{aligned} z_{n,left}^{tot} &= z_n + \frac{z_{n-1}^{tot} + j\tan(\beta_{10}^{rad} d_x)}{1 + jz_{n-1}^{tot}\tan(\beta_{10}^{rad} d_x)}, n = 2,\ 3,...,\ 8 \\ z_{n,right}^{tot} &= z_n + \frac{z_{n+1}^{tot} + j\tan(\beta_{10}^{rad} d_x)}{1 + jz_{n+1}^{tot}\tan(\beta_{10}^{rad} d_x)}, n = 15,\ 14,...,\ 9 \end{aligned} \tag{2.4}$$

where

$$z_m^{tot} = z_m + j\tan(\beta_{10}^{rad} d_x),\ m = 1, 16 \quad . \tag{2.5}$$

The reflection coefficients as seen from slot #8 and #9 toward both ends can be obtained by

$$\begin{aligned} \Gamma_{8,left} &= \frac{z_{8,left}^{tot} - 1}{z_{8,left}^{tot} + 1} \\ \Gamma_{9,right} &= \frac{z_{9,rightt}^{tot} - 1}{z_{9,right}^{tot} + 1}. \end{aligned} \tag{2.6}$$

Meanwhile, the reflection coefficients to the coupling slot location can be calculated with (2.6) and transformed by the $\lambda_{gr}/4$ length of the transmission line (in Fig. 2.5) as follows:

$$\begin{aligned} \Gamma_{left} &= \Gamma_{8,left} \cdot e^{-j2(\beta_{10}^{rad} \cdot \lambda_{gr}/4)} \\ \Gamma_{right} &= \Gamma_{9,right} \cdot e^{-j2(\beta_{10}^{rad} \cdot \lambda_{gr}/4)} \end{aligned} \tag{2.7}$$

where λ_{gr} is a guided wavelength of a radiating SIW.

2.2.4 Centered-Inclined Series-to-Series Coupling Slot

The input power injected from the wideband coax-to-SIW transition is coupled

to the radiating SIW through the series-to-series coupling slots that are etched on both the lower and upper copper plates of the radiating and feeding SIWs, respectively. The design parameters of the centered-inclined coupling slot, such as the tilt angle (p) and the length (l_s) can be determined under the resonant condition of 35 GHz in order to satisfy the impedance matching and phase distribution requirements **[10]**.

A radiating SIW is transformed to series impedance that is connected to the feeding SIW by the series-to-series coupling slot **[11]**. As a result, the total input impedance of the proposed series slot array antenna is

$$z^{tot} = z^{Rad.WG} + j\tan(\beta_{10} g_m) \tag{2.8}$$

where $z^{Rad.WG}$ is the transformed series impedance of the radiating SIW and g_m is the distance from coupling slot to shorting wall and set to the one-half guided wavelength of the feeding SIW at the operating frequency. The optimized values for the coupling slot are obtained from a full-wave simulation with $p = 20°$ and $l_s = 2.27$ mm, as shown in TABLE 2.1.

TABLE 2.1

OPTIMIZED VALUES FOR THE DESIGN PARAMETERS OF THE PROPOSED ANTENNA

SIW single module	d	s	w_s		
Value	0.4	0.7	3.44		
Radiating SIW	d_b	l_c	l_i	g_b	w_b
Value	3.4	3.6116	2.3842	3.4	10
Feeding SIW	g_m	l_s	p		
Value	2.3842	2.27	20		
Antenna dimension	L	W	h_b	h_l	h_u
Value	60.6	17	0.11	0.75	1.52

(Units: mm; degree for parameter 'p' only)

2.3 Simulation and Measurement

Initially, the lengths of the alternating reactance slot pair are set to 2.3842 mm (l_i) and 3.6116 mm (l_c) as inductive and capacitive loads. The corresponding normalized self impedances can be obtained from the results of Fig. 2.2(b) and are 0.123+j0.7269 and 0.1253−j0.7523, respectively. Because all radiating slots have almost equal impedance magnitudes, it is expected that uniform field distributions can be easily obtained. The total impedance of a radiating SIW looking into the series-to-series coupling slot and the line current of the series connected equivalent circuit are calculated based on recursive formulas (2.4) and (2.5). As a result, the induced slot voltages of each radiating slots are calculated. Notice that the external

TABLE 2.2

SIMULATED AND CALCULATED RESULTS FOR THE NORMALIZED ELECTRIC FIELD OF THE RADIATING SLOTS

	Magnitude		*Phase*	
	Max.	Min.	Max.	Min.
EM result	1	0.957	0	-18.65°
Calculated result	1	0.964	0	-19.07°
Error (%)	0.73		2.25	

mutual coupling effects are not taken into consideration in this case.

For verification, the results of the full-wave simulation are compared with the equivalent circuit calculation with respect to the magnitude and phase of the electric fields generated by each radiating slots, as presented in Fig. 2.6. Specifically, the electric field distribution along the center line and 1 mm above the radiating SIW broad wall was checked. The magnitude (min/max) and the phase (max–min) ratio of the EM-obtained electric field are 0.957 and 18.65°, respectively (TABLE 2.2). Also, the transverse (*y*-axis) and longitudinal (*x*-axis) field components show symmetrical and identical patterns. Moreover, the calculated results using equivalent circuit analysis are well matched to the EM data, with an observed error range of 2.25% (TABLE 2.2).

The simulated and experimental results of reflection coefficient are presented

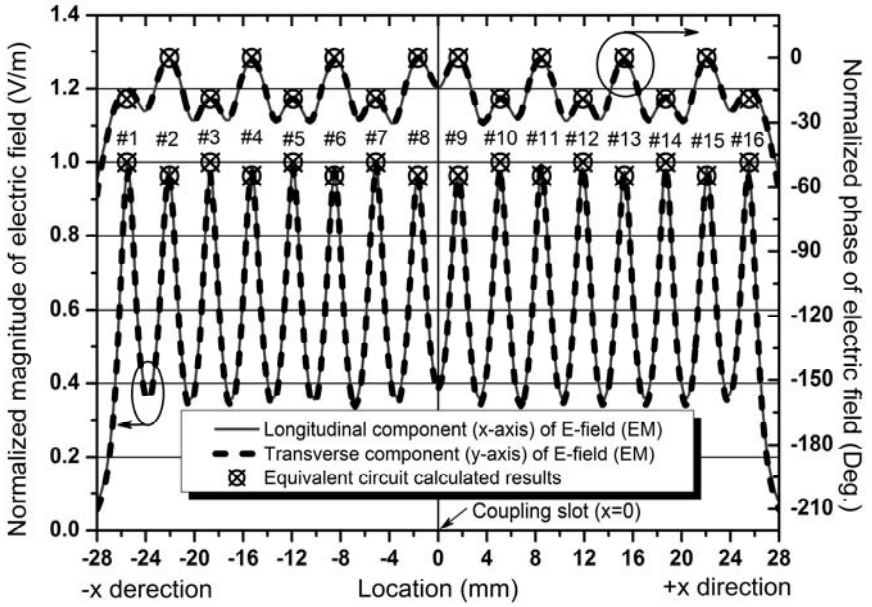

Fig. 2.6 Simulated and calculated results of magnitude and phase of uniformly excited electric field generated by 16 series radiating slots.

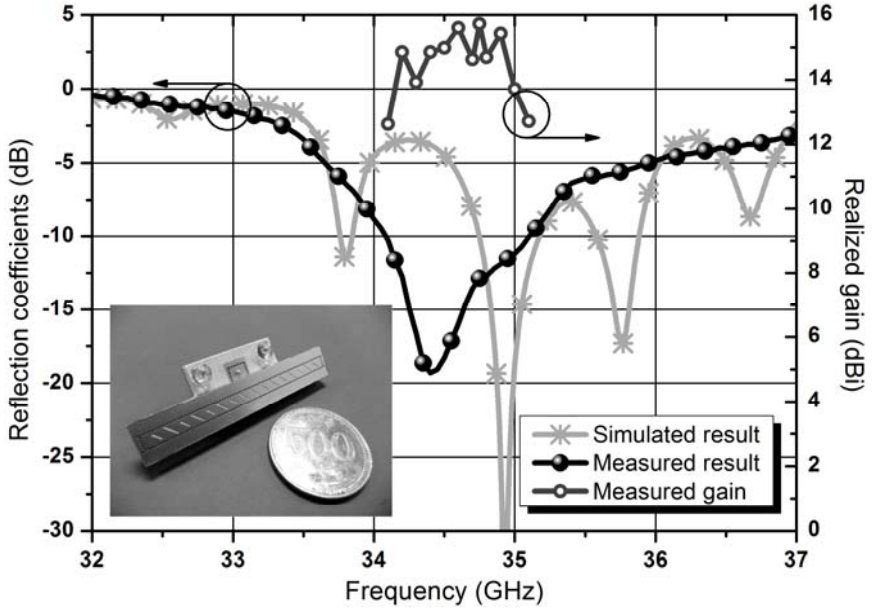

Fig. 2.7 Reflection coefficients and realized gain results. Inset shows a photograph of a fabricated antenna; Antenna size is 60.6 (L) × 17 (W) mm.

along with a photograph of a fabricated antenna in Fig. 2.7. The reflection coefficient is measured with a bandwidth of 2.7% (i.e. 34.07 ~ 35.1 GHz) under the criterion of a result of less than −10 dB. Theoretically, the discrepancy between the simulated and experimental results is due to the distorted self impedances of the radiating slots and the coupling slot, assumed to be the result of inaccurate fabrication of the components. In addition, the radiation patterns were tested in an anechoic chamber for the *zx*- and *yz*-planes as depicted in Fig. 2.8(a) and (b), respectively. The results were found to be in good agreement with the simulation. The measured realized gain of 15.64 dBi matches well with the simulated result of 15.3 dBi. The measured radiation efficiency is about 72.4 %. Moreover, the obtained side-lobe levels (SLL), half-power beam width (HPBW), and the ratio between co- and cross-polarizations at the bore-sight are 15.66 dB, 8.11°, and 13.81 dB, respectively. The electrical performance of the proposed antenna is summarized in TABLE 2.3.

2.4 Summary

In this Section, a SIW 45°-inclined series slot array antenna operating at Ka band was described. The design features were verified using calculated, simulated, and experimental results. The entire antenna can be easily fabricated by using a double-layered structure consisting of radiating and feeding SIWs. In addition,

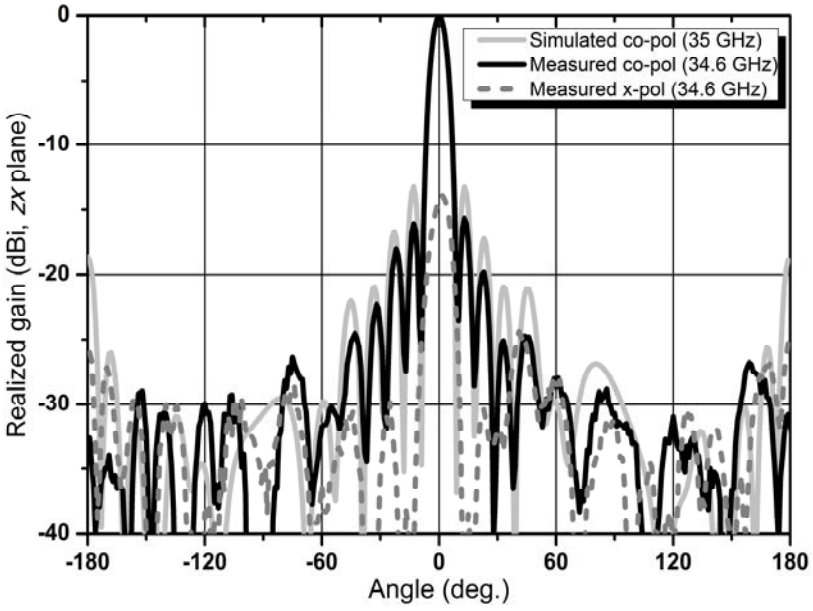

(a)

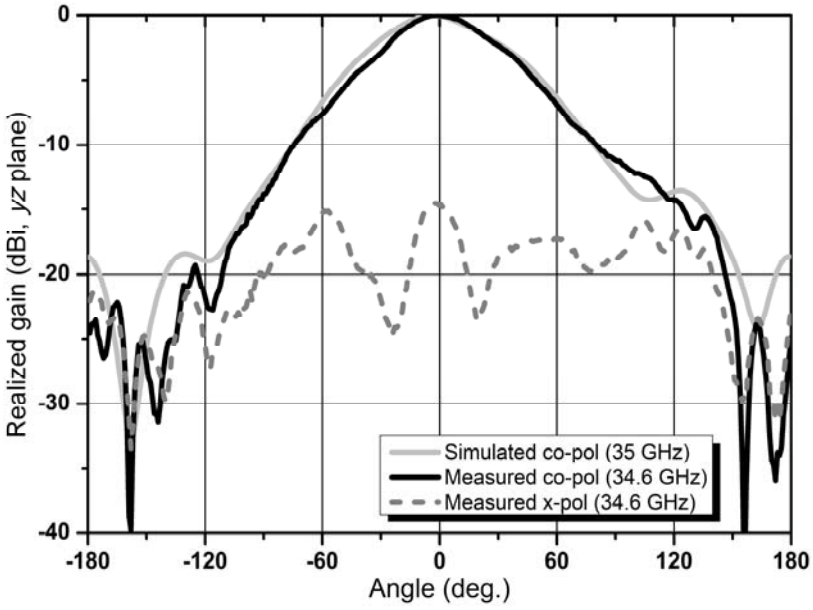

(b)

Fig. 2.8 Simulated and measured radiation patterns. (a) *zx*-plane and (b) *yz*-plane.

TABLE 2.3

MEASURED ELECTRICAL PERFORMANCE OF THE PROPOSED ANTENNA

	Bandwidth	*At 34.6 GHz*			
	(<−10 dB)	Gain	SLL	HPBW	XPD
Values	1.03 GHz (2.7%)	15.64 dBi	15.66 dB	8.11°	13.81 dB

impedance matching and uniform excitation were simultaneously and easily accomplished through the use of arrays that were formed by alternating reactance slot pairs. By using alternating reactance slot pairs, the slot spacing is one-half guided wavelength at the design frequency, resulting in the elimination of grating lobes in the longitudinal direction. We expect that the proposed antenna can be widely applied to 45°-inclined LP radiating systems in the millimeter-wavelength range.

Reference

[1] R. S. Elliott, “An improved design procedure for small arrays of shunt slots,” *IEEE Trans. Antennas Propag*., vol. AP-31, pp. 48–53, Jan. 1983.

[2] M. Orefice and R. S. Elliott, “Design of waveguide-fed series slot arrays,” *IEE Proc*., vol. 129, pp. 165–169, Aug. 1982, Dt. H.

[3] J. Hirokawa, and M. Ando, “45° linearly polarized post-wall waveguide-fed parallel-plate slot arrays,” *IEE Proc.-Microw. Antennas Propag.*, vol. 147, no. 6, pp. 515–519, Dec. 2000.

[4] S. Park, Y. Okajima, J. Hirokawa, and M. Ando, “A slotted post-wall waveguide array with interdigital structure for 45° linear and dual polarization,” *IEEE Trans. Antennas Propag.*, vol. 53, no. 9, pp. 2865–2871, 2005.

[5] A. Mizutani, K. Sakakibara, N. Kikuma, and H. Hirayama, “Grating lobe suppression of narrow-wall slotted hollow waveguide millimeter-wave planar antenna for arbitrarily linear polarization,” *IEEE Trans. Antennas Propag.*, vol. 55, no. 2, pp. 313–320, Feb. 2007.

[6] Z. Chen, W. Hong, Z. Kuai, H. Tang, and J. Chen, “45° linearly polarized resonant slot array antenna based on substrate integrated waveguide,” in

Proceedings of Asia-Pacific Microw. Conf. Dec. 2007.

[7] M. Bozzi, M. Pasian, L. Perregrini, and K. Wu, "On the losses in substrate integrated waveguides," in *37th European Microw. Conf.*, Munich, Germany, Oct. 8-12, 2007.

[8] CST Microwave Studio (MWS) 2010, CST Corporation. Available: http://www.cst.com

[9] D. M. Pozar, *Microwave Engineering*, 2nd ed. New York: Wiley, 1998, ch. 4.

[10] S. R. Rengarajan, "Analysis of a centered-inclined waveguide slot coupler," *IEEE Trans. Microwave Theory Tech.*, vol. 37, no. 5, May 1989.

[11] J. C. Coetzee, J. Joubert, and D. A. McNamara, "Off-center-frequency analysis of a complete planar slotted-waveguide array consisting of subarray," *IEEE Trans. Antennas Propag.*, vol. 48, no. 11, Nov. 2000.

Chapter 3

Planar Slot Array Antenna for 45°-Inclined Linear Polarization

3.1 Introduction

WG-fed slot array antennas are widely used for many millimeter-wave communication systems due to their electrical and physical advantages such as high gain, efficiency, and low-profile. Especially in many radar systems like collision avoidance automotive radar, monopulse radar, and synthesis aperture radar (SAR), the WG-fed slot array antennas are promising candidates for accurate beam forming as well as low side lobe levels (SLLs). Furthermore, these antennas can be used for high-speed wireless communication and direct broadcast satellite (DBS) systems requiring specific linear or circular polarization (LP or CP) **[1]**, **[2]**.

Over the past few decades, conventional WG-fed shunt slot array antennas have been designed with well-established design equations, which take into consideration both internal and external coupling effects **[3]**. The series slot array antennas also have been investigated and analyzed by Orefice and Elliott oriented parallel to the shunt slot array design procedure **[4]**. Both the shunt and series slot array elements are cut on the upper rectangular waveguide (RWG) broad wall with a slot spacing of one-half guided wavelength at the operating frequency. In order to generate in-phase electric field distributions on every radiating slot, alternating offsets and tilt angles should be adopted for WG-fed shunt and series slot array antennas, respectively.

Meanwhile, in some specific radar applications such as collision avoidance automotive radar systems, a 45°-inclined LP is required to alleviate the interference coming from the opposite direction. It is difficult to generate an arbitrary polarization using fundamental shunt and series WG-fed slot array antennas, which generate only the vertical or horizontal LP. Furthermore, the element spacing of a guided wavelength is inevitable for the in-phase electric field distribution of 45°-inclined series slot array elements, which consist of the resonant slot length only **[4]**. As a result, the grating lobes can easily occur in the longitudinal direction of the radiating lines and the radiation efficiency will be decreased. Besides, as the tilt angle of a centered-inclined series slot increases, the corresponding self-impedance also increases, and eventually, the maximum self-resistance appears when the tilt

angle reaches 45° **[5]**. In other words, the number of series connected slot elements for an arbitrary LP should be restricted for impedance matching to the input wave impedance of a given air-filled WG.

Various slot array antennas have been proposed for the 45°-inclined LP with different operating mechanisms for the traveling-wave excitation **[6-8]**. The post-wall WG-fed parallel plate slot array antenna was designed with two reflection-cancelling slots and a main radiating slot to generate a 45°-inclined LP **[6]**. In addition, to minimize the reflection, which can occur from the radiating elements, reflection-cancelling inductive posts located on each radiating slot with the proper spacing were introduced **[7]**. In addition, the traveling-wave-fed slot array antenna that has open-ended circular cavities surrounding each series of slots etched on the narrow wall of the radiating WGs is presented in **[8]**. The posts under every radiating slot contribute to the coupling amount to the air boundary by means of their location and height. Nevertheless, these traveling-wave-fed slot array antennas, which adopt the end-fed structure, are susceptible to beam tilting for frequency variation as well as asymmetric radiation patterns.

This Chapter III presents a new design method and analyzes with equivalent circuit models the standing-wave-fed series slot array antenna generating a 45°-inclined LP. We proposed an alternating reactance slot pair for a radiating unit that

has both an inductive and a capacitive reactance with relative low resistance to design the element arrangement with one-half guided wavelength slot spacing. Furthermore, the proposed antenna was realized through substrate integrated waveguide (SIW) technology with low costs and lightweight features. In Chapter 3.2, the proposed antenna configuration will be described. In addition, the detailed design method for the SIW transmission line, alternating reactance slot pair, and grating lobe suppression will follow from Chapter 3.3. Furthermore, equivalent circuit analysis was done for a linear and planar slot array antenna as well as the dual-resonant coax-to-SIW transition. Finally, in Chapter 3.6, the electrical performance of the proposed antenna will be presented with full-wave simulation and experimental results to verify the validity of the design method.

3.3 Proposed Antenna Structure

As described in Fig. 3.1(a), the centered-inclined series slot arrays are etched on the upper broad wall of the radiating SIWs along the center line to generate a 45°-inclined LP **[11]**. Every radiating slot is designed to acquire the bore sight main beam through an in-phase and uniform field distribution. Beam tilting also can be easily avoided by the center-fed method with series-to-series coupling slots as shown in Fig. 3.1(b). These coupling slots are etched on the bottom and top metal plates of the upper and lower PCBs, respectively, and aligned with each other

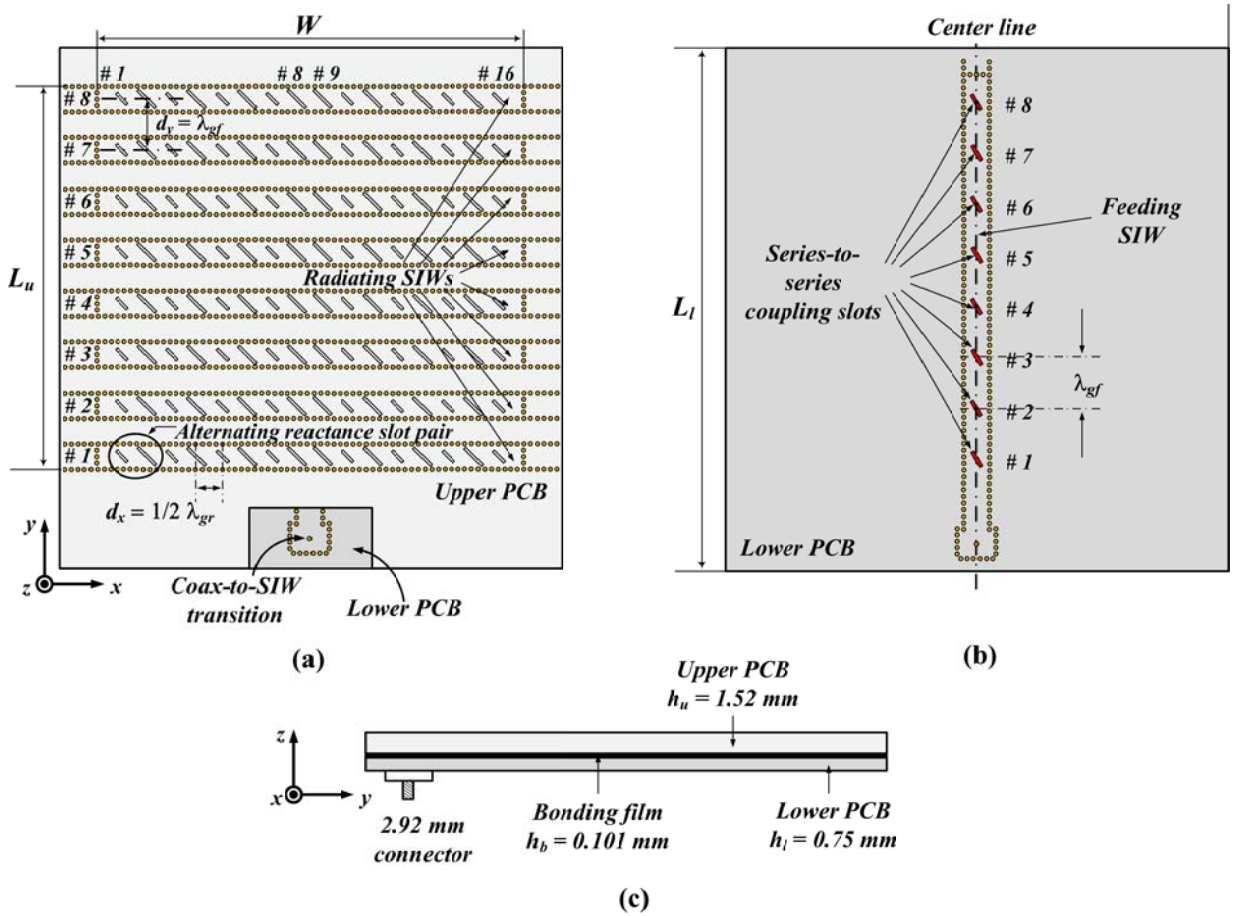

Fig. 3.1 The proposed planar antenna geometry. (a) Top view. (b) The feeding structure that has series-to-series coupling slot arrays. (c) Lateral view.

precisely. Each radiating SIWs have sixteen 45°-inclined radiating elements with the precise spacing of one-half guided wavelength ($d_x = \lambda_{gr}/2$) not to exceed a wavelength (λ_0) in free space. On this occasion, shorter and longer lengths of slots rather than a resonant one are arranged alternatively and periodically. The operating principle of the above alternating reactance slot pairs is clarified in Chapter 2.2.2 in detail. In addition, all series-to-series coupling slots are separated from each other with a guided wavelength ($d_y = \lambda_{rf}$) of a feeding SIW with an equal tilt angle referenced from the center line to provide power with in-phase and equal amplitude.

The proposed antenna was designed with the SIW technology, which can be used in general PCBs with the standard process such as via holes. Radiating and feeding SIWs are inserted in the RO3035^{TM} substrates with a dielectric constant of 3.5, a loss tangent of 0.0018, and a thickness of 1.52 mm (h_u) and 0.75 mm (h_l), respectively, as shown in Fig. 3.1(c) for the lateral view. The upper and lower PCBs were adhered to each other with a RO4450B^{TM} bonding film with a dielectric constant of 3.3, a tangent loss of 0.004, and a thickness (h_b) of 0.101 mm. Furthermore, the selected PCBs had the thinnest metal cladding of 17 μm to minimize undesired phase variation from the thickness of the metal plates.

3.3 Feeding Network Design and Analysis

A coupling slot arrangement was chosen with an equal tilt angle and with the

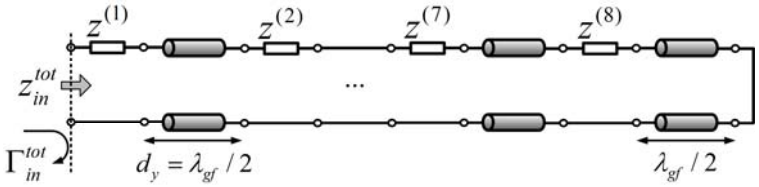

Fig. 3.2 The equivalent circuit of a feeding SIW.

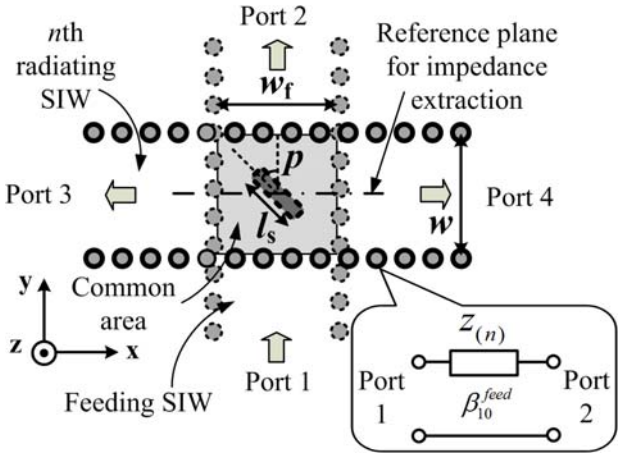

Fig. 3.3 The four-port series-to-series coupling slot junction and an equivalent circuit, where β_{10}^{rad} is the propagation constant of the TE_{10} mode.

spacing of a guided wavelength (λ_{gf}) of a feeding SIW, as shown in Fig. 3.1(b). The distance between each radiating SIWs were set as $d_y = 2 \cdot w$. Therefore, the width (w_f) of a feeding SIW can be set as 3.38 mm to identify the guided wavelength of a feeding SIW with the spacing between the radiating SIWs.

A series-to-series coupling slot plays the role of a transformer, which converts

the total input impedance of the radiating elements obtained from (2.4) to an arbitrary impedance according to the variation in the tilt angle and length of a coupling slot. The proposed planar slot array antenna can be simplified (Fig. 3.2) with a feeding SIW transmission line. The last radiating SIW is terminated with the short-circuited SIW stub of one-half guided wavelength of a feeding SIW and the total normalized input impedance of the planar slot array antenna is

$$
\begin{aligned}
z_{(8)}^{tot} &= z_{(8)} + j\tan(\beta_{10}^{feed} d_y) \\
z_{(n)}^{tot} &= z_{(n)} + \frac{z_{(n+1)}^{tot} + j\tan(\beta_{10}^{feed} d_y)}{1 + jz_{(n+1)}^{tot}\tan(\beta_{10}^{feed} d_y)}, n = 7,\ 6,...,\ 1
\end{aligned}
\tag{3.1}
$$

where β_{10}^{feed} and $z_{(n)}$ are the propagation constant of the TE_{10} mode of a feeding SIW and the transformed normalized series impedance of the n^{th} radiating SIW, respectively. The final total input impedance of a planar slot array antenna is $z_{(1)}^{tot}$.

The transformed impedance of a radiating SIW containing eight alternating reactance slot pairs can be determined by the tilt angle (p) and length (l_s) of the coupling slot as shown in Fig. 3.3. Specifically, the tilt angle and length of the coupling slot control the coupling amount and the phase, respectively. The series-to-series coupling slot can be modeled as an ideal transformer at the resonant frequency; however, it is hard to preserve that model at the off-resonant frequency.

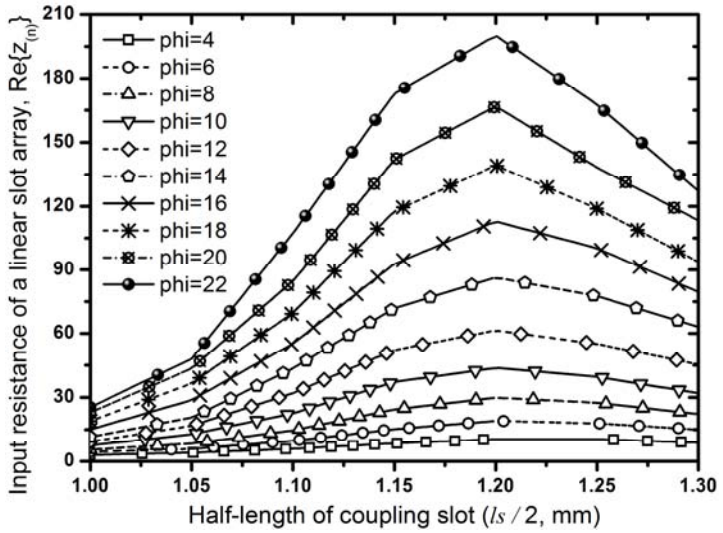

(a)

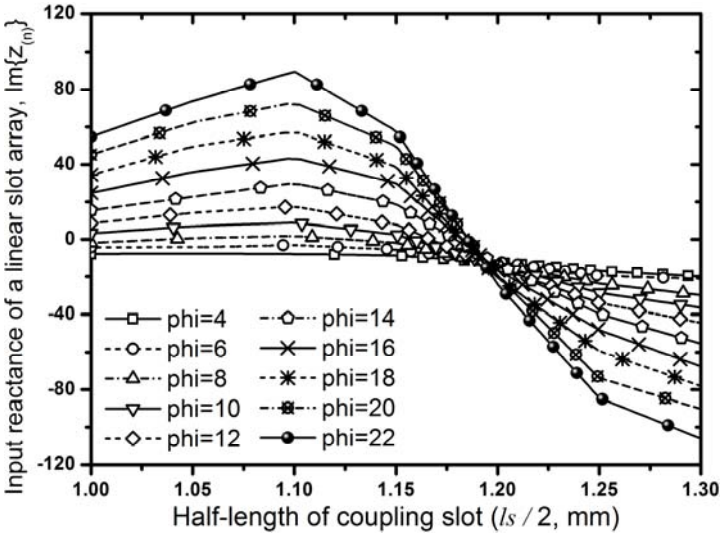

(b)

Fig. 3.4 The input impedance characteristics of a linear slot array as a function of the coupling slot length (l_i) and the tilt angle (p) when the width (w_c) of the coupling slot is 0.5 mm. (a) Input resistance and (b) Input susceptance.

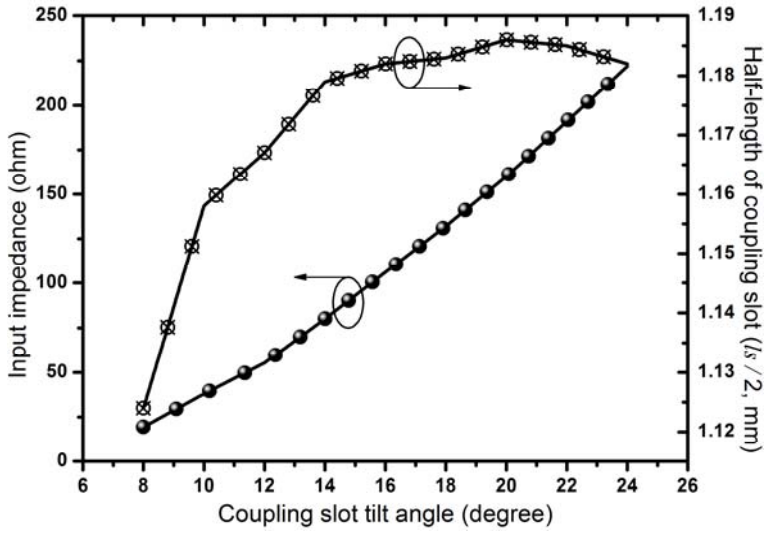

Fig. 3.5 The resonant condition for the series-to-series coupling slot which is terminated with a linear slot array at port 3 and 4.

Therefore, an ideal transformer with a parallel resonator has been suggested to provide the exact model for a wide frequency bandwidth **[13]**. Meanwhile, a more accurate analysis is required for the proposed coupling junction comprised of a SIW structure and the bonding film, which has a finite thickness and a dielectric constant. As shown in Fig. 3.3, the input impedance of a coupling slot was evaluated when port 3 and 4 are terminated by the impedance obtained from equation (2.4), and port 2 is short-circuited at the same time. The reference plane of an input port is located in a feeding SIW just below the center of a series-to-series coupling slot (Fig. 3.3). The input resistance and reactance can be extracted according to the variation in

design parameters with the full-wave simulator, CST MWS based on the finite-difference time-domain (FDTD) algorithm **[14]**. Fig. 3.4(a) and (b) show the results of the transformed input resistance and reactance characteristics according to the variation in the tilt angle and the half-length of a coupling slot within a range from 4° to 22° and from 1 mm to 1.3 mm, respectively. As a result, the resonant condition can be found for a single linear slot array fed by a coupling slot. The input resistance increases with the tilt angle, and pure real input impedances can be found within the range of a half-length for the coupling slot from 1.12 mm to 1.19 mm. Finally, Fig. 3.5 shows the resonant condition as a function of the series-to-series coupling slot parameters with linear interpolation based on the previous results of Fig. 3.4(a) and (b).

The calculated wave impedance (Z_0^{feed}) of a given feeding SIW is 294.4 Ω. The design parameters of a coupling slot such as the tilt angle and half-length can be obtained from the results of Fig. 3.5. For uniform field distribution and impedance matching, the individual normalized impedance of a single radiating SIW series connected in a feeding SIW transmission line can be obtained as Z_0^{feed}/(n) where *n* means the total number of linear slot arrays. Consequently, the tilt angle and half-length of a coupling slot were 9.87° and 1.1557 mm, respectively, for pure real input impedance ($z_{(n)} = Z_0^{feed}/8 = 36.8\ \Omega$) as a single linear slot array antenna. Furthermore, for the efficient design of the planar slot array antenna with low sidelobe levels

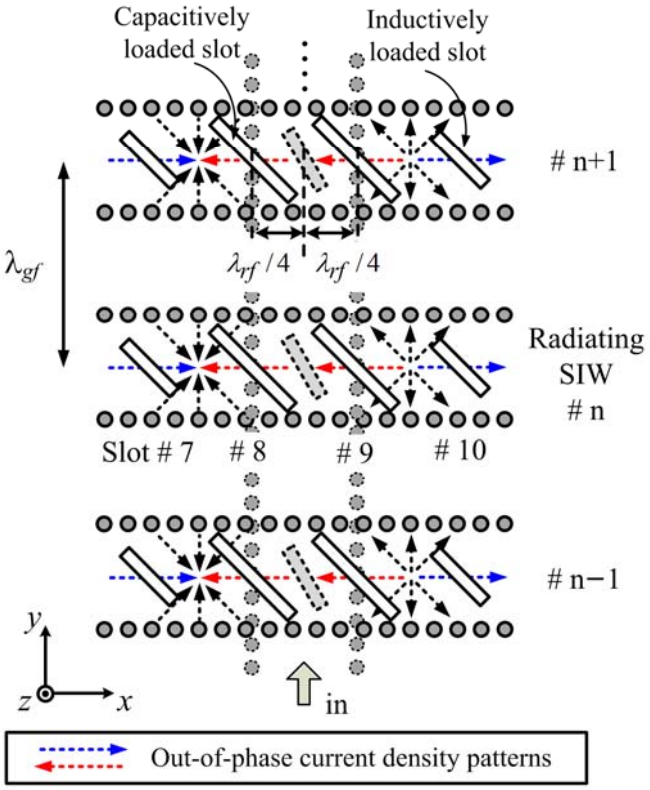

Fig. 3.6 The arrangement of the coupling and radiating slots for in-phase distribution with surface current density patterns.

(SLLs) in *yz*-plane as well as input matching, it is necessary to decide the input impedance of a given linear slot array as a function of the coupling slot tilt angle and half-length.

3.4 Coupling and Radiating Slot Arrangement for In-Phase

Excitation

There are two radiating slots adjacent to the coupling slot and they are separated with one quarter guided wavelength from the coupling slot location as shown in Fig. 3.6. In general, the coupled input signals toward the left ($-x$) and right ($+x$) sides of a radiating SIW are excited with the out-of-phase field distribution from the center of a series-to-series coupling slot. Furthermore, these coupled signals have alternative signs ($\pm x$) due to the opposite direction of the propagation. As a result, the surface current density patterns on the upper metal plates of the radiating SIWs can generate, consequently, two adjacent radiating slots (slot #8 and #9) from a coupling slot and should have an equal length (i.e., inductive or capacitive slot) for the in-phase electric field distribution as depicted in Fig. 3.6. In addition, every coupling and radiating slot can be recursively arranged under the same orientation with the guided wavelength of a feeding SIW.

3.5 Wideband Coax-to-SIW Transition Design and Analysis

The wideband coax-to-SIW transition is advantageous for the feeding network of antennas or circuits for which they are easily affected by the external electromagnetic coupling noises on account of their enclosed structure with the metal plates and via arrays. The coax-to-SIW transitions with an inductive matching via and asymmetric diaphragm have been invented for application to antenna

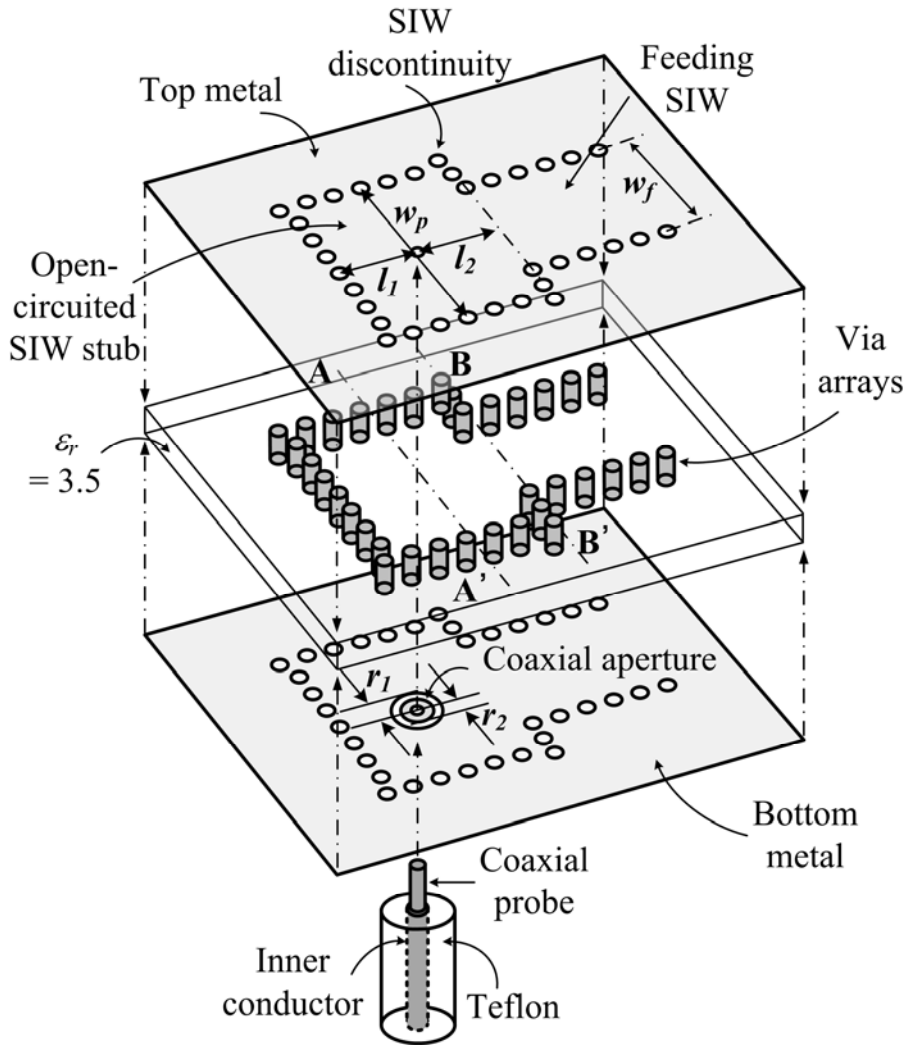

Fig. 3.7 The wideband stepped coax-to-SIW transition structure.

feeding networks **[15]**, **[16]**. In order to overcome the narrow bandwidth, the discontinuous width of the SIW for dual resonance was applied. This structure was

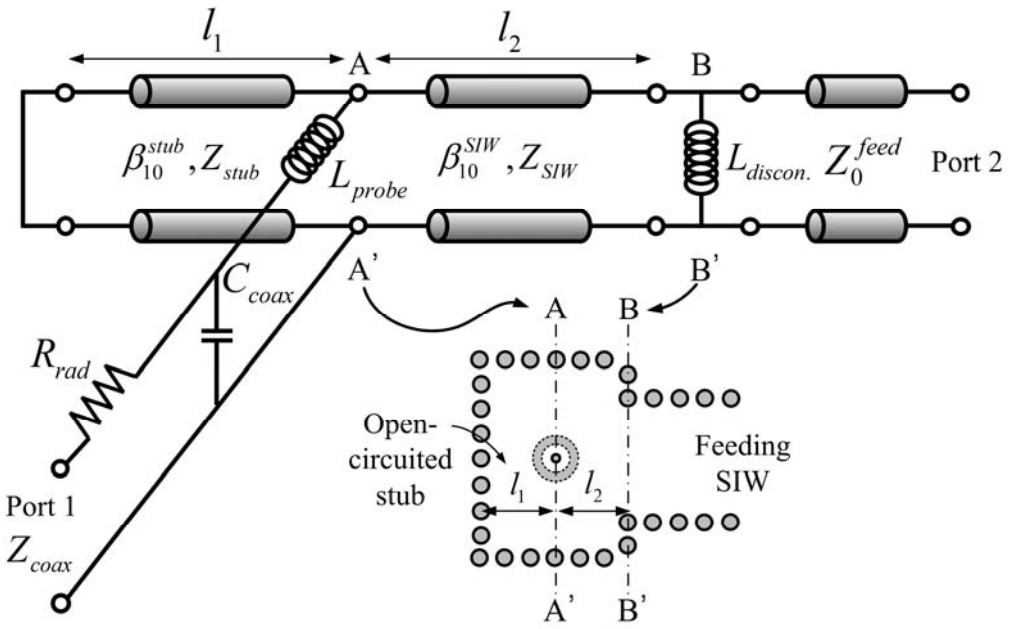

Fig. 3.8 The equivalent circuit model of the proposed wideband stepped coax-to-SIW transition.

previously suggested for the application of a transition between a metallic RWG and a post-wall waveguide **[17]**.

As described in Fig. 3.7, in the bottom metal plate, the pattern of a coaxial aperture is formed with an outer (r_1) and inner (r_2) radius of 0.5 mm and 0.254 mm, respectively, for convenient and flexible matching. The open-ended rectangular cavity has a wider width (w_p) than the width (w_f) of a given feeding SIW. Therefore, a discontinuity is surely formed at the reference plane (BB') as depicted in Fig. 3.7.

In addition, the open-circuited SIW stub consisting of a shorting via wall is located with the length of l_1 from the position of the coaxial probe that is the reference plane, AA'.

The equivalent circuit of the proposed stepped coax-to-SIW transition is illustrated in Fig. 3.8. The coaxial probe can be modeled as the series connected resistance (R_{rad}) and inductance (L_{probe}), which represent the radiation loss to the internal bounded SIW medium and reactive near field of a coaxial probe, respectively **[18]**. The open-circuited SIW stub with the length and width of l_1 and w_p are represented by the transmission line with a wave impedance of Z_{stub} and a propagation constant of β_{10}^{stub}. In addition, the intermediate SIW line section between a coaxial probe (AA') and the discontinuity of the SIW (BB') has a length of l_2 with a wave impedance of Z_{SIW} (= Z_{stub}) as shown in Fig. 3.8. As the last part of the transition, the discontinuity at BB' can be modeled with the shunt inductance, L_{discon}, which can be controlled by the ratio of w_f / w_p **[19]**.

The validity of the proposed equivalent circuit model was confirmed with full-wave and circuit s-parameter simulation results with CST MWS and ADS **[14]**, **[20]**. The dual resonant characteristic that occurred at 28.77 GHz and 37.31 GHz were found to be in good agreement with each other as depicted in Fig. 3.9. It was also found that this dual resonance is independently generated by two sections of the

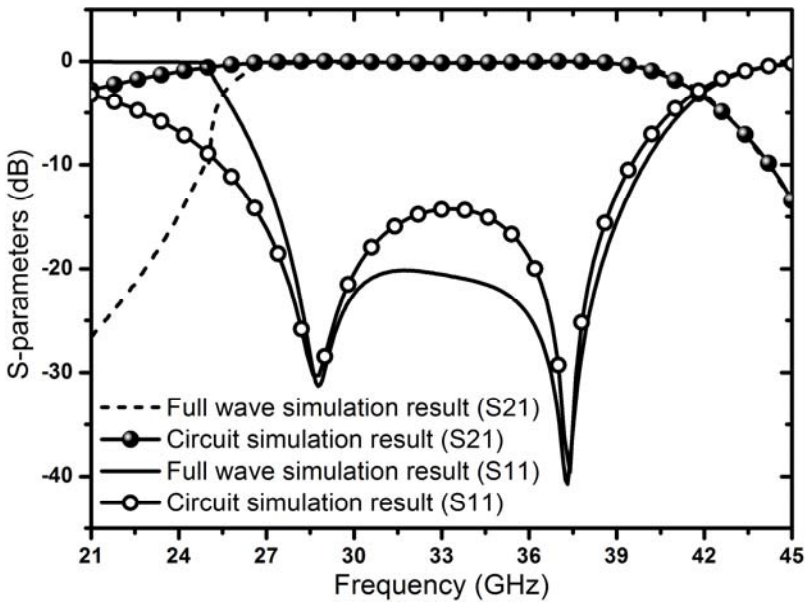

Fig. 3.9 S-parameter results of circuit and full-wave simulations for a single-ended stepped coax-to-SIW transition.

transition. Specifically, the first and second resonant frequencies are controlled by the SIW discontinuity and open-circuited SIW stub, respectively. The electrical performances through the resonant frequency variation for the return loss with respect to the design parameters were verified. Fig. 3.10(a) shows that the first resonant frequency moves toward the lower bands as the width of a feeding SIW increases. This means that the transmission for the lower bands mainly relies on the cut-off frequency decided by the width of a feeding SIW. In addition, the second resonant frequency is dominantly controlled by the length of the open-circuited SIW

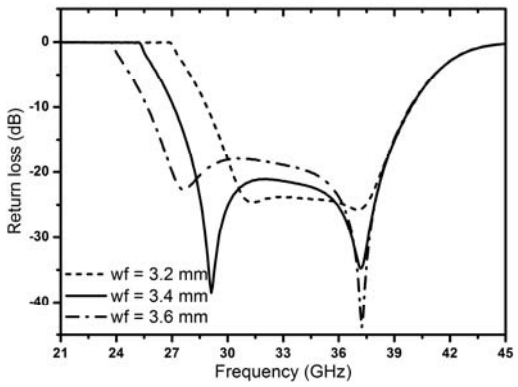

(a)

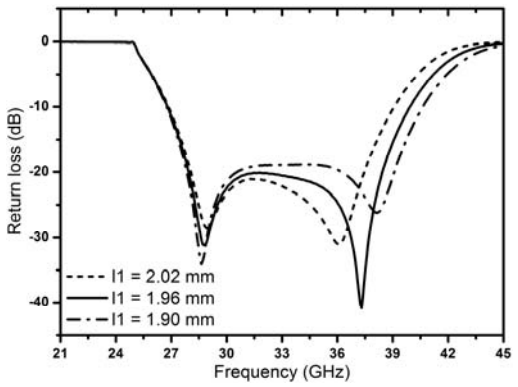

(b)

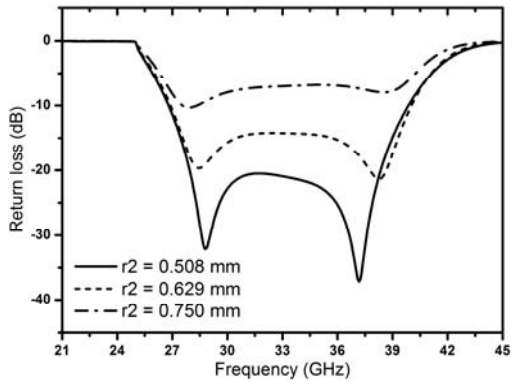

(c)

Fig. 3.10 The return loss variation according to (a) the width of a feeding SIW (w_f), (b) the length of an open-circuited SIW stub (l_1), and (c) the radius of the coaxial aperture radius (r_2).

stub as shown in Fig. 3.10(b). Likewise, the SIW stub can be seen as an open-circuit when the length of a stub is about a one-quarter guided wavelength. Therefore, the lower frequency component can be transferred with minimum reflection as the length of a SIW stub increases. Besides, the overall matching improvement of the transition is feasible with the coaxial aperture design parameter, r_2, as shown in Fig. 3.10(c). Eventually, a wideband transmission characteristic within a shielded structure can be realized. The design parameters and corresponding optimized values of the proposed planar slot array antenna including stepped coax-to-SIW transition are summarized in TABLE 3.1.

3.6 Simulation and Measurement

The electrical performances of the proposed planar slot array antenna designed following the procedures of Chapter 3.3 were analyzed with the results from the full-wave simulation and experimentation.

3.6.1 Uniform Electric Field Distribution

To confirm the uniform electric field distributions on the antenna aperture, the amplitude and phase of the 45°-inclined electric field components were checked just above the aperture plane based on the design values summarized in TABLE 3.1. The field uniformity for the radiating slots arrayed on the radiating SIW #1 was verified as depicted in Fig. 3.11(a). Specifically, the electric field distribution along the

TABLE 3.1

DESIGN PARAMETERS AND OPTIMIZED VALUES

Radiating SIW	*Parameter*	d	d_x	d_y
	Value	0.4	3.34	6.88
	Parameter	h_u	l_c	s
	Value	1.52	3.4	0.7
	Parameter	w	w_s	l_i
	Value	3.44	0.4	2.32
Feeding SIW	*Parameter*	h_l	h_b	l_s
	Value	0.75	0.101	1.1557
	Parameter	p	w_f	w_c
	Value	9.87	3.38	0.5
Coax-to-SIW transition	*Parameter*	l_1	l_2	r_1
	Value	1.96	2.15	0.5
	Parameter	r_2	w_p	
	Value	0.254	5.44	
Total structure	*Parameter*	L_l	L_u	W
	Value	78	51.6	57.4

(Units: mm; degree for parameter 'p' only)

center line and 2 mm above the radiating SIW was verified. The sixteen peak values for the phase and amplitude were in the corresponding radiating slot locations along the x-axis and normalized to their maximum value. The difference between the maximum and minimum values of the phase distribution was 30° when their corresponding locations were –21.7 mm (slot #2) and 5.166 mm (slot #10), respectively. It was larger than that of the calculated result (19.07°) from Chapter

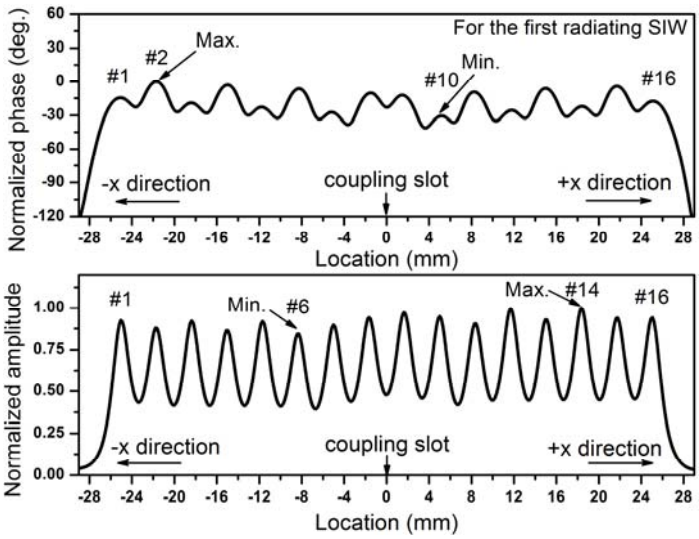

(a)

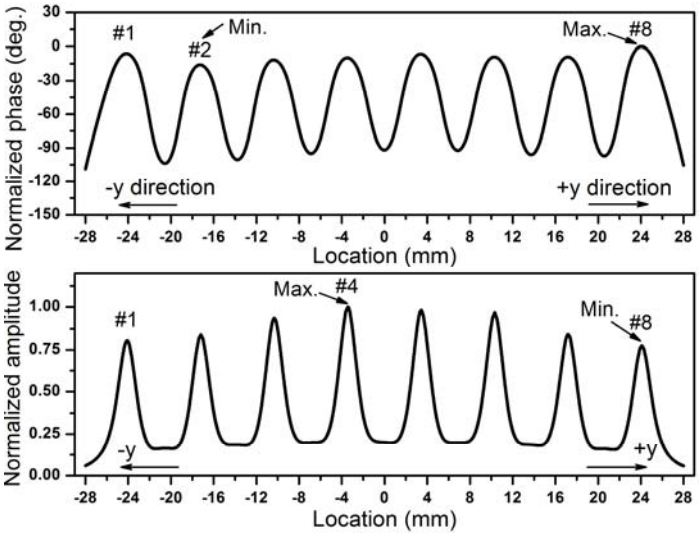

(b)

Fig. 3.11 The near aperture field distribution with respect to the phase and amplitude (a) for the radiating SIW #1 and (b) for 9th radiating elements (slot #9) of every radiating SIW.

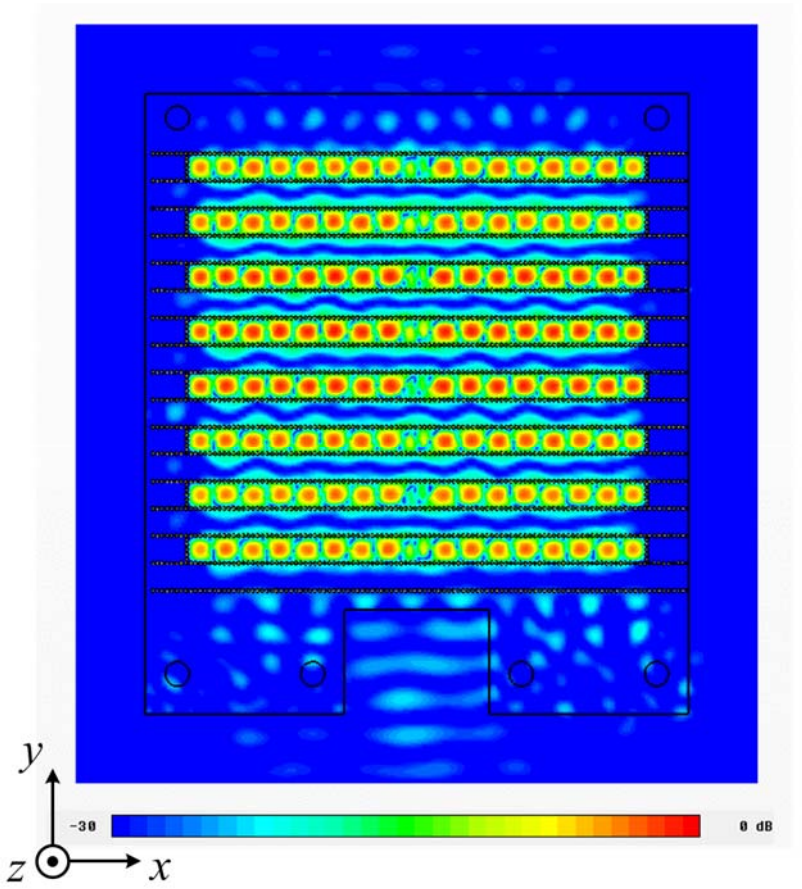

Fig. 3.12 The simulated aperture distribution with respect to the electric field amplitude.

2.2.2. It is conjectured that the self-impedances turn into active-impedances due to the mutual coupling affected by the adjacent radiating slots, as proved in preceding researches **[3]**, **[4]** for shunt slot array antennas. In addition, the uniformity of the normalized amplitude was obtained from the ratio (Min. / Max.) of 0.843 (–1.48 dB)

when their maximum and minimum fields were generated by slot #14 and slot #6, respectively. Moreover, the uniformity for the *yz* cutting plane was also evaluated (Fig. 3.11(b)). There were eight peak values, which originated from every 9^{th} radiating element for each radiating SIW. The phase difference and amplitude uniformity were 15.86° and 0.775 (–2.21 dB), respectively. Even though every radiating SIW had identical design values for the alternating reactance slot pairs and series-to-series coupling slots, there were asymmetric properties for the phase and amplitude. Nevertheless, the acceptable uniform aperture field distribution was realized and verified with the full-wave simulation result (Fig. 3.12).

3.6.2 Back-to-Back Coax-to-SIW Transition

The back-to-back transition was designed and fabricated as shown in Fig. 3.13. The Teflon and inner conductor were inserted into the hole of a metal housing and connected with a 2.92 mm connector. The fabricated PCB patterns were firmly adhered with a metal housing using plastic screws and shared a common ground without any air gaps between them. The experiment was done with an E8361A network analyzer from Agilent. The *S*-parameter results showed wide band-pass characteristics for the Ka-band (Fig. 3.14). The simulated bandwidth was 33.4% ranging from 27.347 to 38.314 GHz under the criteria of VSWR 1.5:1 whereas the measured bandwidth was 30.13% ranging from 27.8 to 37.66 GHz. In addition, the measured insertion loss of the back-to-back transition was less than 1 dB within the

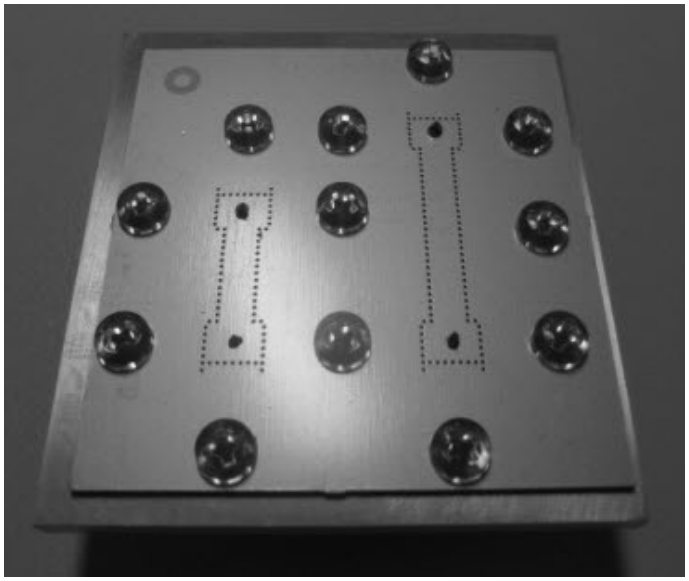

Fig. 3.13 The fabricated back-to-back stepped coax-to-SIW transition.

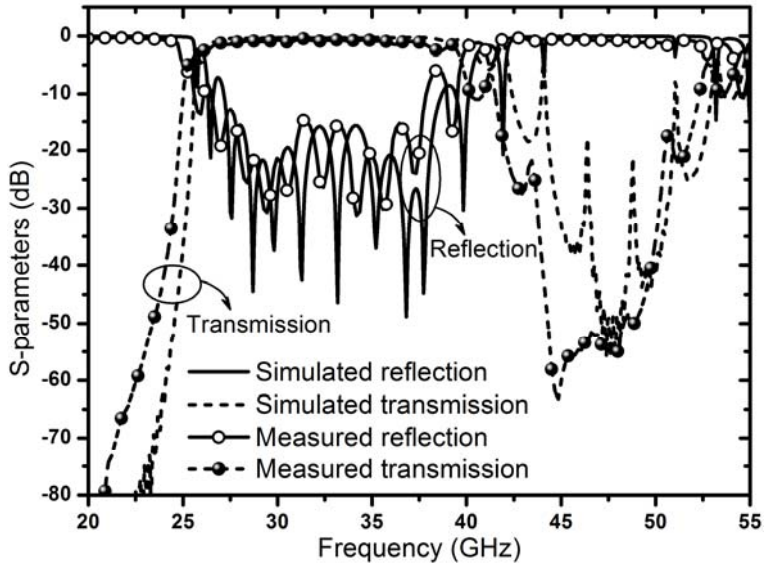

Fig. 3.14 The simulated and measured s-parameter results of the proposed coax-to-SIW transition.

pass-band frequency range.

3.6.3 Reflection Coefficient, Gain, and Radiation Patterns

The proposed series slot array antenna was fabricated and set up for experiments to investigate the reflection coefficient, gain, and radiation patterns. A wideband transition imbedded planar slot array antenna was combined with metal housing to use a 50 Ω input port. The bottom metal plate of a feeding SIW shared a common ground with the metal housing (Fig. 3.15) for improved stability of electrical performance. The simulated and measured impedance bandwidths were from 34.46 to 35.34 GHz (2.52%) and from 33.86 to 34.85 GHz (2.88%) under the condition of less than VSWR 2:1, respectively. The center frequency shift was about 1.7% between the simulation and the measurement as described in Fig. 3.16 due to the etching error, which contributes to the variations in the self-impedances of the radiating slots.

The realized gain and radiation patterns for a 45°-inclined LP were proven in an anechoic chamber. The simulated and experimental maximum gains were 25.8 and 24.3 dBi at 35 and 34.8 GHz, respectively. Likewise, the aperture efficiency was 53.7% from a given aperture area of 57.4 × 51.6 mm and measured gain. The radiation patterns in *zx* and *yz* planes are depicted in Fig. 3.17. The simulated and experimental results were well matched each other. The simulated SLLs for each

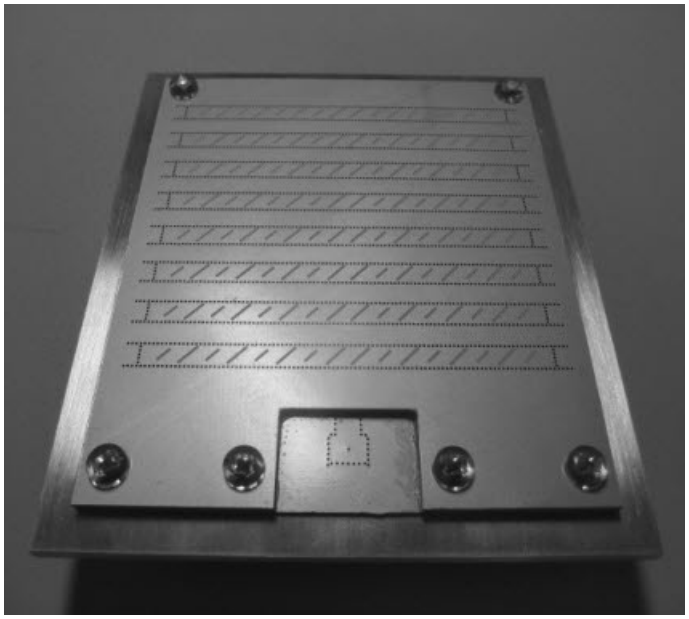

Fig. 3.15 The fabricated slot array antenna for 45º-inclined LP.

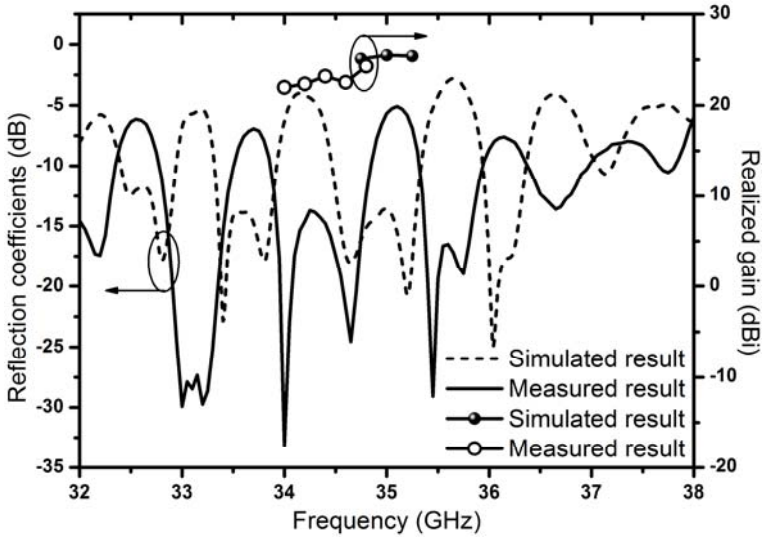

Fig. 3.16 The simulated and measured reflection coefficients and realized gain.

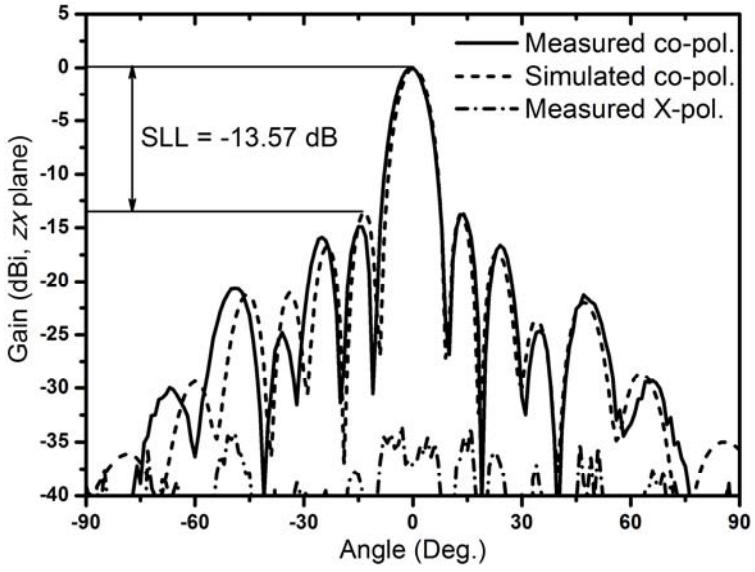

(a)

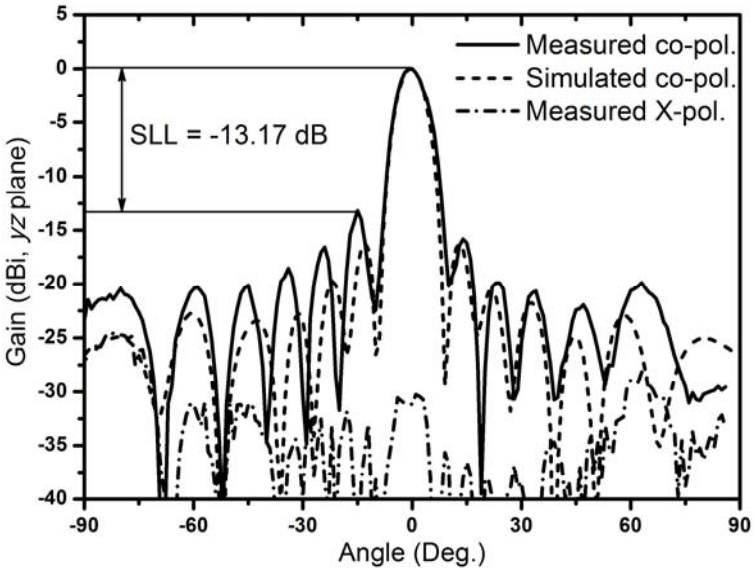

(b)

Fig. 3.17 Radiation patterns for (a) *zx* plane and (b) *yz* plane, respectively.

TABLE 3.2

MEASURED ELECTRICAL PERFORMANCES

Bandwidth	*HPBW*		*Gain*
	zx	*yz*	
2.88%	8.2°	7.9°	24.3 dBi
XPD	*SLL*		*Aperture efficiency*
	zx	*yz*	
–30.26 dB	–13.57 dB	–13.17 dB	53.7%

cutting planes were –13.6 and –16.2 dB and the measured values were –13.57 and –13.17 dB, respectively. It was verified that a uniform field distribution was realized based on the measured SLLs despite their slight increase of about 3 dB. It was revealed that the proposed slot array antenna radiates purely 45°-inclined LP because the measured cross polarization discrimination (XPD) was less than –30 dB for all cutting planes. The measured electric performances of the proposed antenna as well as the half power beam width (HPBW) for each cutting plane are presented in TABLE 3.2.

3.7 Summary

A standing-wave-fed series slot array was proposed for a 45°-inclined LP in the Ka-band. All radiating and feeding lines were integrated in a multi-layered PCB with the SIW technique. Alternating reactance slot pairs with non-resonant slot

lengths and equal slot spacing were adopted to implement impedance matching and uniform field distribution as well as side lobe suppression. The equivalent circuit models with the transmission line were presented and analyzed for the antenna components such as the linear slot array and total planar slot array antenna. Furthermore, the wideband stepped coax-to-SIW transition was also evaluated by an equivalent circuit model and verified from the circuit and full-wave simulation results. It was confirmed that the imbedded and enclosed transition helps the proposed antenna to radiate stable 45°-inclined LP without any distortion. The proposed antenna showed highly efficient electrical performances such as aperture efficiency and realized gain of 53.7 % and 24.3 dBi, respectively, at 34.8 GHz with a XPD level of less than –30 dB. Furthermore, the measured SLLs for each cutting plane with –13.57 dB and –13.17 dB confirmed the uniform aperture field distribution. As a result, we expect that the lightweight and low costs features of a SIW slot array antenna with stable electrical performances can be designed with the proposed design method for millimeter-wave radiating systems.

Reference

[1] K. Hashimoto, J. Hirokawa, and M. Ando, “A post-wall waveguide center-feed parallel plate slot array antenna in the millimeter-wave band,” *IEEE Trans. Antennas Propag.*, vol. 58, no. 11, pp. 3532–3538, Nov. 2010.

[2] K. Sakakibara, Y. Kimura, J. Hirokawa, and M. Ando, “A two-beam slotted leaky waveguide array for mobile reception of dual-polarization DBS,” *IEEE Trans. Veh. Tech.*, vol. 48, no. 1, pp. 1–7, Jan. 1999.

[3] R. S. Elliott, “An improved design procedure for small arrays of shunt slots,” *IEEE Trans. Antennas Propag.*, vol. AP-31, pp. 48–53, Jan. 1983.

[4] M. Orefice and R. S. Elliott, “Design of waveguide-fed series slot arrays,” *IEE Proc.*, vol. 129, pp. 165–169, Aug. 1982, Dt. H.

[5] H. Oraizi and M. T. Noghani, “Design and optimization of waveguide-fed centered inclined slot arrays,” *IEEE Trans. Antennas Propag.*, vol. 57, no. 12, pp. 3991–3995, Dec. 2009.

[6] J. Hirokawa and M. Ando, “45° linearly polarized post-wall waveguide-fed parallel-plate slot arrays,” *IEE Proc.-Microw. Antennas Propag.*, vol. 147, no. 6, pp. 515–519, Dec. 2000.

[7] S. Park, Y. Okajima, J. Hirokawa, and M. Ando, “A slotted post-wall

waveguide array with interdigital structure for 45° linear and dual polarization," *IEEE Trans. Antennas Propag.*, vol. 53, no. 9, pp. 2865–2871, 2005.

[8] A. Mizutani, K. Sakakibara, N. Kikuma, and H. Hirayama, "Grating lobe suppression of narrow-wall slotted hollow waveguide millimeter-wave planar antenna for arbitrarily linear polarization," *IEEE Trans. Antennas Propag.*, vol. 55, no. 2, pp. 313–320, Feb. 2007.

[9] F. Xu and K. Wu, "Guided-wave and leakage characteristics of substrate integrated waveguide," *IEEE Trans. Microwave Theory Tech.*, vol. 53, no. 1, pp. 66–73, Jan. 2005.

[10] D. Kim, W. Chung, C. Park, S. Lee, and S. Nam, "Design of a 45°-inclined SIW resonant series slot array antenna for Ka band," *IEEE Antennas Wirelelss Propag. Lett.*, vol. 10, pp. 318–321, 2011.

[11] D. Kim and S. Nam, "A Ka band planar slot array antenna for 45 degree linear polarization using substrate integrated waveguide," *European Conference on Antennas and Propagation* (*EuCAP2011*), Rome, Italy, 11-15, Apr. pp. 2351-2353.

[12] J. C. Coetzee, J. Joubert, and D. A. McNamara, "Off-center-frequency analysis of a complete planar slotted-waveguide array consisting of

subarray," *IEEE Trans. Antennas Propag.*, vol. 48, no. 11, pp. 1746–1755, Nov. 2000.

[13] G. Mazzarella and G. Montisci, "Wideband equivalent circuit of a centered-inclined waveguide slot coupler," J. Electromagn. Waves Applicat., vol. 14, pp. 133–151, 2000.

[14] CST Microwave Studio (MWS) 2010, CST Corporation. Available: http://www.cst.com

[15] T. Kai, Y. Katou, J. Hirokawa, M. Ando, H. Nakano, and Y. Hirachi, "A coaxial line to post-wall waveguide transition for a cost-effective transformer between a RF-device and a planar slot-array antenna in 60 GHz band," *IEICE Trans. Commun.*, vol. E89–B, no. 5, pp. 1646–1653, May 2006.

[16] D. Kim, J. W. Lee, T. K. Lee, and C. S. Cho, "Design of SIW cavity-backed circular-polarized antennas using two different feeding transitions," *IEEE Trans. Antennas Propag.*, vol. 59, no. 4, pp. 1398–1403, Apr. 2011.

[17] T. Kai, J. Hirokawa, and M. Ando, "A stepped post-wall waveguide with aperture interface to standard waveguide," in *IEEE AP-S Int. Symp. Dig.*, 2004, pp. 1527–1530.

[18] G. K. C. Kwan and N. K. Das, "Excitation of a parallel-plate dielectric

waveguide using a coaxial probe–Basic characteristics and experiments," *IEEE Trans. Microwave Theory Tech.*, vol. 50, no. 6, pp. 1609–1619, Jun. 2002.

[19] N. Marcuvitz, *Waveguide Handbook*. New York: McGraw–Hill, 1951, pp. 296–298.

[20] Advanced Design System (ADS) 2009, Agilent technologies. Available: http://www.agilent.com

Chapter 4

Excitation Control Method for Low Sidelobe Level

4.1 Introduction

WG slot array antennas are quite suitable for millimeter-wave radiating systems that require not only high gain, efficiency, and a robust structure but also low cross-polarization and SLLs. Despite the above advantages, three-dimensional metallic waveguide slot array antennas are associated with massive volumes, complex manufacturing, and a high cost. Recently, alternative solutions for efficient millimeter-wave antenna manufacturing processes have been studied, such as a "laminated waveguide" or a "substrate integrated waveguide" (SIW) with low conduction and radiation losses **[1]**, **[2-3]**. Owing to their simple manufacturing process, involving only drilling and chemical etching on general PCBs, low-cost,

simply fabricated, and lightweight features are possible. Furthermore, SIW transmission lines are especially compatible with complex feeding networks compared to conventional microstrip transmission lines for millimeter-wave antenna systems due to their low radiation leakage, which typically deteriorates their inherent radiation characteristics. As a result, many recent studies of SIW slot array antenna designs have been conducted **[4-9]**.

Slot array antennas with highly accurate 45°-inclined LP are promising candidates for collision avoidance systems as well as dual-polarized radar systems. In these antennas, lower SLLs and higher cross-polarization discrimination (XPD) should be imposed for compatibility against the surrounding electromagnetic (EM) environment effect, such as ghost effects. The SLLs of conventional resonant (i.e. resonantly spaced with a half guided-wavelength) shunt and series slot array antennas can be suppressed by the excitation control using the offsets and tilt angles of every slot because the self-conductance and -resistance of individual shunt and series resonant slots are the function of offsets and tilt angles, respectively **[11, 12]**.

In contrast with the conventional SLL suppression method for the radiating elements having resonant length, we propose the SLL suppression method based on a uniform series slot array antenna suggested in **[8]** by the authors using axial displacements for inductively and capacitively loaded slots along the center line of a broad wall. The axial displacements control the mode currents on reactively loaded

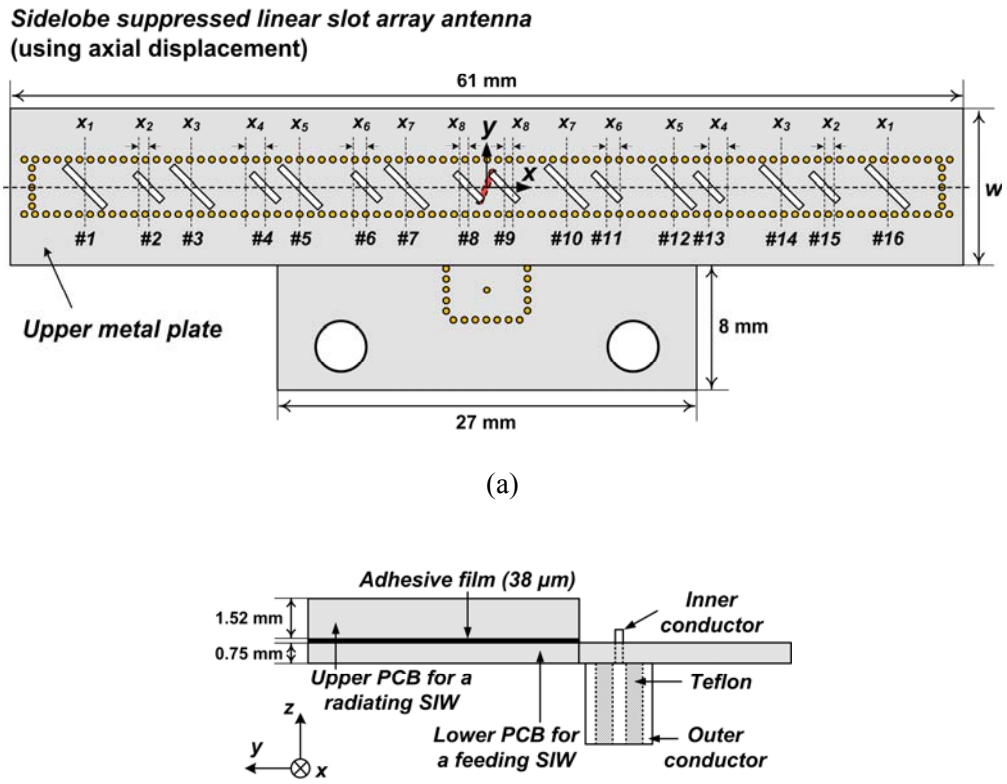

Fig. 4.1 SIW linear slot array antenna structure (a) for arbitrary excitation coefficients using axial displacements (from x_1 to x_8). In this case, the axial displacements are employed just for inductive radiating slots (x_2, x_4, x_6, and x_8) not capacitive radiating slots (x_1, x_3, x_5, and x_7). (b) Lateral view.

radiating slots, allowing arbitrary excitation coefficients to be determined. As a conventional structure for a uniform 45°-inclined LP, a previously suggested resonantly excited series slot array antenna which has a constant slot spacing

distance with a half guided-wavelength is considered in the application of the axial displacement parameters. Also, the validity of the proposed method is evaluated from the calculation results using an equivalent circuit analysis and a commercially available full-wave EM simulation (CST MWS) **[13]**. Two types of low SLL linear slot array antennas with Dolph-Chebyshev polynomials for –20 dB and –26 dB SLLs are designed and evaluated in terms of the measured electrical performances of the reflection coefficients, realized gains, XPDs, and SLLs.

4.2 Axial Displacements for Excitation Control

A conventional uniform linear series slot array antenna as shown in Fig. 2.1 of Chapter 2.2.1. In this antenna, sixteen centered-inclined radiating slots (i.e., eight alternating reactance slot pairs) are separated with the half guided-wavelength of a radiating SIW as a resonantly excited feature. As a result, these radiating units ensure stable radiation characteristics without any grating lobes in the longitudinal direction (*zx*-plane). In addition, the symmetric radiation patterns can be guaranteed due to their center-fed structure from a series-to-series coupling slot that is located between a radiating and a feeding SIW, as shown in Fig. 2.1.

The excitation coefficient design starts from a conventional uniform linear slot array antenna [Fig. 2.1] using the axial displacements along the longitudinal axis (*x*-axis) of a radiating SIW, as shown in Fig. 4.1(a). Eight resonantly spaced radiating

slots on the left side of a radiating SIW are numbered from the shorted-end to the center of a series-to-series coupling slot location. Furthermore, the axial displacements are set for the inductive (even n) and capacitive (odd n) slots with inward and outward directions of (x_2, x_4, x_6, and x_8) and (x_1, x_3, x_5, and x_7), respectively, from the resonantly excited positions. All of these displacement values are symmetric with respect to the center of the antenna.

In our research, two types of PCBs with the same dielectric constant of 3.5 are used for a radiating and a feeding SIW with different thicknesses of 1.52 mm and 0.75 mm, respectively. They are precisely aligned using adhesive film with a dielectric constant of 2.35 and a thickness of 38 μm. In order to construct the SIW transmission line as a perfectly electric side wall, metallic via arrays are periodically arranged with a diameter of 0.4 mm and a spacing of 0.7 mm for both the radiating and feeding SIW. These blind vias of a multi-layered antenna structure are constructed using sequential lamination method to develop SIW transmission lines. Also, the width of these SIWs is set to 3.44 mm, making the guided-wavelength (λ_g) therefore 6.8 mm. As a result, the fundamental TE_{10} mode at an operating frequency of 35 GHz is able to propagate along the SIW transmission line above a cut-off frequency of 25.06 GHz without any higher-order modes.

Fig. 4.2 shows the equivalent radiating RWG for the left side of the proposed

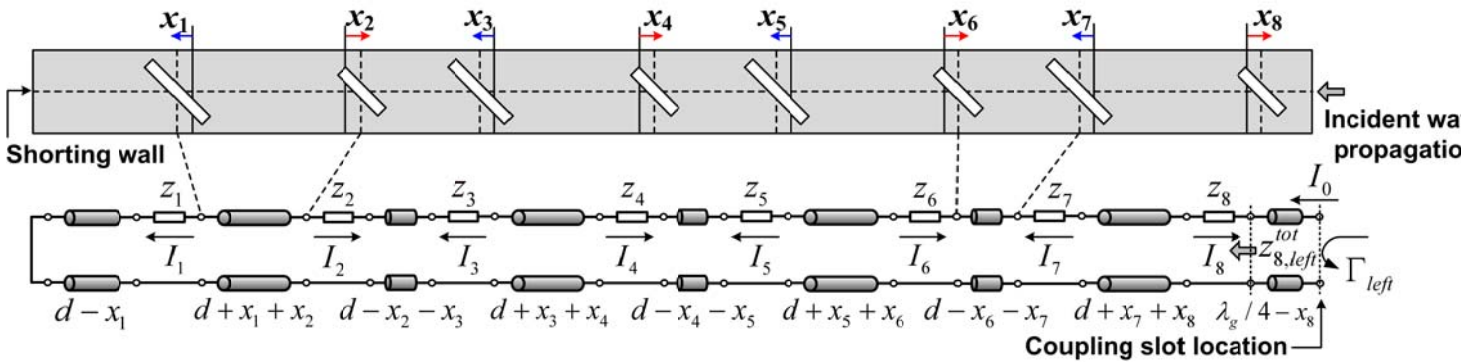

Fig. 4.2 Equivalent rectangular waveguide slot array model with axial displacements on each radiating slots and its transmission line circuit model.

center-fed linear slot array antenna and its equivalent circuit below. There are four alternating reactance slot pairs with axial displacements (x_n) along the center line of a broad wall. Once the axial displacements are applied to each radiating slots, the length of the transmission lines between adjacent series-connected impedances are changed, as shown in Fig. 4.2. When we know the inductive and capacitive self-impedances of an alternating reactance slot pair, the total input impedance looking from the 8th radiating slot toward the shorted-end can be calculated using an impedance recursive formula as a function of the axial displacement:

$$\begin{aligned} z_{1,left}^{tot} &= z_1 + j\tan\left[\beta_{10}\left(d - x_1\right)\right] \\ z_{n,left}^{tot} &= z_n + \frac{z_{n-1,left}^{tot} + j\tan\left[\beta_{10}\left(d + (-1)^n \cdot u_{n-1}\right)\right]}{1 + jz_{n-1,left}^{tot} \cdot \tan\left[\beta_{10}\left(d + (-1)^n \cdot u_{n-1}\right)\right]} \\ &\qquad for\ n = 2,\ 3,\ldots 8 \end{aligned} \tag{4.1}$$

In this equation, β_{10} is the propagation constant of the fundamental TE_{10} mode for a given radiating SIW and $d = \lambda_g/2$ is set for 3.4 mm at an operating frequency of 35 GHz. Also, the index $u_n = x_{n-1} + x_n$ represents the length variation of each transmission line between neighboring radiating slots due to the axial displacement.

The mode currents of each series slot module can be defined by the following recursive formula:

$$I_8 = \frac{I_0}{\cos\left[\beta_{10}\left(d - x_8\right)\right] + jz_{8,left}^{tot} \cdot \sin\left[\beta_{10}\left(d - x_8\right)\right]} \tag{4.2}$$

$$I_n = \frac{I_{n+1}}{\cos\left[\beta_{10}\left(d - \left(-1\right)^n \cdot u_{n+1}\right)\right] + jz_{n,left}^{tot} \cdot \sin\left[\beta_{10}\left(d - \left(-1\right)^n \cdot u_{n+1}\right)\right]}$$

$$for\ n = 7,\ 6,\ldots 1$$

where I_0 is the input current coupled from a series-to-series coupling slot. The impedance and current recursive formulas can be also employed for the right side of a radiating SIW due to their symmetric feature with respect to the center of an antenna, the location of the series-to-series coupling slot. Finally, equations (4.1) and (4.2) yield the magnitudes and phases of the slot voltages applied by the axial displacements.

Meanwhile, the magnitude and phase difference effects of radiating electric fields with respect to the direction of the axial displacements for inductive [x_8 (for slot #8, 9)] and capacitive slots [x_7 (for slot #7, 10)] are investigated using an EM full-wave simulator, CST MWS and equivalent circuit analysis. At this point, the remaining radiating slots are resonantly excited with one-half guided-wavelength spacing. In order to identify the near-field distribution generated by the radiating slots, we set a tracking line 1 mm above a broad wall along the center line of a radiating SIW (x-axis).

As a first example, the single-axial displacement of x_8 for only the two inductive radiating slots of #8 and #9 are adjusted with random values of ± 0.7 mm. In this case, the positive sign indicates that the axial displacement of x_8 moves toward a coupling slot. When a positive x_8 is employed, the magnitudes of the inductive slot voltages are increased until they are nearly double the values of other values, as shown in Fig. 4.3(a). In addition, the phases of their electric fields approach the phases of the capacitive radiating slots. It is important to note that the centered axial displacements scarcely affect the field distribution of the remaining radiating slots. On the other hand, when two inductive slots move toward both ends of the radiating SIW, the magnitudes of their electric fields are inversely proportional to the remaining slots and the phase differences with the neighboring capacitive slots (slot #7 and #10) are increased considerably. Therefore, the axial displacement for the inductive slots should be employed toward the center of a linear slot array antenna in order to realize a tapered distribution and a decreased phase difference at the same time.

As the next example, axial displacement of x_7 is applied for only two capacitive radiating slots, slots #7 and #10, simultaneously. The positive sign for x_7 means that the capacitive slots are moving toward both ends of a radiating SIW. Regarding the magnitudes of the radiated electric fields, there is an insufficient distribution to

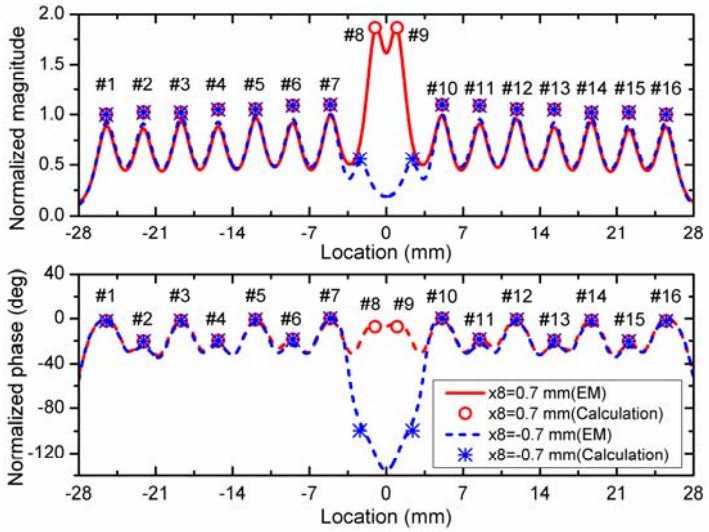

(a)

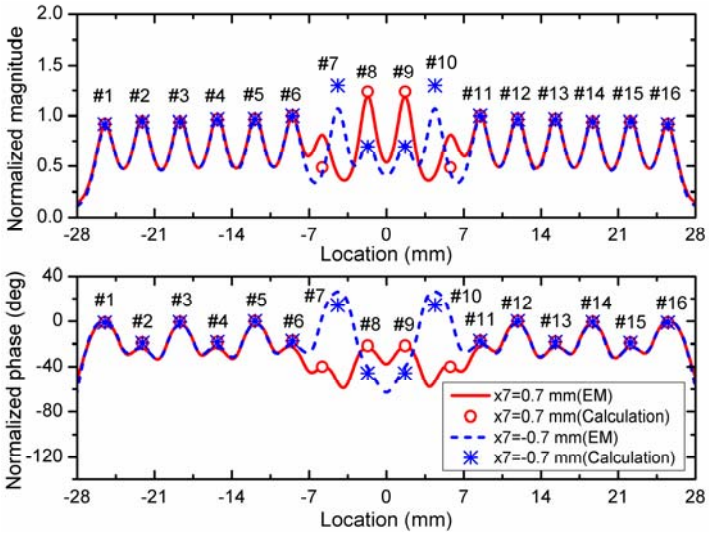

(b)

Fig. 4.3 The magnitude and phase variation of radiating electric fields with respect to the direction of axial displacements for (a) inductive (slots #8 and #9) and (b) capacitive (slots #7 and #10) radiating slots, respectively. For the verification, the calculated results from recursive formulas are depicted.

suppress the sidelobes, especially in the case of negative axial displacement. In addition, for the phase difference, it is obvious that the phase difference as regards the neighboring inductive radiating slots (slots #8 and #9) increases to more than 40° regardless of the direction of the axial displacement as shown in Fig 4.3(b). Consequently, it is suitable and highly advantageous to apply the axial displacement only for the inductive radiating slots associated with the magnitude and phase distribution. From the viewpoint of phase, the properly increased distance between reactively loaded radiating slots compensates their phase difference compared with the spacing of one-half guided-wavelength.

4.3 Design Procedure for Excitation Control

We realize a Dolph–Chebyshev distribution for –20 dB and –26 dB SLLs using the proposed axial displacement scheme. As mentioned in the previous section, the tapered excitation coefficients can be easily controlled by the axial displacement for inductive radiating slots. In order to fit into a smoothly decreasing curve such as a cosine function, the axial displacements are successively adopted from the center of a linear slot array antenna, as shown in Fig. 4.4.

When the axial displacement of x_8 = 0.2 mm is employed for radiating slots #8 and #9, the magnitudes and phase differences are tapered and reduced, respectively.

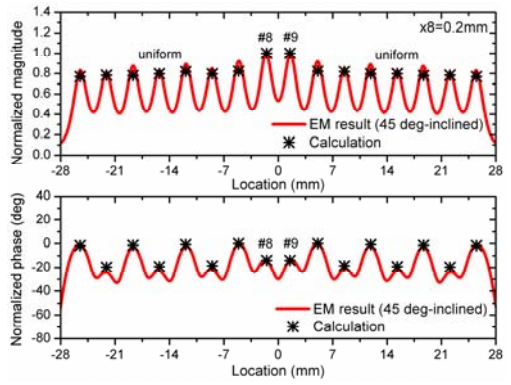

(a)

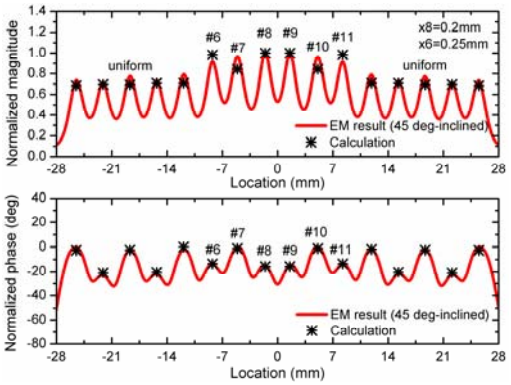

(b)

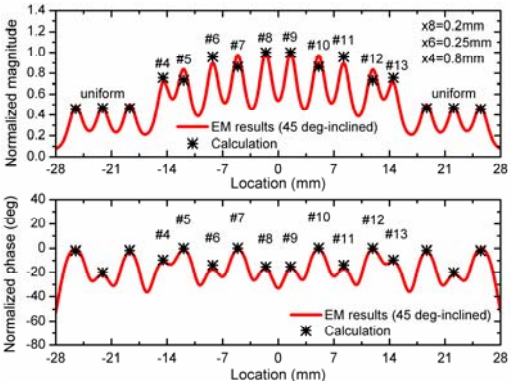

(c)

Fig. 4.4 The slot voltage characteristics according to the progressive axial displacement variations. The calculated results from the equivalent circuit are shown with EM results.

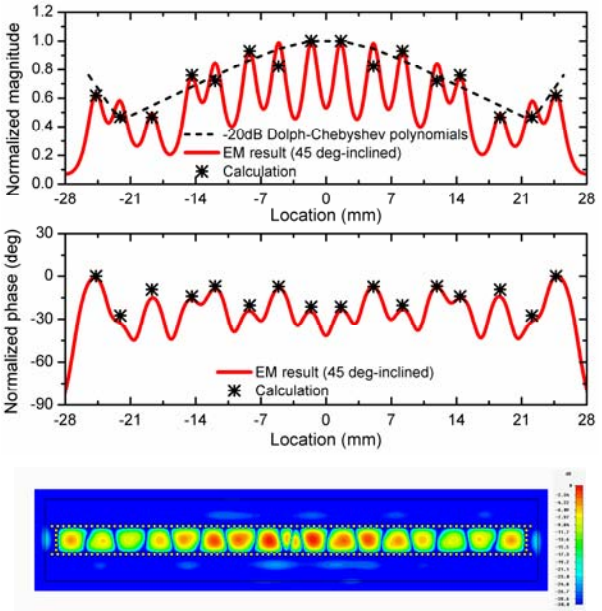

(a)

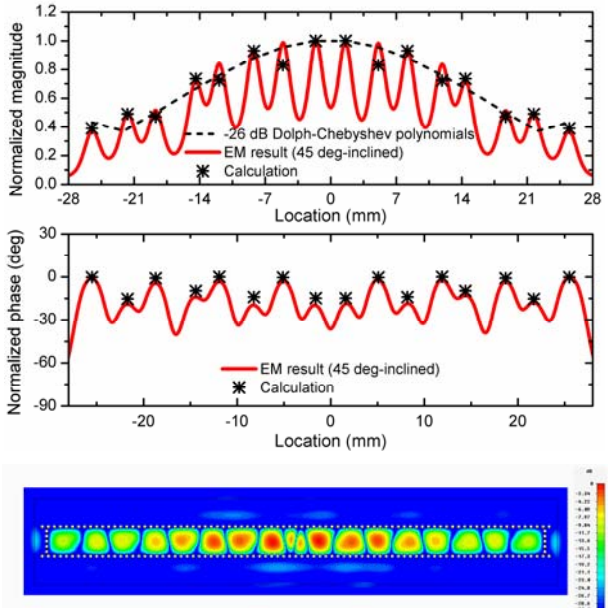

(b)

Fig. 4.5 Excitation coefficient design results for (a) –20 dB and (b) –26 dB, respectively, with electric field distribution (E_z) inside a radiating SIW.

TABLE 4.1

THE DESIGN PARAMETERS AND OPTIMIZED VALUES

Axial displacements Value	x_1		x_2		x_3
	0.8*	0**	0*	0.4**	0
	x_4	x_5	x_6	x_7	x_8
	0.8	0	0.25	0	0.2
Radiating slot length	*Inductive slot* (l_i)		*Capacitive slot* (l_c)		*Slot width*
Value	2.24		3.58		0.4
Coupling slot	*Tilt angle*		*Slot length*		*Slot width*
Value	15°		2.33		0.7

(Units: mm)

(* for –20 dB and ** for –26 dB SLL)

On the other hand, the others are conserved in the form of a uniform field distribution, as shown in Fig. 4.4(a). The next step is to set the axial displacements of x_6 and x_4 sequentially at 0.25 mm and 0.8 mm, respectively. As depicted in Fig. 4(b) and (c), the tapered excitation coefficients can be controlled independently from slots #4 to #13, except for the remaining respective three radiating slots located in both shorted walls.

The inversely proportional excitation coefficient is required for –20 dB SLL for the precise design of the excitation coefficients, especially for the last two radiating slots, slots #1 and #16. Therefore, the capacitive slots #1 and #16 inevitably move in

a positive direction (i.e., x_1 = 0.8 mm) without any movement of x_2, whereas the –26 dB SLL is relatively easy to design due to the gradually decreasing feature in this case. Hence, x_2 is set to 0.4 mm without any capacitive axial displacement. In addition, we calculate the slot voltages using an equivalent circuit model and compare the results to the EM simulation results, as shown in Fig. 4.5. The calculated voltage of capacitive slot #7 is slightly lower than the simulated result.

Nevertheless, the error is hardly affects SLLs because of insignificant amount of error. The axial displacement amounts as well as the other design parameters, such as the length of the radiating slots and the series-to-series coupling slot, are listed in TABLE 4.1 with their optimized values.

4.4 Simulation and Measurement

The proposed design method for low SLL slot array antennas is verified from measurements of the reflection coefficient, realized gain, SLL, and XPD. The proposed antennas are fed from a wideband coax-to-SIW transition to provide the input power without any external electromagnetic coupling noise **[9]**. The reflection coefficients are measured using the N5230A network analyzer of Agilent Technologies. These are shown in Fig. 4.6 with the simulation results. The measured impedance bandwidths of the two types of SLLs respectively ranged from 34.36 to 35.04 GHz (Fig. 4.6(a)) and from 34.88 to 35.48 GHz (Fig. 4.6(b)) with a VSWR of

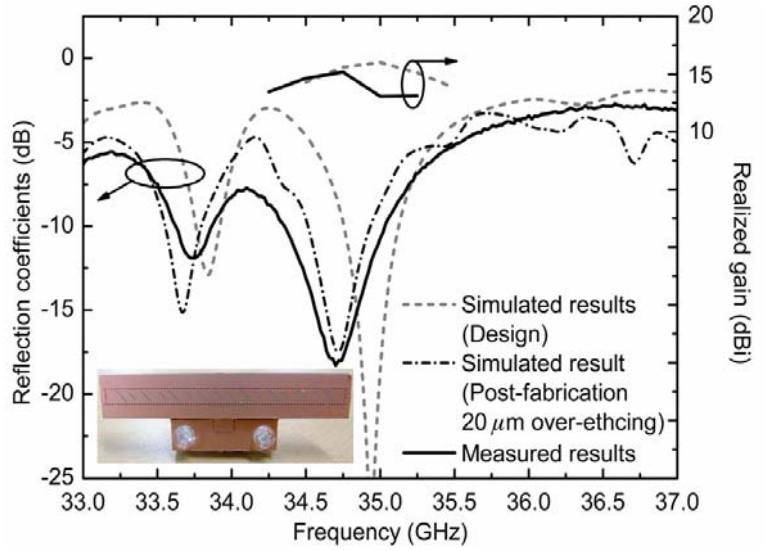

(a)

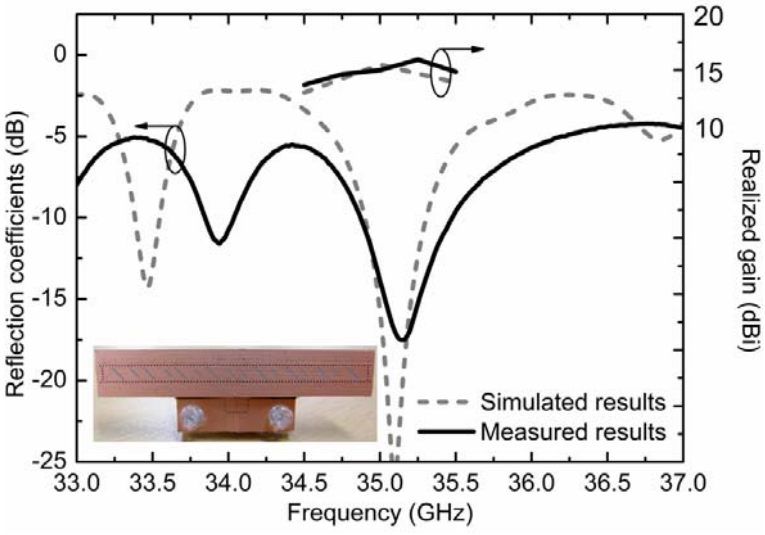

(b)

Fig. 4.6 The reflection coefficients and realized gain results with fabricated antenna pictures of (a) –20 dB SLL and (b) –26 dB SLL slot array antennas, respectively.

less than 2:1 for the two cases. The measured center frequency of –20 dB SLL slot array antenna is slightly changed from 34.93 GHz to 34.7 GHz with 0.66% frequency shift error and the reflection is somewhat increased from –27 dB to –18 dB. This discrepancy is mainly due to etching error and thus the post-fabrication simulation was conducted with 20 μm over-etched radiating and coupling slots for the proposed –20 dB SLL slot array antenna. As a result, the similar result with measured reflection coefficient was obtained for resonant frequency and reflection as shown in Fig. 4.6(a). Meanwhile, the measured resonant frequency of 35 GHz for –26 dB SLL slot array antenna in Fig. 4.6(b) shows similar tendency with simulation, even if there are some differences at lower frequency range.

The realized gain and radiation patterns are depicted in Fig. 4.6 and 4.7. The peak gains are 15.17 dBi at 34.75 GHz and 15.95 dBi at 35 GHz for the –20 dB and –26 dB SLL array antennas, respectively. Additionally, the proposed antennas show the high efficient radiation characteristics with the total efficiencies of 72.57% and 78.66%, respectively, at the center frequency of 35 GHz. Meanwhile, the calculated array factors using the calculated slot voltages presented in Fig. 4.5(a) and (b) are compared with the radiation patterns of CST MWS in Fig. 4.7. It is found that these calculated and the simulated results are well matched each other. Furthermore, even though there are phase variations about 27º and 15º among radiating elements for two types of antennas, respectively, the intended SLLs can be successfully realized.

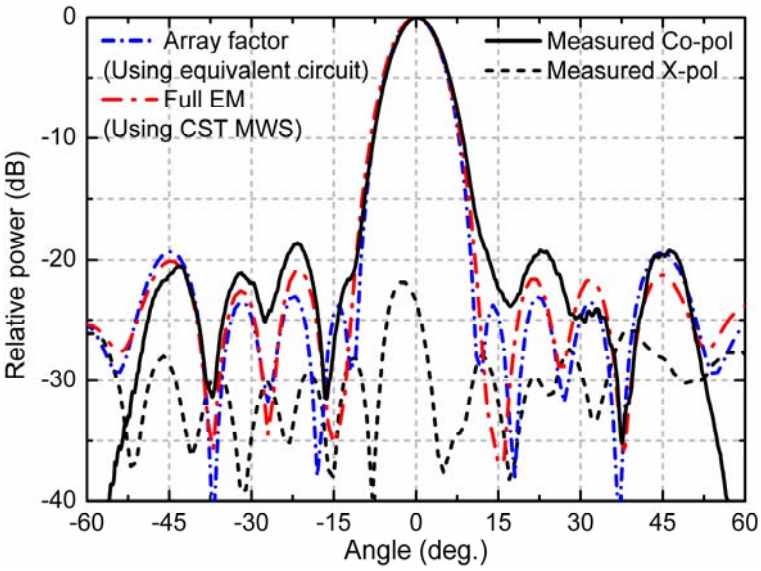

(a)

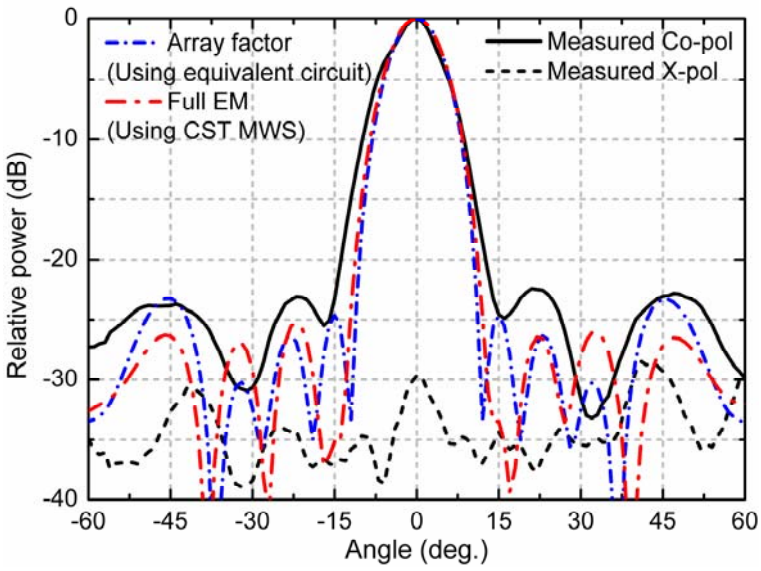

(b)

Fig. 4.7 The measured radiation patterns (*zx*-plane) with calculated array factor and full-wave simulation results for 45°-inclined LP of two types of linear array antennas. (a) –20 dB SLL, (b) –26 dB SLL.

TABLE 4.2

RADIATION CHARACTERISTICS FOR TWO TYPES OF ANTENNAS

Antenna type & Frequency		SLL (dB)	XPD (dB)	Gain (dBi)
-20 dB Antenna	*34.75 GHz*	–18.7	–26.92	15.17
	35.0 GHz	–16.6	–23.46	13.05
	35.25 GHz	–15.6	–23.99	13.11
-26 dB Antenna	*34.75 GHz*	–21.9	–28.39	14.64
	35.0 GHz	–22.5	–29.64	15
	35.25 GHz	–20.2	–23.41	15.95

The measured SLLs are obtained with slightly increased levels of –18.7 dB and –22.5 dB, respectively, and the frequency variations of SLL are summarized in TABLE 4.2 including XPD and realized gain.

It is found that the *x*-directed electric currents on both long edges of an upper metal plate are strongly induced from main radiating slots and ultimately increase cross-polarization levels. In addition, the diffracted and re-radiated fields from a protrudent part of a lower PCB and a coaxial cable for measurement also increase the cross-polarization level, respectively. Therefore, the optimum width of the upper metal plate can be obtained from full-wave EM simulation and is set for 80 mm (= *w* in Fig. 4.1(a)) to suppress cross-polarization. As a result, the lower cross-polarization levels of the proposed antennas are detected respectively as –26.92 dB

and –29.64 dB at the bore-sight.

4.5 Summary

An excitation control method for a series slot array antenna generating 45° LP is proposed. With the use of axial displacement on each radiating slot along the center line of a broad wall of a SIW, the mode currents on each radiating slot can be controlled, which allows the arbitrary excitation coefficients to be determined. In addition, –20 dB and –26 dB linear slot array antennas are designed and fabricated for verification. It is expected that the proposed low sidelobe level design method for series slot array antennas can help one realize arbitrary radiation of 45°-inclined LP.

Reference

[1] H. Uchimura, T. Takenoshita, and M. Fujii, “Development of a “Laminated Waveguide”,” *IEEE Trans. Microwave Theory Tech.*, vol. 46, no. 12, pp. 2438–2443, Dec. 1998.

[2] F. Xu and K. Wu, “Guided-wave and leakage characteristics of substrate integrated waveguide,” *IEEE Trans. Microwave Theory Tech.*, vol. 53, no. 1, pp. 66–73, Jan. 2005.

[3] Y. J. Cheng, K. Wu, and W. Hong, “Power handling capability of substrate integrated waveguide interconnects and related transmission line systems,” *IEEE Trans. Adv. Packag.*, vol. 31, no. 4, pp. 900–909, Nov. 2008.

[4] K. Hashimoto, J. Hirokawa, and M. Ando, “A post-wall waveguide center-feed parallel plate slot array antenna in the millimeter-wave band,” *IEEE Trans. Antennas Propag.*, vol. 58, no. 11, pp. 3532–3538, Nov. 2010.

[5] J. Hirokawa and M. Ando, “45° linearly polarized post-wall wave- guide-fed parallel-plate slot arrays,” *Proc. Inst. Elect. Eng., Microw. Antennas Propag.*, vol. 147, no. 6, pp. 515–519, Dec. 2000.

[6] S. Park, Y. Okajima, J. Hirokawa, and M. Ando, “A slotted post-wall waveguide array with interdigital structure for 45° linear and dual polarization,” *IEEE Trans. Antennas Propag.*, vol. 53, no. 9, pp. 2865–2871, Sep. 2005.

[7] X. –P. Chen, K. Wu, L. Han, and F. He, “Low-cost high gain planar antenna array for 60-GHz band applications,” *IEEE Trans. Antennas Propag.*, vol. 58, no. 6, pp. 2126–2129, Jun. 2010.

[8] D. Kim, W. –S. Chung, C. –H. Park, S. –J. Lee, and S. Nam, “Design of a 45°-inclined SIW resonant series slot array antenna for Ka band,” *IEEE Antennas Wireless Propag. Lett.*, vol. 10, pp. 318–321, 2011.

[9] D. Kim, W. –S. Chung, C. –H. Park, S. –J. Lee, and S. Nam, “A series slot array antenna for 45°-inclined linear polarization with SIW technology,” *IEEE Trans. Antennas Propag.*, vol. 60, no. 4, pp. 1785–1795, Apr. 2012.

[10] A. F. Stevenson, “Theory of slots in rectangular wave-guides,” *J. Appl. Phys.*, vol. 19, pp. 24–38, Jan. 1948.

[11] R. S. Elliott, “An improved design procedure for small arrays of shunt slots,” *IEEE Trans. Antennas Propag.*, vol. AP–31, no. 1, pp. 48–53, Jan. 1983.

[12] M. Orefice and R. S. Elliott, “Design of waveguide-fed series slot arrays,” *IEE Proc*., vol. 129, pp. 165–169, Aug. 1982, Dt. H.

[13] CST Microwave Studio (MWS) 2012, CST Corporation. Available: http://www.cst.com

Chapter 5

Dual Linear Polarized SIW Monopulse Antenna for Dual-Plane Tracking Radar

5.1 Introduction

A monopulse antenna has more than two radiation patterns such as a sum (Σ) and a difference (Δ) in order to find target direction. Sum and difference pattern ratio is a function of angle-of-arrival (AoA) and target angle can be extracted from the amplitude and phase information of the received incoming signal. Two orthogonal pattern functions such as azimuth and elevation directions are required for simultaneous dual-plane monopulse operation [1]. In addition, it is possible to get more exact target direction from stable and symmetric aperture field distribution of a radiator with balanced amplitude and phase excitation from a feeding network (i.e. a comparator).

The conventional monopulse systems have employed lens or reflector type antennas that are relatively heavy and bulky [1]. However, the operating frequency is getting higher up to millimeter-wave bands and the antenna is required to be integrated in a small room with low-profile such as microstrip patch antennas [2, 3]. In [2] and [3], microstrip patch monopulse antennas are suggested for sub-millimeter-wave C- and Ku-bands, respectively, and show that stable radiation patterns can be obtained with a deep null for difference patterns. However, it is likely to decrease radiation efficiency and deteriorate radiation patterns from feeding network transmission line losses (i.e. dielectric, conductor, and leakage losses) especially for millimeter-wave operation. For that reason, shunt slot array monopulse antennas are commonly used using rectangular waveguides (RWGs) for radiating and feeding lines [4]. The injected powers from the air-filled RWG feed network are mostly radiated without dielectric losses or spurious emissions. These high efficient slot array antennas, however, are heavy and expensive for mass production.

Recently, many substrate integrated waveguide (SIW) antennas have been suggested for various millimeter-wave systems in order to overcome the disadvantages of conventional RWG slot array antennas, starting with [5]. Furthermore, some SIW monopulse antennas are investigated for light-weight and miniaturization [6-9]. The Ka- and W-band SIW monopulse antennas that employ

shunt slot arrays are proposed in [6, 7] for dual-plane tracking, respectively. These SIW antennas are integrated in a single-layered PCB including several power dividers, couplers, and delay lines using only through hole via arrays. But overall antenna dimensions are relatively large. A dual V-type linearly tapered slot radiator was developed for a 1-D tracking using a multimode SIW feeder [8]. In [9], H-plane dielectric loading horn antennas are suggested for a 1-D search. The proposed comparator is composed of some hybrid couplers and 90º delay lines for amplitude and phase control and consequently more than –25 dB null-depth of a difference pattern can be achieved.

Meanwhile, most radars are desire to enhance the resolution of the target because there are several interference such as scintillation and glint noises generated by scattering. The enhancement of channel capacity using polarization diversity is a great alternative to overcome amplitude and angle noises of the received signal; indeed, this technology is already employed for various communication or radar systems using RWG slot array antennas [10-12].

The most important design issue for dual LP array antennas is to suppress mutual coupling without any grating lobes. The mutual coupling between dual polarized radiators influences on unintended impedance change of each polarized input ports as well as an isolation level between them. Likewise, for a feeding part,

the balanced amplitude and phase output characteristics between output ports of a comparator should be guaranteed for stable and symmetric radiation patterns. In this dissertation, the 16 × 16 dual LP SIW monopulse antenna using ±45º radiating slots for Ka-band is applied based on the previously confirmed design methodology [13]. The orthogonal conditions between dual radiators are suggested to maximize isolation levels and improve the purity of a LP at the same time. In contrast with [14], the proposed antenna is realized on a multi-layered SIW structure, and the complex feeding SIWs are underneath the radiating SIWs. Furthermore, the dual LP monopulse operations are accomplished by using fabricated RWG comparator as a hybrid system.

5.2 Design Considerations for Dual LP Radiating SIWs

The most important design issue is to minimize the coupling effects between dual polarized radiators that are sharing a common radiating aperture area. Additionally, the slot spacing should be adjustable for suppression of grating lobes. Fig. 5.1 shows the arrangement of orthogonalized dual LP slots on each radiating SIWs. Four adjacent cross-polarized radiating slots are orthogonalized to a centered one with a constant radius. As a result, the mutual coupling can be minimized and it is similar to a previous research [14]. This orthogonal condition can be satisfied when the slot spacing of an alternating reactance slot pair is equal to the separation

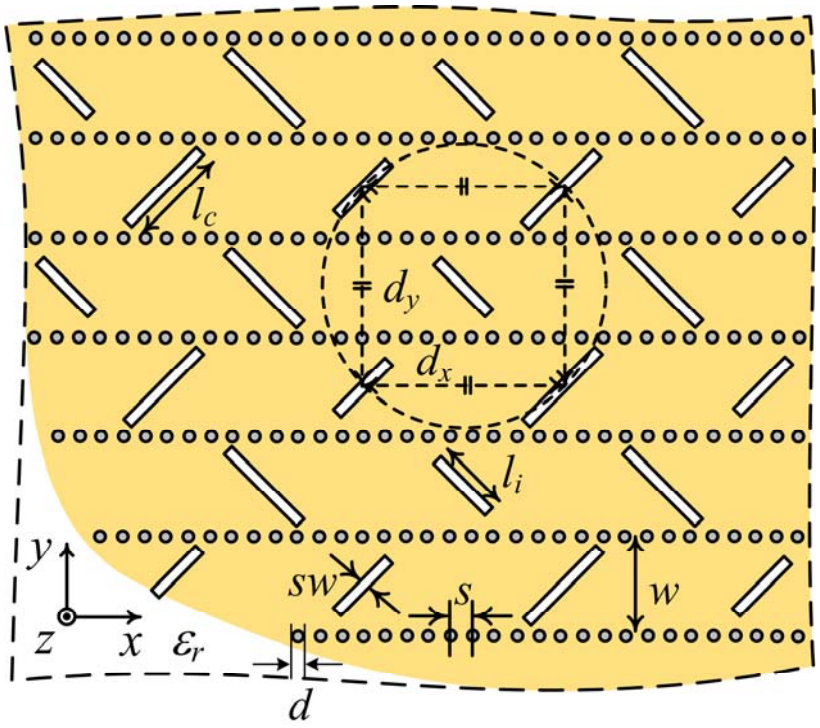

Fig. 5.1 The arrangement of ±45º dual linear polarized radiating slots on radiating SIWs. The SIW transmission lines consist of via arrays with a diameter (d) and spacing (s) of 0.4 mm and 0.75 mm. The length of the alternating reactance slot pair are set to 2.9 mm (l_i) and 3.6 mm (l_c) as inductive and capacitive loads. The width of all radiating slots is 0.4 mm (sw).

distance between neighboring co-polarized radiating SIWs. As described in [13], the slot spacing of an alternating reactance slot pair is a half guided-wavelength that is a function of the dielectric constant (ε_r) and the width (w) of a radiating SIW as follows:

$$\frac{d_x(\varepsilon_r, w)}{\lambda_0} = \frac{\lambda_g(\varepsilon_r, w)}{2 \cdot \lambda_0} = \frac{1}{2\sqrt{\varepsilon_r - \left(\frac{\lambda_0}{2 \cdot w_{eff}}\right)^2}} . \quad (5.1)$$

The x-directed slot spacing (d_x) is normalized to the free space wavelength (λ_0) and w_{eff} means the effective width of a radiating SIW as described in [15]. The normalized y-directed slot spacing is a function of the width of radiating SIWs as

$$\frac{d_y}{\lambda_0} = \frac{2 \cdot w}{\lambda_0} . \quad (5.2)$$

In order to satisfy the orthogonal condition between dual LPs, the width and the dielectric constant of radiating SIWs should be considered simultaneously. The orthogonal conditions are plotted with respect to the width variation of a radiating SIW for given different dielectric constants of 1, 2.2, and 3.5 as depicted in Fig. 5.2. The black line with inverted triangles means the normalized y-directed slot spacing depending on the width of radiating SIWs as mentioned in (5.2). If a radiating SIW is filled with air, the width of SIWs can be set for 4.975 mm under the orthogonal condition at 35 GHz and the corresponding slot spacing is $1.162 \cdot \lambda_0$. It is likely to generate grating lobes and then decrease the radiation efficiency. On the other hand,

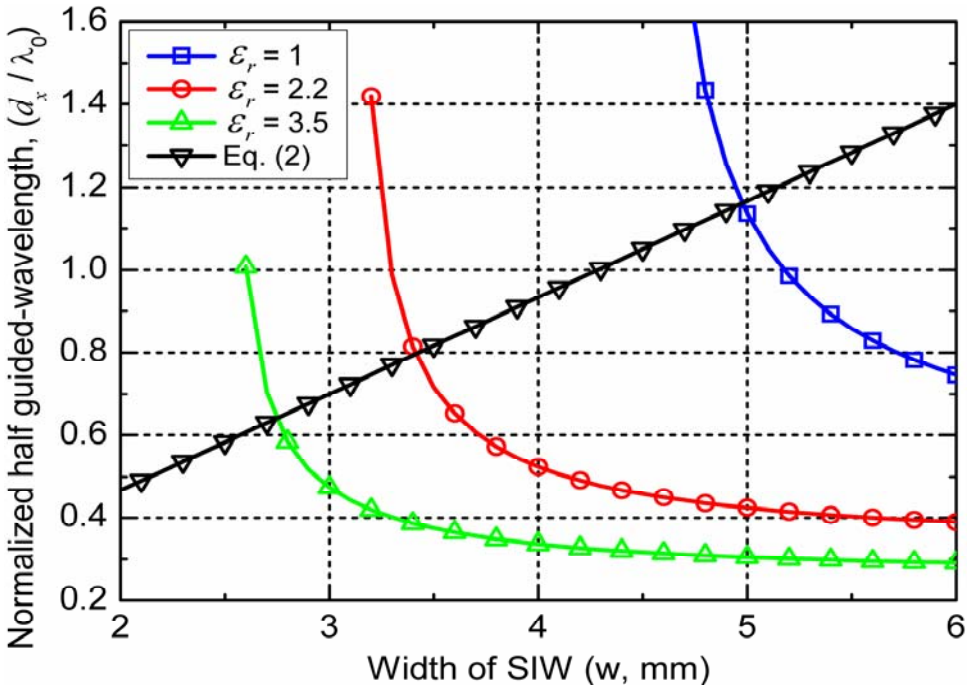

Fig. 5.2 The orthogonal conditions for a dual linear polarized slot array antenna with respect to the width variation of a radiating SIW for given PCBs.

the slot spacing becomes narrow to $0.641 \cdot \lambda_0$ when a dielectric constant is 3.5. But, the width of SIWs is too narrow with 2.745 mm to make the antenna without fabrication error. In conclusion, when the dielectric constant and the width of a SIW is set for 2.2 and 3.42 mm (= $0.8 \cdot \lambda_0$), respectively, the grating lobes can be suppressed under the orthogonal condition. In addition, these radiating SIWs operate over cut-off frequency with a fundamental TE_{10}-mode.

5.3 The Proposed Dual LP 8 × 8 SIW Monopulse Prototype Antenna

A 4 × 4 sub-array for each sub-quadrants is designed under orthogonal condition on RT/Duroid5880 laminate with the dielectric constant of 2.2 and the radiating SIWs width of 3.42 mm. The proposed dual LP SIW monopulse antenna is developed by four dual LP sub-arrays that are located in each quadrants as shown in Fig. 5.3. For convenience, all of SIW lines are replaced with equivalent conventional RWGs. All ends of radiating SIWs are terminated with folded short-circuited stubs and excited by shunt-to-series coupling slots of feeding SIWs on a middle PCB. As a result, the proposed monopulse antenna satisfies orthogonal conditions without any slot free regions or blockages between sub-arrays.

The input power are injected through coax-to-SIW transitions and pass along feeding SIWs of a bottom PCB for each LPs and sub-arrays. The series-to-series coupling slots etched in the ends of feeding SIWs transfers the power to the crossed feeding SIWs of a middle PCB. This coupled powers are equally divided toward left and right directions. Then four shunt-to-series coupling slots located between a middle and a top PCBs distribute the powers to each radiating SIWs and 4 × 4 series slots are excited with almost in-phase. The ±45º LP radiating SIWs are alternately placed under the orthogonal condition and form interdigitated boundaries. In

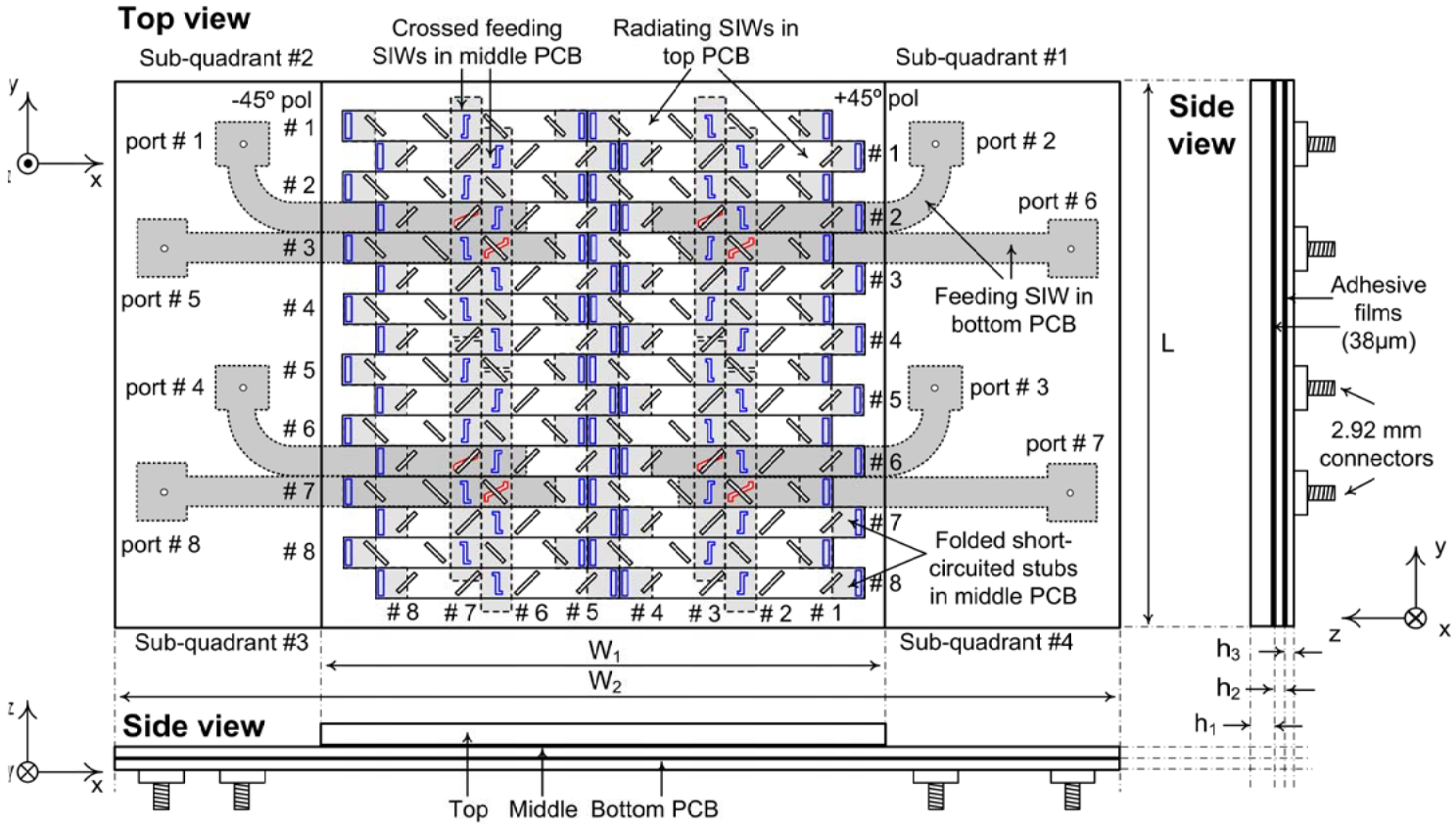

Fig. 5.3 The proposed dual LP monopulse antenna structure with top and side views. (SIW transmission lines that are consisted with metallic via arrays are replaced with equivalent conventional RWGs.)

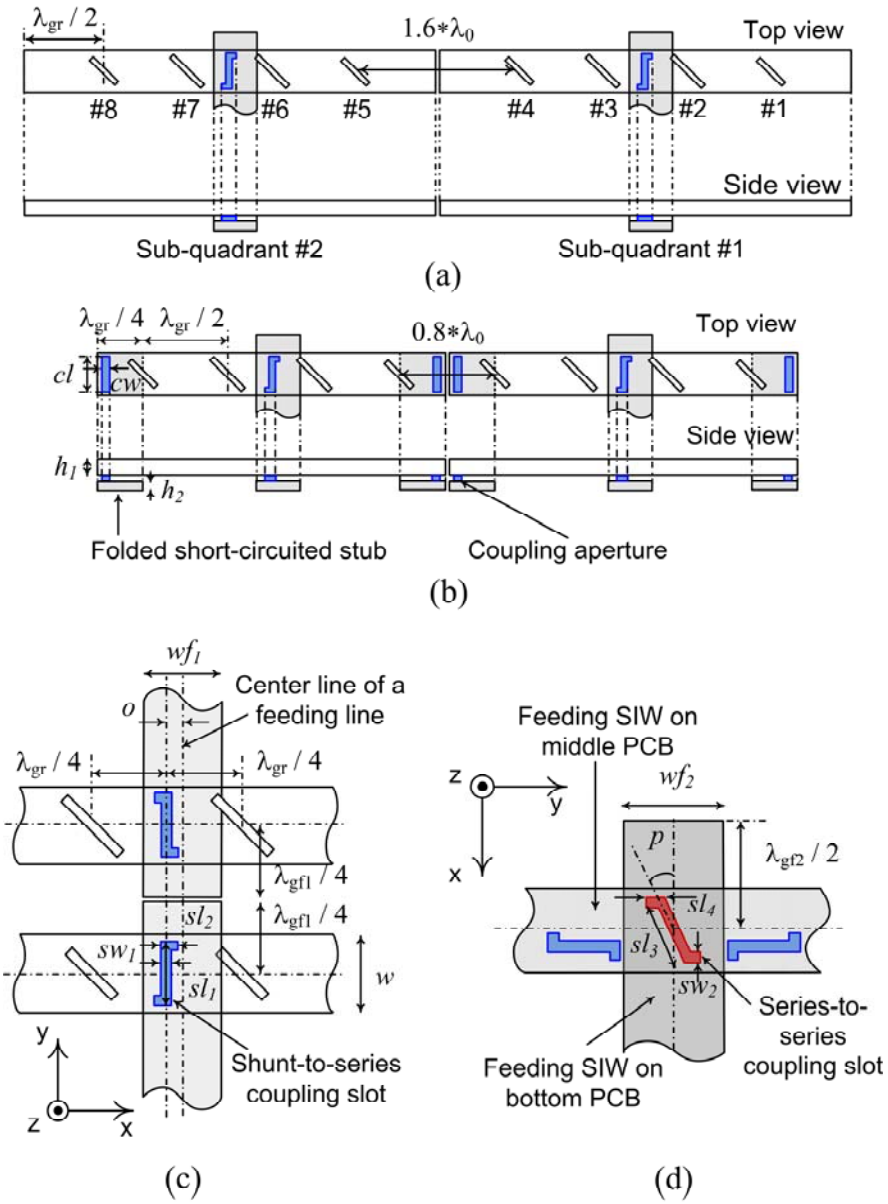

Fig. 5.4 The proposed folded short-circuited stubs. (a) Wide *x*-directed slot spacing between two sub-arrays. (b) Reduced slot spacing as $0.8 \cdot \lambda_0$ without any slot free regions. (c) The arrangements of shunt-to-series coupling slots and radiating slots of two adjacent sub-arrays. (d) The arrangement of a series-to-series coupling slot with adjacent two shunt-to-series coupling slots for in-phase excitation.

addition, the folded short-circuited stubs and shunt-to-series coupling slots of a middle PCB are employed to radiating and feeding SIWs in order to set the *x*- and *y*-directed slot spacings as $0.8 \cdot \lambda_0$, respectively.

5.3.1 Folded Short-Circuited Stubs

Slot free regions generated between sub-arrays may decrease the radiation efficiency due to the high sidelobe levels as reported in [16, 17]. It is important to reduce or eliminate slot free regions for efficient large array antennas. Basically, ±45º LP series slots should be terminated with short-circuited SIW stubs. For examples, the slot spacing between the radiating slot #4 of sub-array #1 and the slot #5 of sub-array #2 becomes $1.6 \cdot \lambda_0$ for operating center frequency as shown in Fig. 5.4(a). Therefore, folded short-circuited stubs are employed at the ends of each radiating SIWs using rectangular coupling apertures, and then the sub-array spacing can be reduced to $0.8 \cdot \lambda_0$ without any input impedance change as shown in Fig. 5.4(b). The impedance matching and bandwidth of the folded short-circuited stub can be controlled by the length (*cl*), width (*cw*) of a coupling aperture, as well as the spacing from a shorting via wall as depicted in Fig. 5.4(b). The coupling aperture located between a top and a middle PCBs is filled with the adhesive film with the dielectric constant of 2.35 and acts like magnetic dipole of an effective half-wavelength of 35 GHz with 2.9 mm (=*cl*).

5.3.2 Shunt-to-Series Coupling Slots

The coupled power can be transferred through series or shunt coupling slots between crossed lines located in different layers each other. The slot is longitudinal and offset from the center line in a main line and is centered transverse in a branch line. This slot is called longitudinal/transverse coupling slot or shunt-to-series coupling slot [18]. The length (sl_1, sl_2) and offset value from the center line of a feeding SIW determines the resonant condition for a pure admittance connected in a main line. The proposed sub-array employs four shunt-to-series coupling slots between a middle and a top PCB metal plates with same offset value and direction for impedance matching, uniform, and in-phase excitation, simultaneously, as shown in Fig. 5.3. In addition, there are not any overlapped areas between crossed feeding SIWs for dual LPs in a middle PCB.

In order to reduce blockages between sub-arrays, a concept of perfect magnetic conductor (PMC) was applied to terminate feeding WGs for a symmetric structure [17]. For the proposed antenna, only $\lambda_{gf1}/4$ length open-circuited lines are required for shunt-to-series coupling slots without any slot free regions in *y*-direction as shown in Fig. 5.4(c). As a result, the last radiating slots on radiating SIW #4 and 5 can keep their slot spacing as $0.8 \cdot \lambda_0$. This is the reason why shunt-to-series coupling slots should be used for the proposed dual LP monopulse antenna

TABLE 5.1

THE DESIGN PARAMETERS AND OPTIMIZED VALUES (UNIT: MM)

SIW Transmission Line	d	0.4		s	0.75	
Radiating Slots and Radiating SIWs	cl	2.9		cw	0.4	
	h_1	1.575		λ_{gr}	13.7	
	l_c	3.6		l_i	2.9	
	w	3.42		ws	0.4	
Coupling Slots and Feeding SIWs	$h_2 = h_3$	0.787		$\lambda_{gf1} = \lambda_{gf2}$	13.7	
	sw_1	0.3		sw_2	0.4	
	sl_1	2.5		sl_2	0.6	
	sl_3	2.8		sl_4	0.7	
	$wf_1 = wf_2$	3.42		p	25º	
Total Structure	L	65	W_1	81	W_2	188

(Units: mm; degree for parameter 'p' only)

feeding network. All shunt-to-series coupling slots are folded to fit in a crossed common area between feeding and radiating SIWs to satisfy the resonant condition under the given height of lines and an operating frequency.

5.3.3 Series-to-Series Coupling Slots

The centered and inclined coupling slots make the branch line equivalent to series connected impedance of a main line. So, it is called the series-to-series coupling slot and can be terminated with the $\lambda_{gf2}/2$ length short-circuited stub [19].

The resonant length (sl_3, sl_4) of the coupling slot can be determined over tilt angle (p) and height of waveguide variation as shown in Fig. 5.4(d). The design parameters and optimized values for dual LP SIW monopulse antenna including coupling apertures and slots are listed on TABLE 5.1.

5.4 RWG Comparator for Monopulse Operation

A single sum pattern and two difference patterns for azimuth and elevation directions are required for dual-plane tracking operation. The operation scheme for the proposed feeding network is depicted in Fig. 5.5(a) with a block diagram. A sum pattern (Σ) can be synthesized by equal (i.e. –6 dB) and in-phase power division for each four output ports, which are connected to each sub-array, for a symmetric radiation pattern. In addition, two difference patterns (Δ_{AZ}, Δ_{EL}) can be realized by four magic-Ts in order to make 180º differences in both azimuth and elevation directions. The proposed comparator for monopulse operation is fabricated based on WR-28 RWG transmission lines and several coax-to-waveguide transitions as shown in Fig. 5.5(b) for outstanding amplitude and phase balances with extremely low-loss.

The results of return losses for each input ports are suggested in Fig. 5.6. All output ports are terminated with 50 ohms and the total comparator is well matched less than –10 dB around operating center frequency of 35 GHz. Besides, the amplitude and phase balances among output ports are confirmed for symmetric

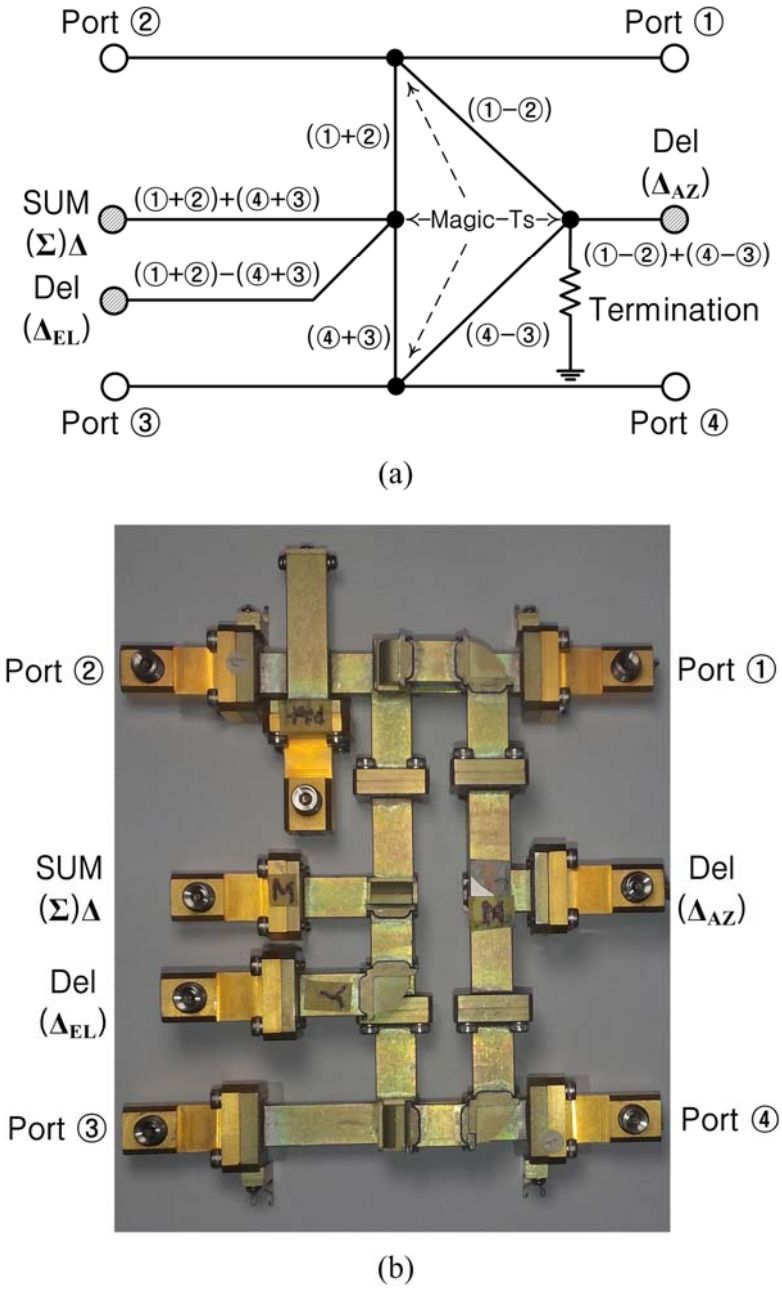

Fig. 5.5 The feeding network for 2-D monopulse operation. (a) A block diagram. (b) The picture of fabricated RWG comparator.

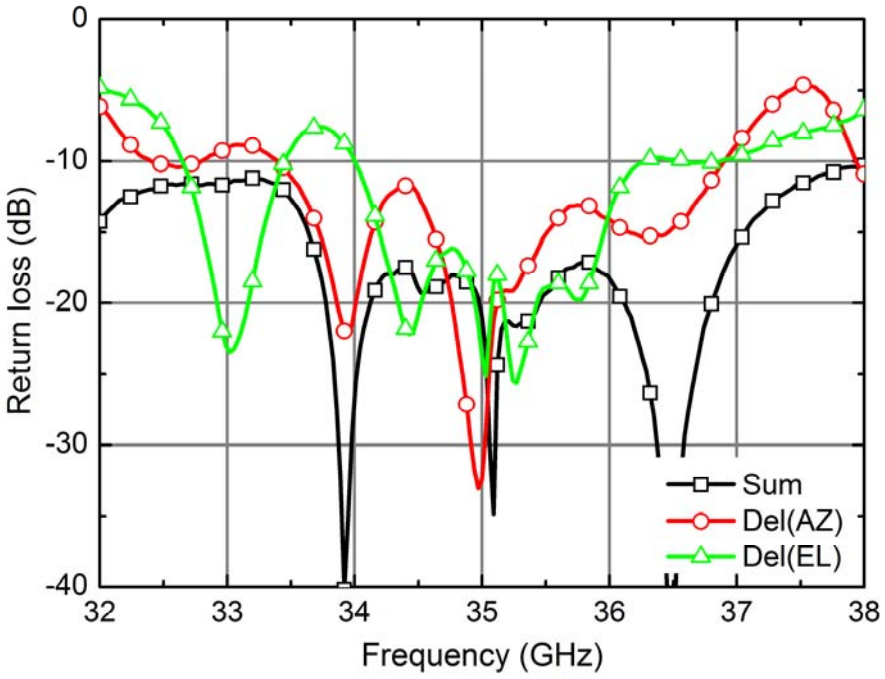

Fig. 5.6 The measured return losses for each input ports of a RWG comparator.

radiation patterns and deep nulls for difference patterns. The results of amplitude and phase difference for the sum input port of the comparator are shown in Fig. 5.7(a) and 8(a), respectively. Comparing with theoretical value of –6 dB, each output values demonstrate balanced distribution within 1 dB variation with low-loss. Besides, the phase differences based on the output port ① are all less than 10º that is considerably accurate in-phase distribution. The results of amplitude and phase difference for remaining two difference input ports (Δ_{AZ}, Δ_{EL}) are shown in Fig.

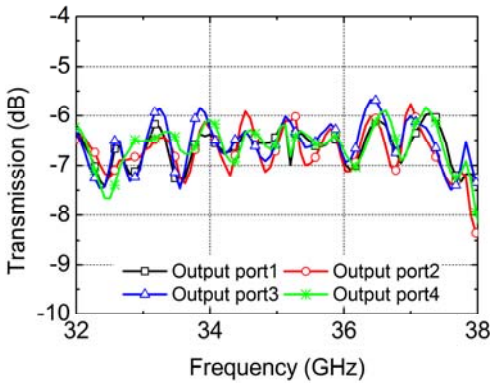

(a)

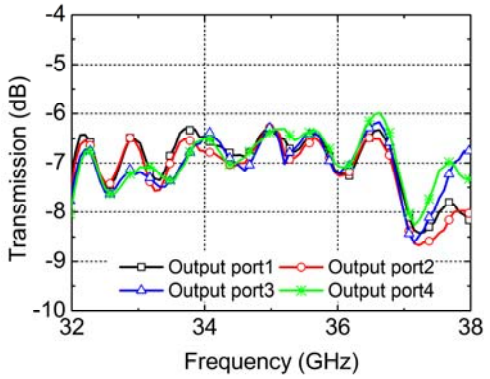

(b)

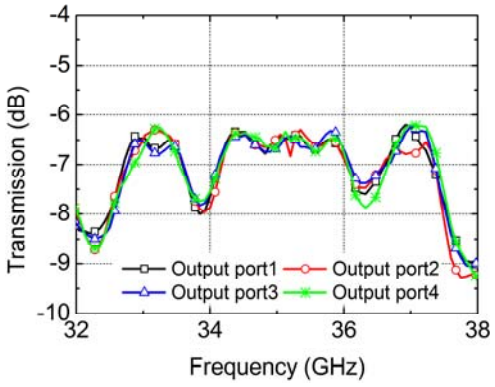

(c)

Fig. 5.7 The measured amplitude results of four output ports for (a) sum (Σ), two difference input ports (b) Δ_{AZ} and (c) Δ_{EL}.

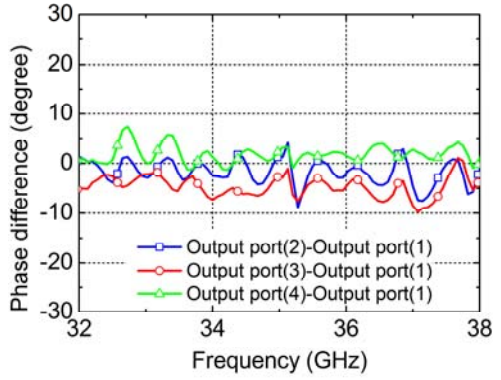

(a)

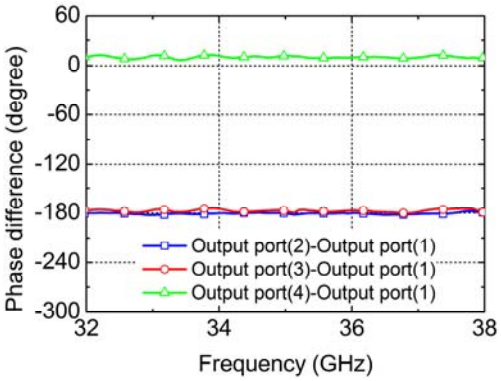

(b)

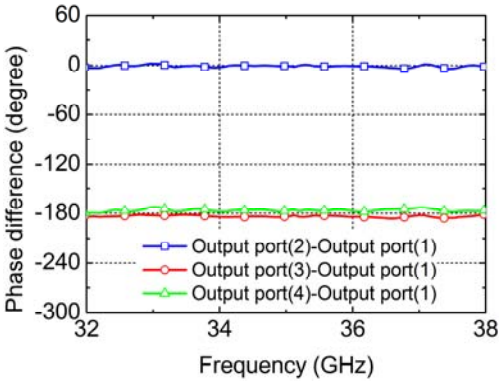

(c)

Fig. 5.8 The measured phase imbalance results for (a) sum (Σ), two difference input ports (b) Δ_{AZ} and (c) Δ_{EL}.

5.7(b), (c) and 8(b), (c), respectively. The transmission losses for both difference input ports are below 1 dB from 34 to 36 GHz. In addition, the exact out-of-phase distributions within 10º error are verified between left and right side output ports as well as up and down output ports for azimuth and elevation directions, respectively.

5.5 Experimental Results

The isolation between orthogonalized dual LPs is verified from S-parameters and radiation pattern results of the fabricated dual LP SIW sub-array antenna. Next, total dual LP SIW monopulse antenna is experimented using a RWG comparator that is connected by rigid cables which have same electrical length to realize exact amplitude and phase balances. The optimization and experiment of all fabricated SIW antennas are conducted by using full-wave EM simulator, CST MWS and an E8316A network analyzer from Agilent, respectively.

5.5.1 Dual LP Sub-Array Antenna

The picture of fabricated multi-layered 4 × 4 dual LP SIW sub-array antenna is shown in Fig. 5.9. All dual LP series radiating slots are arrayed under the orthogonal condition and share the common radiating aperture area of 750.8mm^2. The power injected by two coax-to-SIW transitions for each LPs. The measured reflection coefficients of a two-port sub-array antenna including isolation are shown in Fig.

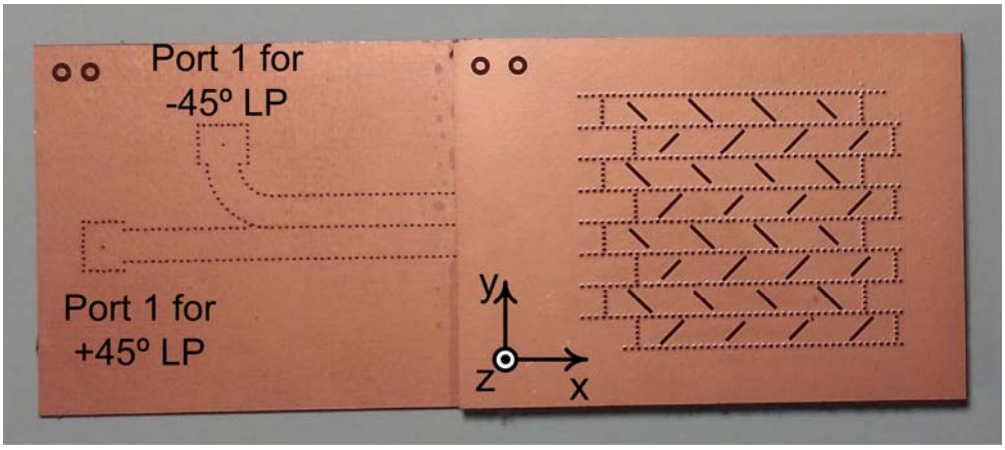

Fig. 5.9 The picture of fabricated dual LP sub-array antenna.

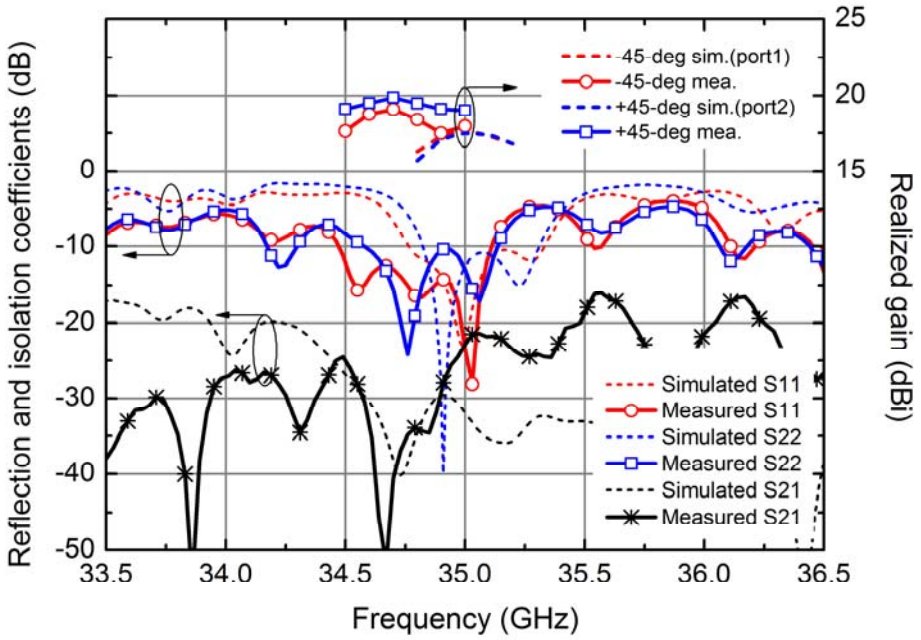

Fig. 5.10 The simulated and measured results of reflection coefficients, isolations, and realized gains for fabricated dual LP SIW sub-array antenna.

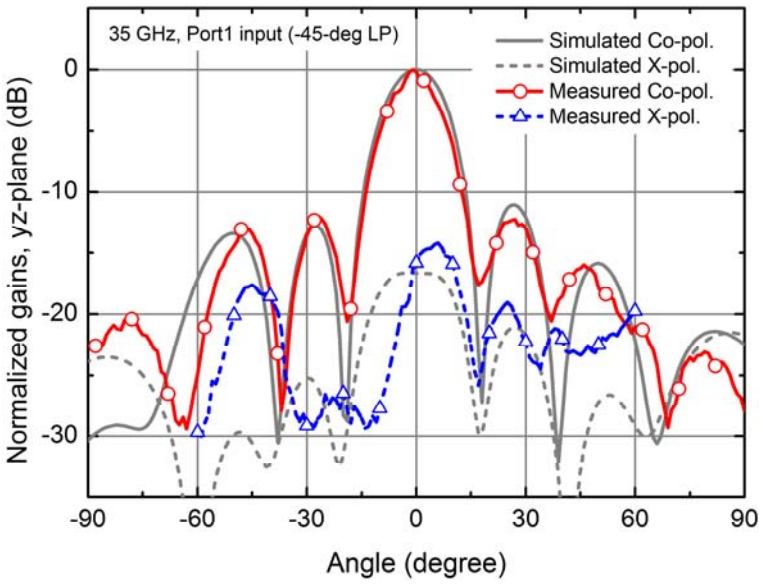

(a)

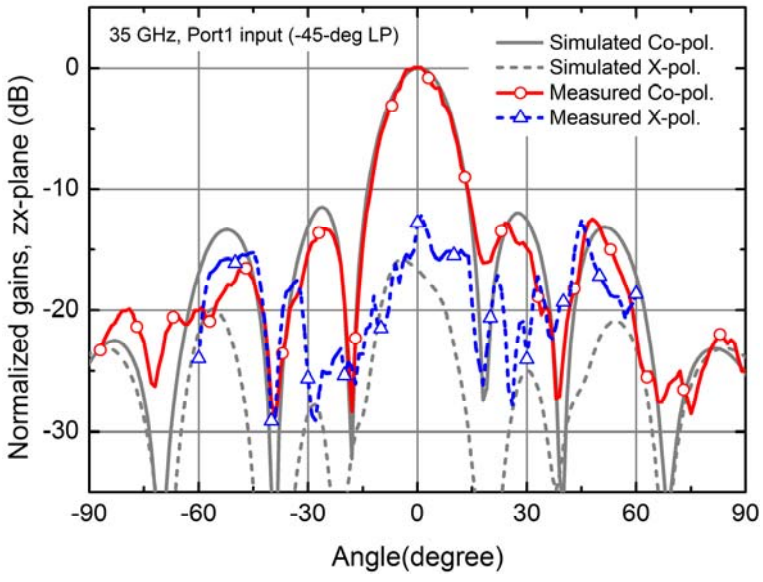

(b)

Fig. 5.11 The simulated and measured radiation patterns for –45º LP (port #1). (a) *yz*-plane. (b) *zx*-plane.

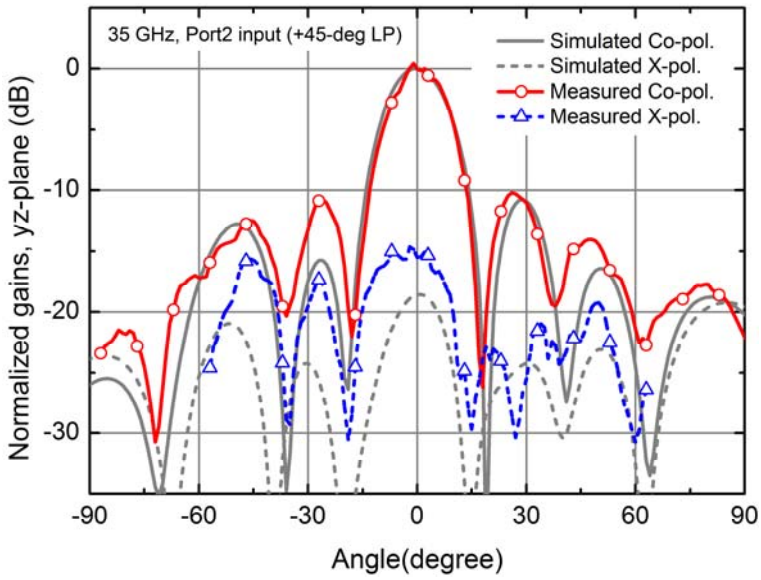

(a)

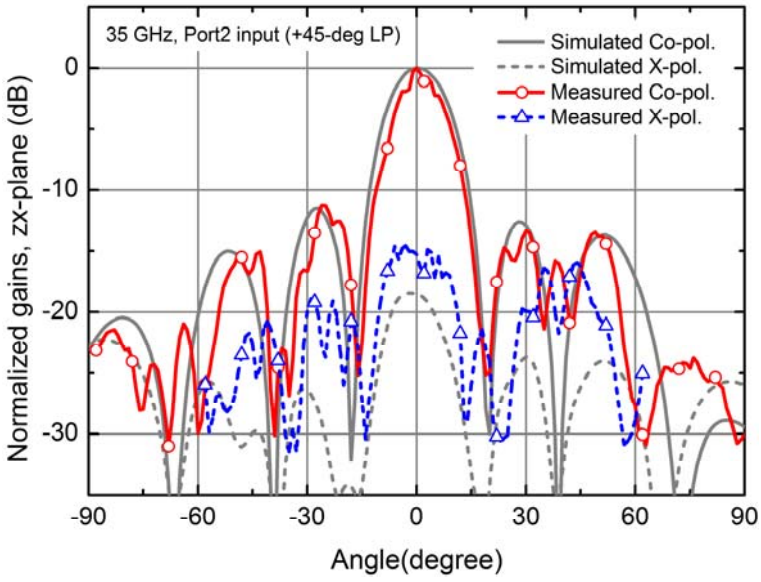

(b)

Fig. 5.12 The simulated and measured radiation patterns for +45º LP (port #2). (a) *yz*-plane. (b) *zx*-plane.

5.10. The measured impedance bandwidths (VSWR < 2) are from 34.47 to 35.11 GHz and from 34.58 to 35.14 GHz for –45º and +45º LPs, respectively. The operating frequencies are lower due to over-etched radiating and coupling slots. Besides, the mutual coupling is sufficiently suppressed under –20 dB at operating frequency bands. The radiation patterns for each LPs and different cutting planes are depicted in Fig. 5.11 and 5.12. The maximum realized gain is 18.08 and 18.88 dBi at 34.7 GHz for –45º and +45º LPs, respectively. In addition, most cross polarization discrimination (XPD) levels at boresight are under –15 dB for dual LPs and cutting planes except for *zx*-plane of –45º LP as shown in Fig. 5.11(b). Considering the theoretical directivity for given aperture area and frequency of 34.7 GHz, the measured aperture efficiency can be calculated as 48.5% and 61.2% for –45º and +45º LPs, respectively.

5.5.2 Dual LP SIW Monopulse Antenna

The total 8 × 8 monopulse slot array antenna structure is fabricated as shown in Fig. 5.13. The orthogonalized dual LP slot radiators are arrayed on SIW structure and a WR-28 comparator feeding network for monopulse operation is mounted on the back side of the antenna. Four input ports for each LP are connected to four comparator input ports using rigid cables that have equal electrical length and low insertion losses for balanced aperture field distributions. Fig. 5.13(b) and 5.13(c)

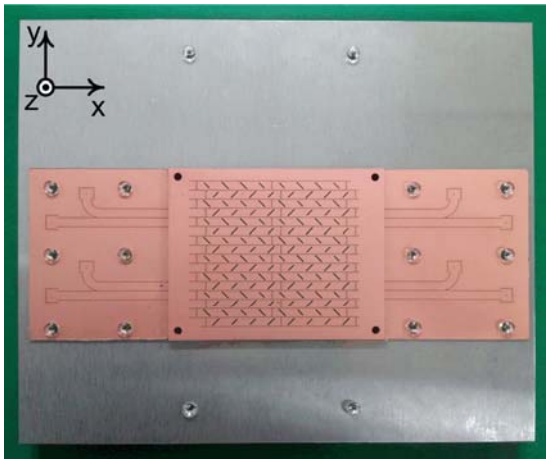

(a)

(b)

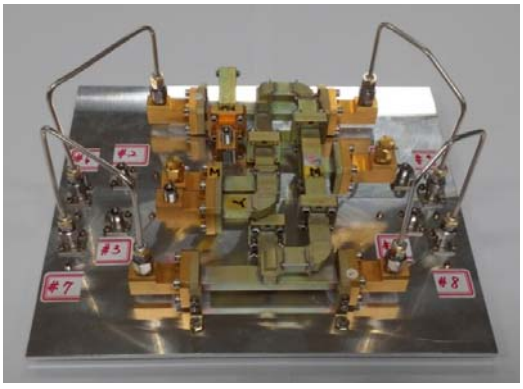

(c)

Fig. 5.13 The fabricated monopulse antenna. (a) SIW main radiator, (b) back view for -45° LP operation, (c) back view for +45° LP operation.

show the assembled antenna structure for –45° (input ports 1~4) and +45° (input ports 5~8) LP operation, respectively.

The simulated and measured +45° LP radiation patterns are depicted in Fig. 5.14 and 5.15. A measured sum pattern at 34.7 GHz in both azimuth and elevation cutting planes are shown in Fig. 5.14(a) and (b), respectively. The operating center frequency is lower to 34.7 GHz due to over-etching for radiating and coupling slots. However, the measured radiation patterns are in good agreement with simulation results. In addition, the null-depth of two difference pattern for azimuth and elevation direction is detected with –19 dB and –20 dB, respectively, as shown in Fig. 5.15(a) and (b). The lower cross-polarization levels for dual LP also can be obtained.

5.6 Summary

A 8 × 8 dual LP monopulse antenna is proposed to minimize mutual coupling effects under orthogonal condition. The monopulse operation for dual-plane and dual polarization was conducted by SIW main radiators and a RWG comparator mounted on the back side of a SIW antenna. Sum and two difference patterns for each LP are verified in azimuth and elevation cutting planes, and it is found that symmetric sum and difference patterns can be obtained with deep nulls from balanced aperture field distributions in terms of an amplitude and a phase. However,

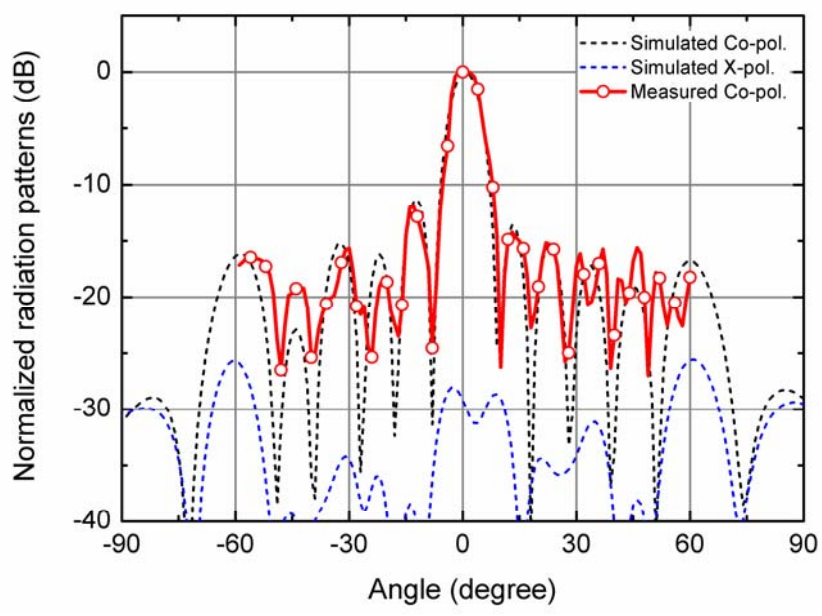

(a)

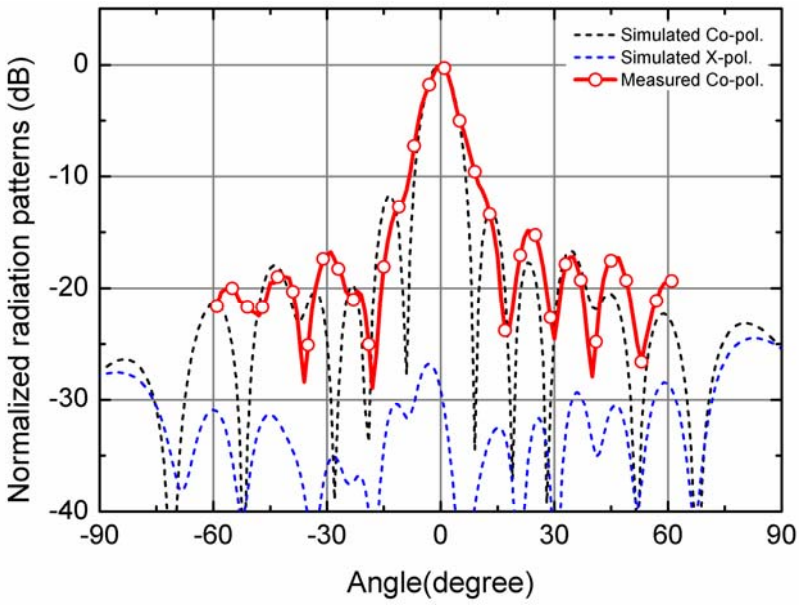

(b)

Fig. 5.14 The +45° LP sum radiation patterns at 34.7 GHz. (a) In azimuth angle (*zx*-plane), (b) In elevation angle (*yz*-plane).

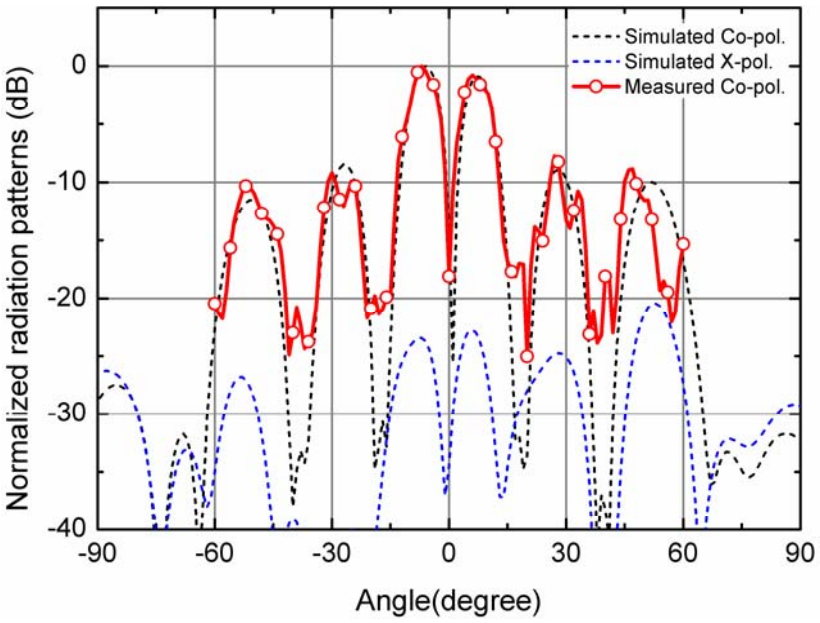

(a)

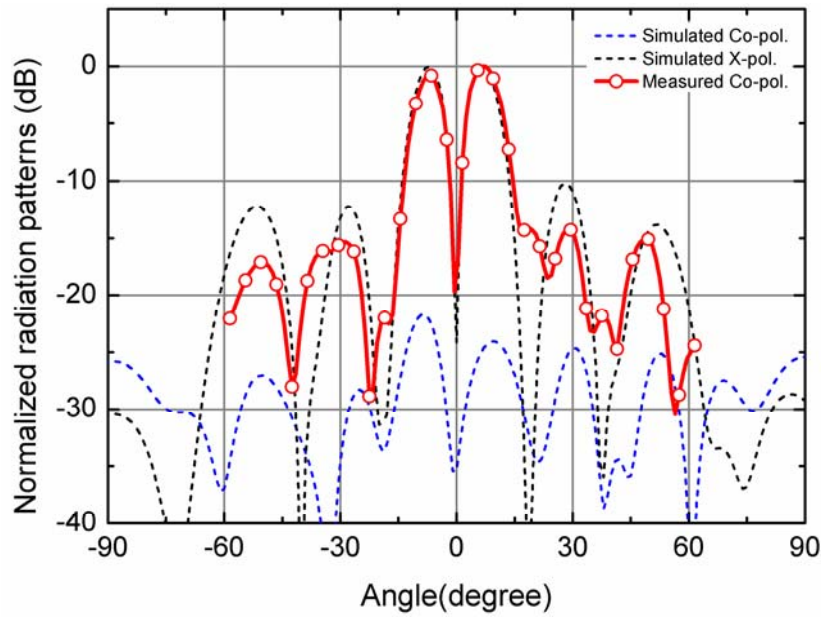

(b)

Fig. 5.15 The +45° LP difference radiation patterns at 34.7 GHz. (a) In azimuth angle (*zx*-plane), (b) In elevation angle (*yz*-plane).

the measured operating frequency is lower due to fabrication error for radiating and coupling slots. Therefore, over-etched patterns should be compensated for more exact monopulse operations.

Reference

[1] S. M. Sherman, *Monopulse Principles and Techniques*. Dedham, MA: Artech House, 1984.

[2] Z.-W. Yu, G.-M. Wang, and C.-X. Zhang, "A broadband planar monopulse antenna array of C-band," *IEEE Antennas Wireless Propag. Lett.*, vol. 8, pp. 1325–1328, 2009.

[3] H. Wang, D.-G. Fang, and X. G. Chen, "A compact single layer monopulse microstrip antenna array," *IEEE Trans. Antennas Propag.*, vol. 54, no. 2, pp. 503–509, Feb. 2006.

[4] R. C. Johnson, *Antenna Engineering Handbook*. New York: McGraw-hill, 1993, ch. 9.

[5] L. Yan, W. Hong, G. Hua, J. Chen, K. Wu, and T. J. Cui, "Simulation and experiment on SIW slot array antennas," *IEEE Microw. Wireless Compon. Lett.*, vol. 14, no. 9, pp. 137–139, Sep. 2004.

[6] B. Liu, W. Hong, Z. Kuai, X. Yin, G. Luo, J. Chen, H. Tang, and K. Wu, "Substrate integrated waveguide (SIW) monopulse slot antenna array," *IEEE Trans. Antennas Propag.*, vol. 57, no. 1, pp. 275–279, Jan. 2009.

[7] Y. J. Cheng, W. Hong, and K. Wu, "94 GHz substrate integrated monopulse antenna array," *IEEE Trans. Antennas Propag.*, vol. 60, no. 1, pp. 121–129, Jan. 2012.

[8] Y. J. Cheng, W. Hong, and K. Wu, “Design of a monopulse antenna using a dual V-type linearly tapered slot antenna (DVLTSA),” *IEEE Trans. Antennas Propag.*, vol. 56, no. 9, pp. 2903–2909, Sep. 2008.

[9] H. Wang, D.-G. Fang, B. Zhang, and W.-Q. Che, “Dielectric loaded substrate integrated waveguide (SIW) H-plane horn antennas,” *IEEE Trans. Antennas Propag.*, vol. 58, no. 3, pp. 640–647, Mar. 2010.

[10] K. Sakakibara, Y. Kimura, J. Hirokawa, M. Ando, and N. Goto, “A two-beam slotted leaky waveguide array for mobile reception of dual-polarization DBS,” *IEEE Trans. Veh. Technol.*, vol. 48, no. 1, pp. 1–7, Jan. 1999.

[11] W. Wang, J. Jin, J.-G. Lu, and S.-S. Zhong, “Waveguide slotted antenna array with broadband, dual-polarization and low cross-polarization for X-band SAR applications,” in *Proc. IEEE Int. Radar Conf.*, Arlington, VA. May 2005, pp. 653–656.

[12] M. Guler and S. Kim, “Dual-polarized, millimeter wave slot array,” *in Proc. Aerospace Conference 2003*, vol. 2, pp. 1077–1083, 2003.

[13] D. Kim, W.-S. Chung, C.-H. Park, S.-J. Lee, and S. Nam, “A series slot array antenna for 45º-inclined linear polarization with SIW technology,” *IEEE Trans. Antennas Propag.*, vol. 60, no. 4, pp. 1785–1795, Apr. 2012.

[14] S. Park, Y. Okajima, J. Hirokawa, and M. Ando, “A slotted post-wall

waveguide array with interdigital structure for 45° linear and dual polarization," *IEEE Trans. Antennas Propag.*, vol. 53, no. 9, pp. 2865–2871, Sep. 2005.

[15] F. Xu and K. Wu, "Guided-wave and leakage characteristics of substrate integrated waveguide," *IEEE Trans. Microwave Theory Tech.*, vol. 53, no. 1, pp. 66–73, Jan. 2005.

[16] K. Hashimoto, J. Hirokawa, and M. Ando, "A post-wall waveguide center-feed parallel plate slot array antenna in the millimeter-wave band," *IEEE Trans. Antennas Propag.*, vol. 58, no. 11, pp. 3532–3538, Nov. 2010.

[17] M. Zhang, J. Hirokawa, and M. Ando, "An E-band partially corporate feed uniform slot array with laminated quasi double-layer waveguide and virtual PMC terminations," *IEEE Trans. Antennas Propag.*, vol. 59, no. 5, pp. 1521–1527, May 2011.

[18] S. R. Rengarajan, "Characteristics of a longitudinal/transverse coupling slot in crossed rectangular waveguides," *IEEE Trans. Microw. Theory Tech.*, vol. 37, no. 8, pp. 1171–1177, Aug. 1989.

[19] S. R. Rengarajan, "Analysis of a centered-inclined waveguide slot coupler," *IEEE Trans. Microw. Theory Tech.*, vol. 37, no. 5, pp. 884–889, May 1989.

Chapter 6

Conclusion

In this thesis, the design methodology of a series slot array antenna for arbitrary inclined linear polarization (LP) is proposed and verified. Especially, 45°-inclined linear polarization is realized for several radar system applications. As a radiating unit, an alternating reactance slot pair is suggested for a impedance matching, uniform field distribution, and suppression of grating lobes, simultaneously. These radiating slot pairs separated with a half guided-wavelength of a radiating line, then resonantly operate as a standing-wave excitation. Also, the proposed antenna structures are realized on printed circuit boards (PCBs) using substrate integrated waveguide (SIW) technology for miniaturization and lightweight features.

A linear and a planar slot array antennas operating at Ka-band are designed and analyzed using equivalent circuit with recursive impedance and current formulas.

The high radiation efficiency for a linear slot array antenna is measured as 72.4% with the realized gain of 15.3 dBi. The excellent high gain of 24.3 dBi is obtained for a 16 × 8 planar slot array antenna with 53.7% aperture efficiency as well. In order to reduce sidelobe levels (SLL) of the proposed 45°-inclined LP, SLL suppression method is also proposed based on a uniform series slot array antenna structure using axial displacements along the center line of radiating SIWs. Two types of low SLL linear slot array antennas with Dolph-Chebyshev polynomials for –20 and –26 dB SLLs are designed and evaluated in terms of the measured electrical performances of the reflection coefficients, realized gain, XPDs, and SLLs.

Lastly, ±45° dual LP slot array antenna design method is proposed. To suppress a mutual coupling and grating lobes, a dielectric constant of a PCB and the width of a radiating SIW are determined for orthogonal arrangements between cross-polarized radiating slots. As a results, the cross-polarized radiation can be reduced and finally improve the radiation purity. Furthermore, dual polarization technique is applied for a dual-plane monopulse radar system. A SIW 8 × 8 dual LP monopulse antenna is designed and operated with a RWG comparator as a feeding network for monopulse operation. It is found that a symmetric sum and difference patterns can be realized by balanced field distributions on a radiating aperture in terms of an amplitude and a phase.

초 록

본 논문에서는 임의의 선형편파 발생을 위한 직렬 슬롯 배열안테나 설계 방법을 제시하였다. 45도 기울어진 선형편파 발생이 가능하고 동시에 임피던스 정합, 균일전장 분포를 형성할 수 있도록 '교차 리액턴스 슬롯 쌍'을 기본 방사체로 제안하였다. 이 기본 방사체를 이용하면 개별 방사 슬롯 간의 간격이 관내 파장의 반 파장 간격으로 위치시킬 수 있기 때문에 grating lobe를 억제할 수 있다. 또한, 제안한 안테나 설계 기법은 기판 집적 도파관 기술 (substrate integrated waveguide, SIW)을 통해 구현하였고 전장 시뮬레이터 및 제작, 측정을 통해 설계 기법의 적합성을 검증하였다.

먼저, Ka-밴드 용 선형 및 평면 배열안테나를 설계하였다. 45도 선형편파를 발생시키기 위해 적층의 SIW 구조로 배열안테나를 구현하였으며 균일 전장이 발생되는 원리를 등가회로 및 임피던스, 전류 순환 방정식을 이용하여 검증하였다. 나아가, 전자장 시뮬레이터를 통한 결과와 비교·분석하였다.

두 번째로, 낮은 부엽레벨을 가지도록 개별 방사체의 전장 계수 조절 방법을 제안하였다. 각 직렬 방사 슬롯을 흐르는 모드 전류의 크기를 조절하기 위해 개별 방사체의 위치를 중심선을 따라 이동시킬 수 있다. 이러한 옵셋 조절 방법을 이용하여 –20 dB 및 –26 dB Dolph-Chebyshev 계수

를 가지는 선형 배열안테나를 설계하였고 제안한 방법의 효용성을 제작 및 측정을 통해 검증하였다.

마지막으로, ±45도 이중 선형편파 발생을 위한 설계 기법을 제안하였다. 동일한 개구면을 공유하는 두 선형편파 간의 격리도를 최대화하기 위해 교차 슬롯 간에 수직 조건을 만족할 수 있도록 기판의 유전율 및 방사 SIW의 폭을 결정하였다. 나아가 제안한 설계 기법을 8 × 8 이중 평면 모노펄스 안테나 설계에 응용하였다. 모노펄스 동작을 위해 기존의 금속 도파관 전송선로를 이용해 제작된 비교기를 결합하였으며 반사손실, 방사패턴, 이득 등의 전기적인 결과를 확인하였다.

주요어: 45도 선형편파, 교차 리액턴스 슬롯 쌍, 이중 선형편파, 격리도, 밀리미터파 안테나, 모노펄스 안테나, 상호 커플링, 공진 슬롯 배열안테나, 직렬 슬롯 배열안테나, 부엽레벨 억제, 기판 집적 도파관, 도파관 비교기
학번: 2010-30211

감사의 글

가장 먼저 지난 4년의 박사 과정 동안 지도해 주신 남상욱 교수님과 지금의 제가 있을 수 있도록 해주신 석사 지도 교수님이신 이재욱 교수님께 깊은 감사를 드립니다. 또한, 더 나은 논문이 될 수 있도록 심사해 주신 서광석 교수님, 김성철 교수님, 권영우 교수님, 김병성 교수님께도 감사 드립니다.

2009년 10월 처음 서울대학교 전파공학 연구실에 와서 연구를 시작하던 기억이 납니다. 세월이 빠름을 다시 한 번 실감하며 박사 과정의 시간들이 헛되지 않도록 최선을 다할 뿐이라 다짐합니다. 4년 동안 같은 시간, 같은 공간에서 동고동락한 연구실의 선·후배님들에게 감사하다는 말을 전하고 싶고 앞으로 사회에 나가 함께 끌어주고 밀어줄 수 있는 돈독한 사이가 될 것임을 믿어 의심치 않습니다.

항상 곁에서 믿어 주고 응원해준 사랑하는 부모님, 동생 동건이, 그리고 보라에게 이 논문을 바칩니다.

2014년 1월 25일

김동연 올림